T. Halpin-Healy, Troisième Cycle de la Physique en Suisse Romande, 12 November 1992

.... merci pour tout!

WITHIN THE REALM OF KPZ: DPRM PHENOMENA & ANOMALOUS KINETIC ROUGHENING

* 1+1 DPRM BETHE ANSATZ SOLUTION
* PHYSICAL REALIZATIONS
* PROBABILITY DISTRIBUTIONS (geometric, free energy)
* KPZ EQUATION ⇝ CONNECTION TO STOCHASTIC GROWTH MODELS (Eden clusters & ballistic deposit)
* COMPLETE CHARACTERIZATION OF KPZ STRONG COUPLING FIXED PT
* POWER-LAW NOISE ⇝ ANOMALOUS ROUGHENING (self-affine fire fronts, bacterial colonies, fluid interfaces)
* MANY DIMENSIONAL DPRM - FINITE TEMPERATURE
* GROUND-STATE INSTABILITIES
* RIVER BASIN DELTAS
* DEPINNING BY QUENCHED RANDOMNESS

* 1+1 DPRM ~ Bethe ansatz solution [M. Kardar, Nucl. Phys. B290, 582 (1987)]

We consider the SOS interface in a random bond (RB) Ising model as a directed polymer in a random medium, with partition function

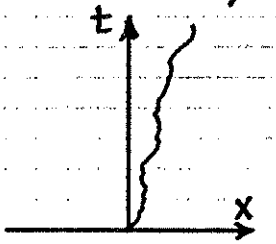

$$\mathcal{Z}_{DPRM} = \int_{\text{POLYMER CONFIGS}} \mathcal{D}x(t)\, e^{-\int dt \left\{ \frac{1}{4\gamma}\left(\frac{dx}{dt}\right)^2 + V(x,t) \right\}}$$

"ELASTICITY" — "PINNING IMPURITIES" disorder has correlator

$$[V(x,t)V(x',t')] = \sigma^2 \delta(x-x')\,\delta(t-t')$$

use REPLICA TRICK to perform average over gaussian disorder – obtain replicated Zamiltonian

$$\mathcal{H}_N = -\gamma \sum_{i=1}^{N} \frac{\partial^2}{\partial x_i^2} - \sigma^2 \sum_{\alpha>\beta} \delta(x_\alpha - x_\beta)$$

← N bosons in one spatial dimension interacting via ATTRACTIVE δ fn potential. (one of the few exactly solvable problems of MANY-BODY PHYSICS)

Bethe ⇒ groundstate wave function of the form

$$\psi_0 \sim \exp\left(-K \sum_{\alpha>\beta} |x_\alpha - x_\beta|\right)$$

discontinuity in slope of wave fn as two particles cross must be matched to the strength σ^2 of the attractive potential ⇒ $K = \sigma^2/\gamma$. Phase space divided into segments depending on ordering of particles. In each segment, the particles are "free" since we have contact potential. Wave function can be written as product of exponentials ⇝ allowed momenta are determined by requiring different segments to match – N! possible orderings of particles. Choose one & expand absolute value

$$\psi_0 \sim \prod_{i=1}^{N} e^{-k_i x_i} \quad \text{with} \quad k_i = (N+1-2i)K \quad \text{where } x_1 < x_2 < \dots < x_N$$

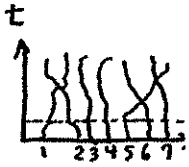

As two particles go thru each other, they just exchange their momenta (ELASTIC SCATTERING!) ⇒ kinetic energy is the same in all segments. We have $\mathcal{H}_N \psi_0 = E_N \psi_0$, with the ground state energy of the N-boson system $E_N = -\frac{1}{3}\gamma K^2 (N^3 - N)$, a famous result of many body physics. Of course, the transfer matrix associated with our replicated DPRM partition function will be dominated by this GS energy ⇒ for a directed polymer of length L, we have

$$[\mathcal{Z}^N] = e^{-E_N L} = e^{-\frac{1}{3}\gamma K^2 N L + \frac{1}{3}\gamma K N^3 L}$$

BUT $[\mathcal{Z}^N] = [\exp(N \ln \mathcal{Z})] = \exp\left\{ \sum_{j=1}^{\infty} \frac{N^j}{j!} C_j(\ln \mathcal{Z}) \right\} \Rightarrow [\mathcal{Z}^N] =$ "CHARACTERISTIC FUNCTION" for random variable $\ln \mathcal{Z} = f$

SO disorder averaged free energy fluctuations of 1+1 DPRM governed by the THIRD CUMULANT ➡ $|\Delta f| \sim L^{1/3}$, ∞ $\{\omega_{1+1} = \frac{1}{3}\}$ ENERGY EXPONENT

NOTA BENE

① it is crucial to keep in mind that, because of the average over many realizations of the "RANDOM ENERGY LANDSCAPE," the quenched free energy is a fluctuating quantity ← to describe it properly, we need probability distribution (mean, higher moments, ...)

② non-standard REPLICA TRICK! We never consider limit $N \to 0$. Indeed, it is an extraordinary feature of the DPRM that the REPLICATED PARTITION FUNCTION $[Z^N]$, being the characteristic function for the fluctuating random variable $\ln Z$, gives us complete information about the quenched free energy probability distribution by providing us with its CUMULANTS.

③ by construction, CUMULANTS ⇝ measure deviation of probability distribution from Gaussian

GAUSSIAN $\equiv 0$
$C_{j>3}$

$$C_1(f) = [f]$$
$$C_2(f) = [f^2] - [f]^2$$
$$C_3(f) = [f^3] - 3[f^2][f] + 2[f]^3$$

■ generally not the same as connected moment!

BUT

$$C_4(f) = [f^4] - 4[f^3][f] - 3[f^2]^2 + 12[f^2][f]^2 - 6[f]^4 \neq [f - [f]]^4$$

④ naive Bethe ansatz calculation assumes GROUND-STATE DOMINANCE and only yields the energy fluctuation exponent $\omega = 1/3$. Inclusion of center of mass motion (see J.P. Bouchaud & M. Orland, J. Stat. Phys. 61, 877 (1990)) gives wandering exponent $\zeta = 2/3$ directly, as well as index relation $\omega = 2\zeta - 1$, various scaling amplitudes, $C_4(f)$ and higher cumulants, finite size corrections, geometric and free energy probability distributions

⑤ Kardar Nucl. Phys. B290, 582 (1987)
Zhang, Phys. Rev. B42, 4897 (1990).

generally: $[Z^N] = e^{-E(N)L}$

would like to know this function for cases of CORRELATED DISORDER:

* QUADRATIC CASE ⇝ Ponson, Morton, Zhang
* LINEAR, BF DPRM ⇝ Jacquet & Zhang

* PHYSICAL REALIZATIONS - Directed Polymers in Random Media

1) STATISTICS OF TORN SHEETS

J. Kertész, V. Horváth, & F. Weber, Les Houches '92 - KINETIC ROUGHENING

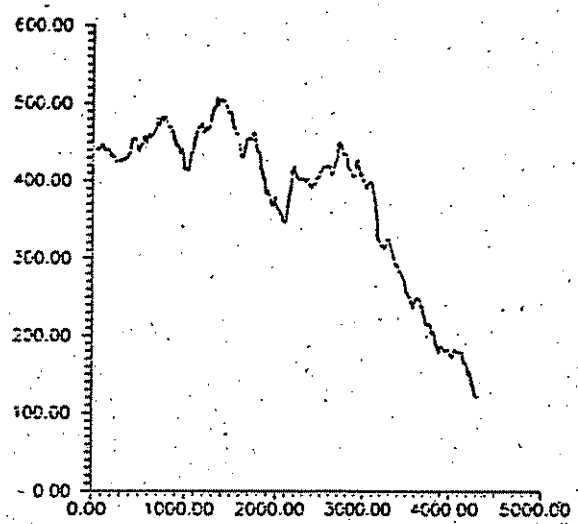

Figure 1. A digitized tear line. Note the different scales on the axes

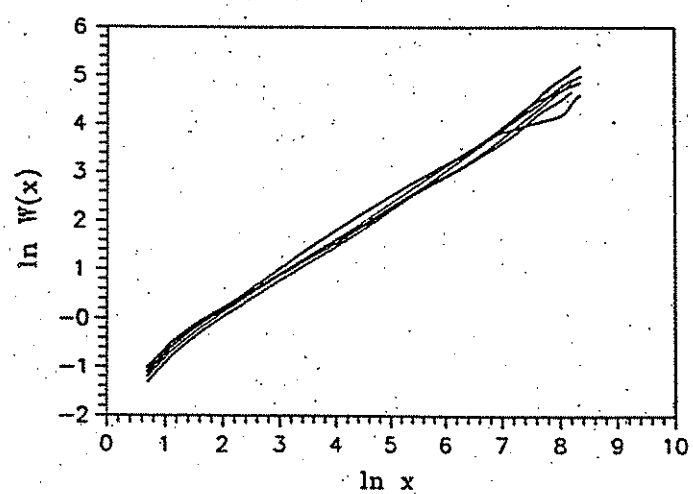

Figure 2. Scaling plots of tear lines in paper

studied the morphology of self-affine fractal tear lines in paper, resulting from equilaterally applied tensile stress.

* sheets 30 × 45 cm
* 5 different kinds of paper from Institute for Paper Research, Hungary
* properties such as strength, density, thickness varied by factors of two or three

NEVERTHELESS, they find

$$\zeta = 0.67 \pm 0.05$$

in (rather) extraordinary agreement with the 1+1 DPRM wandering exponent.

* see also,
  - M. Baird & I. Hopkin-Healy, unpublish

2) RB INTERFACES IN DIRTY 2d MAGNETS

D. Huse & C. Henley, Phys. Rev. Lett. 54, 2708 (1985).

3) BLOWN FUSE NETWORKS

A. Hansen, E. Hinrichsen, & D. Roux, Phys. Rev. Lett. 66, 2476 (1991)

for related work on RB surfaces (roughness of brittle cracks) by same authors see, ibid, 68, 213 (1992).

4) VORTICES IN CERAMIC SUPERCONDUCTORS

T. Nattermann & R. Lipowsky, Phys. Rev. Lett. 61, 2508 (1988).

5) DISLOCATION LINES IN DISORDERED SOLIDS – L. Golubchik & V.M. Vinokur, J. Phys. C 20, 6149 (1987)

RAPID COMMUNICATION

PHYSICAL REVIEW A VOLUME 44, NUMBER 6 15 SEPTEMBER 1991

Directed polymers in random media: Probability distributions

Timothy Halpin-Healy

Physics Department, Barnard College, Columbia University, New York, New York 10027-6598

(Received 17 June 1991)

Using transfer-matrix methods, we have investigated numerically the probability distributions that govern geometric and free-energy fluctuations in the (1+1)-dimensional directed polymer subject to quenched, uncorrelated Gaussian disorder. Exhaustive averaging, over many realizations of the random energy landscape, have permitted us to observe scaling of the third cumulant of the free energy as predicted by Kardar [Phys. Rev. Lett. 55, 2235 (1985)], to address issues concerning finite-size effects, and to discern the *asymmetric* form of the free-energy probability distribution. In addition, we have determined precisely the amplitudes of various transverse moments in order to compare to recent estimates of Bouchaud and Orland [J. Stat. Phys. 61, 877 (1990)].

* see also Kim, Bray & Moore Phys. Rev. A44, 2345 (1991).

The statistical mechanics of directed polymers in random media, a testing grounds of sorts for the basic rules that constitute our understanding of ill-condensed matter, has proven to be a most engaging subject since its introduction [1–4] a few years ago. Because of a mapping via the stochastic Burgers' equation [5], which ties it to a host of other interesting issues, such as the dynamic scaling of surface growth in Eden clusters and ballistic deposits, the long-time behavior of randomly stirred fluids, as well as the asymptotic evolution of propagating flame fronts, the problem of directed polymers in random media (DPRM) enjoys an extraordinary richness. Though much effort was expended initially in pinning down the critical exponents [6–11] and phase diagram [12–15] for the many-dimensional DPRM, recent work has returned to the statistics of optimal paths in 1+1 dimensions, being especially attentive to the implications of non-Gaussian noise [16,17], the nature of the full scaling functions [18,19], and the possibility of replica symmetry breaking [20,21] within the model. Recall that, aside from the infinite-dimensional case of the Cayley tree [22], the only exact result, due to Kardar [1(a)], is in 1+1 dimensions with uncorrelated white noise. His analysis, based on a Bethe ansatz assuming ground-state dominance, established the fact that free-energy fluctuations of the directed polymer scale with an index $\omega=1/3$. The primary purpose of the present paper is to render this statement somewhat more precisely and investigate the full free-energy probability distribution. Invoking an exponent equality of Huse and Henley [2(a)], $\omega=2\zeta-1$, Kardar was then able to infer the wandering exponent $\zeta=2/3$. It is this critical index which characterizes the geometric properties of the DPRM, namely the disorder-induced transverse fluctuations of the directed walker traversing a random energy landscape.

So the matter sat until Zhang [18], and later Bouchaud and Orland [19], sought to understand in greater detail the essential features of the (1+1)-dimensional directed polymer subject to quenched, uncorrelated Gaussian disorder. An important aspect of their work was a preliminary attempt to grapple with the precise form of the probability distributions which determine the scaling behavior of the free energy and spatial fluctuations. Zhang [18] has proposed, for example, that for the free-energy probability distribution, $P(F,t)\sim\exp(-|F-f_0t|^{3/2}/t^{1/2})$, where F is the free energy at the time slice t, in a particular realization of randomness, and f_0 is the disorder averaged free-energy per unit length. This result follows from an approximate saddle-point calculation, is consistent with the energy fluctuation exponent $\omega=1/3$, and gives the nonvanishing second-order cumulant observed in the numerical simulations of Kardar [1(b)]. Nevertheless, as an even function, all odd moments vanish, which precludes the possibility of third cumulant scaling as predicted by Kardar [1].

Lastly, Bouchaud and Orland [19], including the center of mass motion in Kardar's original Bethe ansatz solution, were able to relate the 1+1 DPRM to a more manageable toy model, building upon earlier work of Parisi [20] and Mezard [21]. Their toy model involved studying the properties of a Hookian spring subject to a potential energy function of Gaussian random slope. This permitted them to calculate both the *amplitude* and *exponent* of the second cumulant of the free energy, as well as some higher geometric moments. Using transfer-matrix techniques, we have numerically studied the free energy and geometric probability distributions of the 1+1 DPRM, both at finite and zero temperatures, in an effort to test Kardar's predictions regarding the free-energy cumulants [1], Zhang's conjecture [18] for $P(F,t)$, as well as the amplitude estimates and free-energy finite-size corrections of Bouchaud and Orland [19].

GEOMETRIC PROPERTIES

Perhaps the most distinctive feature of the 1+1 DPRM is the fact that the disorder-induced transverse fluctuations scale as the 2/3 power of the length, a considerably greater effect than the simple entropic wandering characteristic of a coin-flipping random walker. This was first observed numerically for $x_{\rm rms}$ in the zero-temperature case by Huse and Henley [2(a)] and at finite temperature by Kardar [1(b)]. That the exponent $\zeta=2/3$, precisely, was not established directly till the work of Bouchaud and Orland [19], though the result was, of course, much anticipated since the previous efforts of Huse, Henley, and Fisher [2(b)] had uncovered a fluctuation-dissipation theorem that implied $\zeta=2\omega$.

With all published work on the matter having concentrated on x_{rms}, we decided greater understanding might be had by way of studying the higher moments, as well as the full probability distribution $P(x,t)$, which gives the probability of finding the optimal path with a transverse fluctuation x in a particular time slice t. This distribution function, along with that of the free energy to be discussed later, are in a crucial sense the central scaling functions of the DPRM problem. Technical treatments of the DPRM, and the related problem of dynamic scaling of surface growth in Eden clusters and ballistic deposits, have only recently reached the level of sophistication that questions regarding these probability distributions could be broached.

The results presented and figures illustrated in this section are pulled from zero-temperature numerical simulations done in the manner of Zhang [4]. One considers a directed walker who, starting at the origin of a square lattice, has the option of making an immediate step diagonally left or right to $(x,t)=(\pm 1,1)$. These and succeeding diagonal bonds have random energies drawn uniformly between 0 and s, the distribution having variance $\sigma^2 = s^2/12$. Neighboring bonds are uncorrelated. At the time slice t there are $t+1$ possible end points to the 2^t paths emanating from (0,0). For zero temperature, the DPRM becomes a matter of *global optimization* in which, for a given realization of the random energy landscape, one seeks the path of overall least energy—the total energy of a path being given by the sum of the random bonds visited along the way. This contrasts with Kardar's finite-temperature method [1(b)] where all paths are included, weighted by the appropriate Boltzmann factor. Furthermore, Kardar's trajectories follow the traditional links of the square lattice, there being an energy cost $-\ln(\gamma)$ for each horizontal bond traversed, while the vertical bonds carry the uniformly distributed random energies. It should be stressed that these simulations done at finite temperature, in the manner of Kardar, yield essentially identical results as the $T=0$ DPRM. For example, the ratios of even positional moments are the same in both cases. Subtle, but important distinctions will be discussed as they arise. These differences, while interesting in themselves, are insubstantial in the sense that our numerical work suggests that a solitary fixed point controls the two cases. This phase diagram topology is consistent with an earlier conjecture [12], in addition to more recent work [23] that has convincingly established the notion of a single universality class.

In Fig. 1, we show the first four even moments in a logarithmic plot. The numerical work involves calculating the nth root of the disorder average of x^n, following from 100000 realizations of a random energy landscape traversed by directed paths of length 500 steps. As is evident from the figure, the large number of disorder complexions have permitted us to minimize the statistical noise of the data and we obtain reasonably good scaling as soon as the walker has taken a dozen steps or so. Performing a least-squares fit to the data to pick off the scaling index, we find 0.667 ± 0.005 in all cases. The smallness of the uncertainty, which represents our own subjective assessment of ambiguities arising in doing the fit, is a simple consequence of the extensive averaging that we have done. A major goal of the present work was to determine the amplitude ratios of the moments. Normalizing to the second moment, we find 1.00:1.28:1.52:1.72, which immediately suggests a probability distribution that is somewhat sharper than a Gaussian [24]. For the second moment proper, we find an amplitude $A_2 = \lim_{t\to\infty}(x_{rms}/t^{2/3}) = 0.355 \pm 0.005$, independent of the disorder strength, since there is no energy scale at $T=0$. At finite temperatures, we find essentially the same ratios, differences being smaller than 1%–2%. For these finite temperature simulations, we were particularly interested in ascertaining the precise value of the amplitude of the second moment, in order to compare to the predictions of Bouchaud and Orland [19]. We find, for temperature-dictated elastic parameter $\gamma=0.1$ and a disorder strength $\sigma^2=5/6$ [the notation is that of Ref. [1(b)], that the amplitude settles down to value $A_2=0.29\pm0.01$, which is rather close to the value following from the formula of Bouchaud and Orland, $A_2=1.02(D\sigma^2)^{1/3}$, assuming, as they do, that $D\approx\gamma/3$ is the continuum diffusion constant. This good agreement may be entirely fortuitous, however, since recent work [25] indicates that, due to renormalization effects, the relationship between D and γ is considerably more subtle. Along with this serious caveat, we note strong disagreement with the Bouchaud-Orland prediction for amplitude ratios of the geometric moments.

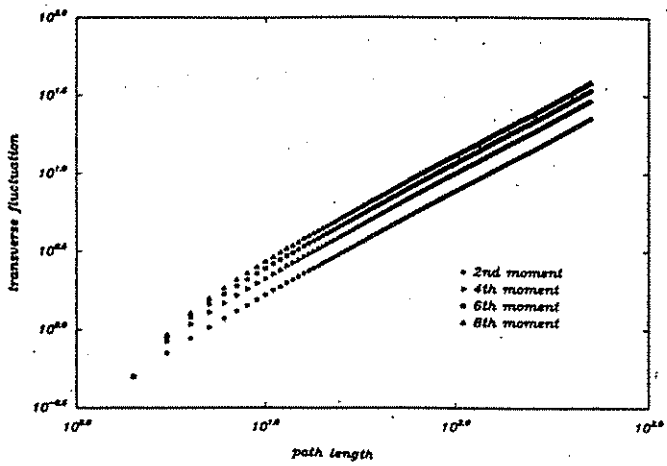

FIG. 1. Log-log plot of the first four even *positional* moments of the zero-temperature (1+1)-dimensional directed polymer in a random medium as a function of path length. The disorder average is performed over 10^5 realizations of the random energy landscape. Paths are 500 steps long. All geometric moments scale with the characteristic wandering exponent 2/3. The second moment, given by the lowest curve, has an amplitude 0.355 ± 0.005. The amplitude ratios are 1.00:1.28:1.52:1.72.

Figure 2 explores the geometric probability distribution $P(x,t)$ that is responsible for generating the above moments. Our numerical data comes from the zero-temperature simulation that included a disorder average over 10^5 realizations of the randomness. In Fig. 2(a), which plots $\ln[P(x,t)/P(0,t)]$, the data for three separate time slices, $t=100$, 200, and 500, are collapsed to a single universal curve that is evidently symmetric and entirely consistent with the scaling form $P(x,t)\sim\exp-(x/t^{2/3})^{\rho}$.

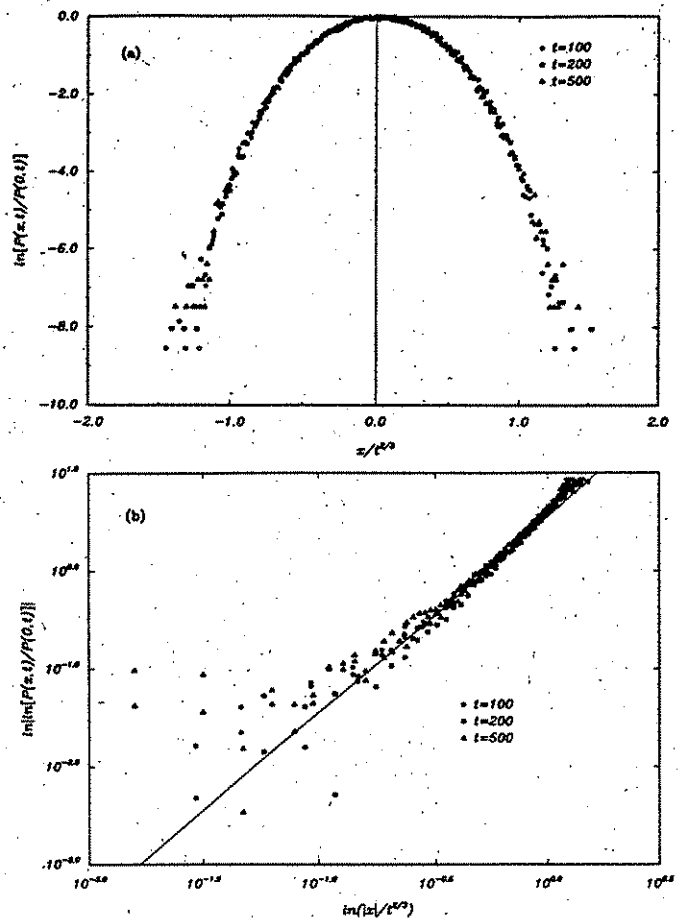

FIG. 2. *Symmetric* positional probability distribution function $P(x,t)$; zero-temperature simulation of 1+1 DPRM, 10^5 realizations. (a) $\ln[P(x,t)/P(0,t)]$ vs $|x|/t^{2/3}$, exhibiting data collapse for three separate time slices $t=100$, 200, and 500; (b) $\ln|\ln[P(x,t)/P(0,t)]|$ vs $\ln(|x|/t^{2/3})$; for increasing abscissa, the data pull away from the line of slope 2, indicating that transverse fluctuations of the directed polymer are governed by a distribution that is eventually *sharper* than Gaussian.

Numerically, we find that the odd moments are effectively zero [26] and do not scale. Taking a logarithm of the collapsed data, we find that the distribution has some Gaussian character, but the slope certainly begins to exceed two at $x/t^{2/3}\approx 1$. In fact, a least-squares fit in this regime gives an effective exponent $\rho\approx 2.2$. Unfortunately, even with 10^5 realizations of the disorder, we could not access sufficiently the depth of the tail to test the prediction [19] that asymptotically $\rho=3$.

FREE-ENERGY PROPERTIES

It is the scaling behavior of the free energy and its higher cumulants that are responsible for the most intriguing aspects of the DPRM problem. In Kardar's Bethe ansatz analysis [1], performing the disorder average over quenched randomness leads, within the replica formalism, to the consideration of a well-known but solvable problem of many-body physics; namely, N bosons in one spatial dimension interacting via an attractive δ-function potential. The ground-state energy of such a system scales as N-N^3. This fact has severe consequences for the probability distribution of the DPRM free-energy probability distribution $P(F,t)$. Foremost among these is a nontrivial scaling of the third cumulant, a most striking prediction which, despite its unusual nature, has remained to this date untested numerically. In addition, if one accepts verbatim the results of the Bethe ansatz solution, fourth- and higher-order cumulants vanish in the thermodynamic limit. These distinctive features greatly constrain the free-energy probability distribution. It was our primary purpose to study in detail the functional form of $P(F,t)$ to settle many of these issues.

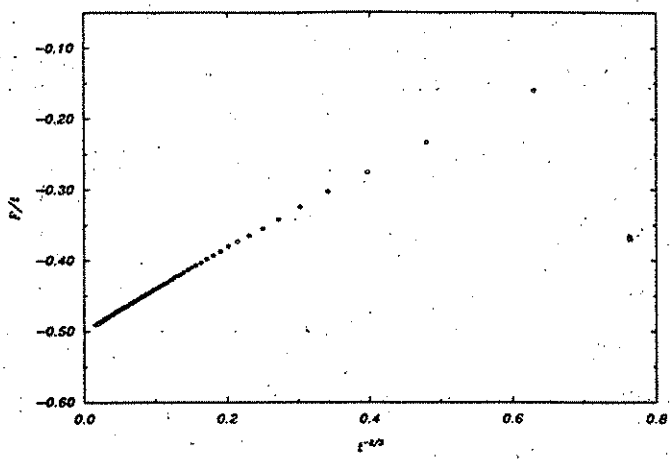

FIG. 3. Finite-size correction to the disorder averaged free energy per unit length. Plot shows F/t vs $t^{-2/3}$ for 10^4 realizations of randomness for directed walks of 500 steps. Finite-temperature simulation with $\gamma=0.1$ and $\sigma^2=5/6$.

In addition, it is also possible to check some of the conjectures of Bouchaud and Orland [19] regarding the free energy. For example, their work allows them to calculate the scaling behavior of the finite-size correction to the free energy per unit length of the DPRM. This quantity ought

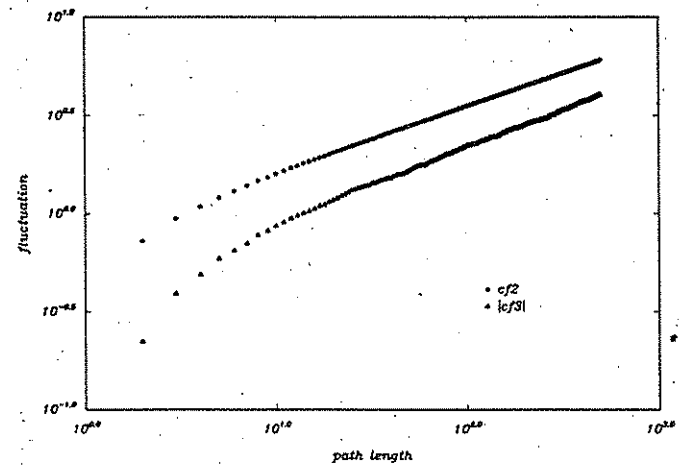

FIG. 4. Negative, third-order cumulant of the free energy (cf3) scales with an exponent 0.37 ± 0.02, in agreement with, though a bit larger than Kardar's predicted value. The second-order cumulant (cf2), with $\omega=0.333\pm0.003$, is in complete accord with the characteristic free-energy scaling index of 1/3. Same parameters as in Fig. 3, but 5×10^4 realizations of disorder are necessary to elicit reasonably good scaling of the third-order cumulant.

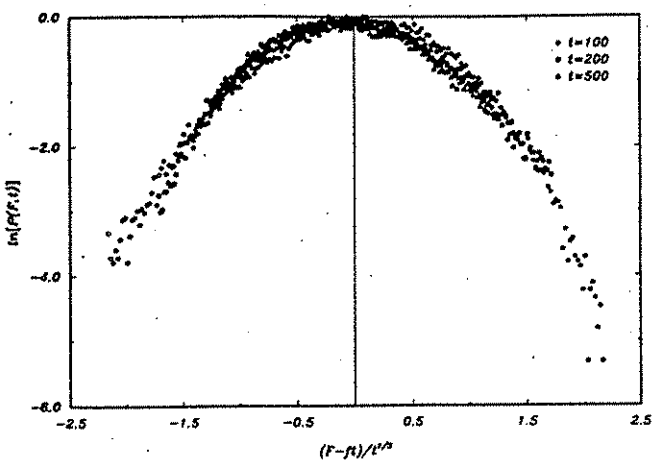

FIG. 5. *Skewed* free-energy probability distribution $P(F,t)$ of the 1+1 DPRM at finite temperature. Plotted is $\ln[P(F,t)]$ vs deviation from mean-free energy, in data collapsed form for times slices $t=100$, 200, and 500; 5×10^4 realizations of random energy landscape.

to vanish with an exponent [27] of 2/3. In Fig. 3, we show data for 10^4 realizations of a system characterized by $\gamma=0.1$, $\sigma^2=5/6$. The data fall nicely upon a straight line, confirming the Bouchaud-Orland exponent. We do, however, find disagreement, by a factor of 2, with their prediction for the slope. There is also a discrepancy of sign. Finally, we note that in our zero-temperature simulations, we observe the finite-size correction to scale with the *same* exponent and similar sign; that is, the generic behavior is to settle down to the asymptotic value from above.

Results for the free-energy cumulants are illustrated in Fig. 4, which shows the second- and third-order cumulants of the probability distribution (labeled cf2 and cf3, respectively, in the figure), for the (1+1)-dimensional DPRM at finite temperature. The elasticity parameter and disorder strength are the same as above, but our numerical work here involves 5×10^4 realizations of randomness. Despite the somewhat modest system sizes, the second-order cumulant scales nicely with an exponent $\omega=0.333\pm0.003$. The amplitude of this cumulant is 0.76. The third-order cumulant scales with a slightly higher exponent (indeed, it is consistently so), but one which is in reasonable agreement with Kardar's conjecture. Note that the data for the third-order cumulant are much noisier. In fact, while the second-order cumulant scales well for as few as 10^3 realizations of the random energy landscape, it is nearly impossible to observe proper scaling of the third-order cumulant unless one performs exhaustive averaging [28]. With nonvanishing third-order cumulant, the free-energy probability distribution differs significantly from a Gaussian distribution. This last point is reaffirmed by a moment's glance at $P(F,t)$, see Fig. 5. We find, in contrast to previous but approximate analytical work [18], the strong suggestion that the free-energy probability distribution is asymmetric.

ACKNOWLEDGMENTS

The author would like to thank J. Krug, M. Kardar, and T. Hwa for useful conversations, and L. Kay for Sparc 2 computer time. This research was supported in part by Grants from the Research Corporation and The Petroleum Research Fund, the latter being administered by the American Chemical Society.

[1] (a) M. Kardar, Phys. Rev. Lett. **55**, 2235 (1985); (b) **55**, 2923 (1985); (c) see also M. Kardar, Nucl. Phys. **B290**[FS20], 582 (1987).
[2] (a) D. A. Huse and C. L. Henley, Phys. Rev. Lett. **54**, 2708 (1985); (b) D. A. Huse, C. L. Henley, and D. S. Fisher, *ibid.* **55**, 2924 (1985).
[3] M. Kardar and Y.-C. Zhang, Phys. Rev. Lett. **58**, 2087 (1987).
[4] Y.-C. Zhang, Phys. Rev. Lett. **59**, 2125 (1987).
[5] M. Kardar, G. Parisi, and Y.-C. Zhang, Phys. Rev. Lett. **56**, 889 (1986).
[6] D. E. Wolf and J. Kertész, Europhys. Lett. **4**, 651 (1987).
[7] T. Halpin-Healy, Phys. Rev. Lett. **62**, 445 (1989).
[8] T. Halpin-Healy, Phys. Rev. Lett. **63**, 917 (1989).
[9] J. M. Kim and J. M. Kosterlitz, Phys. Rev. Lett. **62**, 2289 (1989).
[10] W. Renz (unpublished).
[11] H. G. E. Hentschel and F. Family, Phys. Rev. Lett. **66**, 1982 (1991).
[12] T. Halpin-Healy, Phys. Rev. A **42**, 711 (1990).
[13] Y. P. Pellegrini and R. Jullien, Phys. Rev. Lett. **64**, 1745 (1990).
[14] B. Derrida and O. Golinelli, Phys. Rev. A **41**, 4160 (1990).
[15] L. H. Tang, T. Nattermann, and B. M. Forrest, Phys. Rev. Lett. **65**, 2422 (1990).
[16] Y. C. Zhang, J. Phys. (Paris) **51**, 2129 (1990).
[17] J. Krug, J. Phys. I (France) **1**, 9 (1991).
[18] Y. C. Zhang, Europhys. Lett. **9**, 113 (1989); J. Stat. Phys. **57**, 1123 (1989).
[19] J. P. Bouchaud and H. Orland, J. Stat. Phys. **61**, 877 (1990); see also U. Schulz, J. Villain, E. Brézin, and H. Orland, J. Stat. Phys. **51**, 1 (1988).
[20] G. Parisi, J. Phys. (Paris) **51**, 1595 (1990).
[21] M. Mezard, J. Phys. (Paris) **51**, 1831 (1990).
[22] B. Derrida and H. Spohn, J. Stat. Phys. **51**, 817 (1988).
[23] T. Hwa, E. Frey, and D. Fisher (private communication).
[24] For a Gaussian distribution, the corresponding ratios are 1.00:1.32:1.57:1.79.
[25] J. Krug, P. Meakin, and T. Halpin-Healy (unpublished).
[26] That is not to say that they *vanish* numerically. Rather, the odd geometric moments, while increasing, randomly fluctuate in sign from one time slice to the next.
[27] This exponent was derived for stochastic growth models by J. Krug and P. Meakin, J. Phys. A **23**, L987 (1990).
[28] The situation is even worse for the fourth-order cumulant of the free energy. It should be noted that Kardar's Bethe ansatz solution requires this quantity to be zero. Our numerical simulations observe, however, that this cumulant scales as a noisier version of cf3, with similar exponent but smaller amplitude.

COMPLETE CHARACTERIZATION - KPZ STRONG COUPLING FP: ⑧

PHYSICAL REVIEW A VOLUME 45, NUMBER 2 15 JANUARY 1992

Amplitude universality for driven interfaces and directed polymers in random media

Joachim Krug
IBM Research Division, Thomas J. Watson Research Center, Yorktown Heights, New York 10598

Paul Meakin
Central Research and Development, The du Pont Company, Experimental Station E356/153, Wilmington, Delaware 19880-0356

Timothy Halpin-Healy
Physics Department, Barnard College, Columbia University, New York, New York 10027-6598

(Received 5 September 1991)

We present accurate estimates for the prefactors of the second and third moments of the height and free-energy fluctuations, as well as the leading correction to the growth rate and free energy per unit length, obtained from extensive simulations of a wide range of one-dimensional models of growing interfaces and directed polymers in a random environment. When scaled by the appropriate model-dependent parameters the amplitudes reduce to universal numbers which characterize the strong-coupling fixed point of the equation of Kardar, Parisi, and Zhang [Phys. Rev. Lett. 56, 889 (1986)]. To check the expected scaling we use models for which the model parameters can be computed analytically. For other systems, such as ballistic deposition, the restricted solid-on-solid model, and the finite-temperature directed polymer, the parameters are determined numerically from steady-state properties. Apart from the standard transient simulation which starts from a flat interface, we also report results for time-dependent correlations in the steady state, which give rise to different universal amplitudes. We compare our results with recent predictions arising from replica calculations and dynamic renormalization-group treatments, finding agreement in the latter but severe discrepancies in the former case. We speculate that the failure of replica theory may be indicative of replica symmetry breaking.

PACS number(s): 02.50.+s, 05.40.+j, 61.50.Cj, 75.60.Ch

(nb) THIS PAPER USES THE SYMBOL S, RATHER THAN χ, FOR THE SATURATION WIDTH EXPONENT. DO NOT CONFUSE WITH DPRH WANDERING EXPONENT.

I. INTRODUCTION

In the past five years following the seminal work of Kardar, Parisi, and Zhang (KPZ) [1] the kinetic roughening of driven interfaces has aroused a tremendous amount of interest in the statistical-physics community [2]. Indeed, the KPZ theory provides a quantitative understanding of some of the fascinating structures generated in a broad range of stochastic nonequilibrium processes [3]. Moreover, kinetic roughening is of relevance to many applied fields ranging from crystal-growth [4] and deposition [5] processes to two-phase flow in porous media [6]. Hence long-standing problems in materials science, such as the columnar growth morphology observed in thin-film deposition [7], can be expected to benefit from our improved understanding of kinetic roughening. Finally, workers with a background in the statistical mechanics of disordered systems have been attracted to the field by the close formal relation between moving interfaces and directed polymers in a random medium [8], bringing with them a wealth of powerful and inventive methods [9–12].

Here the term kinetic roughening implies the process by which the noisy local displacement dynamics of an interface translates into scale-invariant fluctuations of the interface position. In the commonly employed simulation scheme the interface is prepared in a flat state at time $t=0$ and the evolution of the fluctuations is monitored by measuring the width

$$\xi=\langle[h(\mathbf{x},t)-\langle h(\mathbf{x},t)\rangle]^2\rangle^{1/2}\,, \tag{1}$$

where $h(\mathbf{x},t)$ denotes the height of the interface above a point $\mathbf{x}$ on a d-dimensional substrate, at time t. The width grows with time as a power law up to a saturation time that scales with the substrate size L as L^z, where z is the dynamic scaling exponent. The dependence on t and L can be summarized in the scaling form [13]

$$\xi(t,L)=L^{\zeta}f(t/L^z)\,, \tag{2}$$

where the scaling function $f(x)$ saturates at large x and $f(x\to 0)\sim x^{\zeta/z}$. The width grows as $t^{\zeta/z}$ at early times and saturates at a value proportional to L^{ζ}. The exponent ζ is called the roughness or wandering [14] exponent. The two scaling exponents in (2) satisfy the relation $\zeta+z=2$ [15–17].

A specific symmetry of one-dimensional interfaces [18,19] forces the roughness exponent to take the value $\zeta=\frac{1}{2}$ familiar from thermal equilibrium, and hence $z=\frac{3}{2}$ exactly [1]. Much of the previous numerical work has focused on obtaining accurate estimates for the scaling exponents in dimensions $d=2$ and higher [20,21]. In the present paper we return to the one-dimensional case to look for universal quantities other than the scaling exponents which can be extracted from theory and simulations. Specifically, we investigate the prefactors of the asymptotic power laws governing the divergence of the interface width (1) and higher moments of the height fluctuations. Our motivation is twofold. First, in experimen-

tal applications [4,6] it is important to understand how these amplitudes depend on the system parameters in order to estimate the range in which to expect the asymptotic power laws. Second, since the scaling exponents in one dimension are basically determined by the symmetries of the problem, the fact that different models show the same asymptotic scaling gives only a weak indication of the presence of true universality. Technically speaking, the existence of several fixed points with identical scaling exponents is a conceivable scenario [22] in the renormalization-group context [1,11,17] which can be ruled out only by demonstration of amplitude universality.

Different sets of amplitudes are associated with the two asymptotic regimes combined in (2). Since we wish to characterize the full probability distribution of the height fluctuations, we define one set of amplitudes associated with the transient regime $t \ll L^z$,

$$a_n = \lim_{t\to\infty} \lim_{L\to\infty} t^{-n/3} \langle [h(x,t) - \langle h(x,t) \rangle]^n \rangle_c \ , \tag{3}$$

where $\langle X^n \rangle_c$ denotes the nth cumulant [23] of the random variable X, and one set associated with the stationary regime $t \gg L^z$,

$$b_n = \lim_{L\to\infty} \lim_{t\to\infty} L^{-n/2} \langle [h(x,t) - \langle h(x,t) \rangle]^n \rangle_c \ . \tag{4}$$

Comparing with (2) it is clear that $\lim_{y\to\infty} f(y) = b_2^{1/2}$ and $f(y) \approx a_2^{1/2} y^{1/3}$ for $y \to 0$. It will turn out that, due to the special structure of the one-dimensional problem, the static amplitudes b_n are trivial, while the dynamic amplitudes a_n contain nontrivial information about the KPZ fixed point.

Another quantity of interest is the leading correction to the asymptotic growth rate $v_\infty = \lim_{t,L\to\infty} \langle \partial h/\partial t \rangle$. Two of us have recently shown that [24]

$$\langle \partial h/\partial t \rangle - v_\infty = L^{-1} \bar{f}(t/L^z) \tag{5}$$

for one-dimensional interfaces, where $\bar{f}(y) = \text{const}$ for $y \gg 1$ and $\bar{f}(y) \sim y^{-2/3}$ for $y \ll 1$. This leads to the amplitudes

$$a_v = \lim_{t\to\infty} \lim_{L\to\infty} t^{2/3} (\langle \partial h/\partial t \rangle - v_\infty) \tag{6}$$

and

$$b_v = \lim_{L\to\infty} \lim_{t\to\infty} L (\langle \partial h/\partial t \rangle - v_\infty) \ , \tag{7}$$

hence $b_v = \lim_{x\to\infty} \bar{f}(y)$ and $a_v = \lim_{y\to 0} y^{2/3} \bar{f}(y)$.

The amplitudes defined above are not universal as they stand: They contain model-dependent parameters that have to be determined in order to extract universal numbers. The relevant parameters will be identified in the next section, and it will be shown how they can be numerically measured for a given growth model. To avoid numerical uncertainties associated with the determination of these parameters, we have investigated a family of models for which they can be derived exactly. This will be described in Sec. III. Section IV summarizes our numerical estimates for the universal amplitudes. In particular, we find that all growth models belong to a single universality class. In Sec. V the connection to directed polymers in a random medium is outlined, the relevant parameters are identified, and numerical estimates of the amplitudes are presented that agree with the results obtained from the growth models. In Sec. VI we abandon the conventional setup of starting from a flat interface, and investigate instead dynamic fluctuations in the stationary regime. This leads to a different set of amplitudes. Finally in the last section we conclude by comparing our numerical results to existing theoretical predictions. Some technical details concerning the numerical measurement of the amplitude b_v defined in (7) are discussed in an appendix.

II. MODEL-DEPENDENT PARAMETERS AND UNIVERSAL AMPLITUDES

According to Kardar, Parisi, and Zhang the local position $h(\mathbf{x},t)$ of a moving interface satisfies [1]

$$\frac{\partial}{\partial t} h(\mathbf{x},t) = v_0 + \frac{\lambda}{2} (\nabla h)^2 + \nu \nabla^2 h + \eta(\mathbf{x},t) \ , \tag{8}$$

where the first two terms on the right-hand side arise from a gradient expansion of the macroscopic inclination-dependent growth rate [25] and the last two terms describe the microscopic growth-rate fluctuations. The noise η is Gaussian with zero mean and variance

$$\langle \eta(\mathbf{x},t) \eta(\mathbf{x}',t') \rangle = D \delta^d(\mathbf{x}-\mathbf{x}') \delta(t-t') \ . \tag{9}$$

The major simplifying feature in $d=1$ is that the stationary height fluctuations are *independent* of the nonlinear term in (8), and hence all static (stationary, equal time) correlation functions can be easily computed [18,19]. The stationary distribution is Gaussian, with the variance

$$\lim_{t\to\infty} \langle |\hat{h}(k,t)|^2 \rangle = \frac{D}{2\nu L k^2} \tag{10}$$

for the discrete Fourier modes $\hat{h}(k,t)$, $k = 2\pi m/L$, $m = -L/2, \ldots, -1, 1, \ldots, L/2$. Consequently, the stationary height-difference correlation function in an infinite system is

$$C_h(r) = \lim_{t\to\infty} \langle [h(x+r,t) - h(x,t)]^2 \rangle = Ar \tag{11}$$

for large r, with

$$A = \frac{D}{2\nu} \ , \tag{12}$$

and the stationary width in a finite system with periodic boundary conditions is

$$\lim_{t\to\infty} \xi(t,L) = \left[\frac{A}{12} \right]^{1/2} L^{1/2} \tag{13}$$

for large L, i.e., $b_2 = A/12$. The Gaussian character of the stationary distribution implies that all higher cumulants vanish, $b_n = 0$ for $n > 2$.

The finite-size correction (5) arises from the fluctuation contribution to the growth rate obtained by averaging the right-hand side of (8). Using (10) it follows that [24]

$$b_v = -\frac{\lambda}{2} \langle (\nabla h)^2 \rangle = -\frac{\lambda A}{2} \ . \tag{14}$$

From a practical point of view, the results (11), (13), and (14) for the static amplitudes provide us with a simple method to numerically determine the values of A and λ for any model of interest. In addition, λ can be determined directly from the inclination dependence of the growth rate. Indeed by imposing a small tilt $h(x,t)\to h(x,t)+\epsilon x$ in (8) and computing the response in the average growth rate we find [25]

$$\lambda = v_\infty''(0) . \tag{15}$$

These ideas will be put to work in Sec. IV.

In the transient regime (10) takes on the dynamic scaling form [26–28]

$$\langle |\hat{h}(k,t)|^2 \rangle = \frac{D}{2\nu L k^2} g[(\lambda^2 A)^{1/3} k t^{2/3}] , \tag{16}$$

where g is now a *universal* (model-independent) nontrivial scaling function. The height fluctuations in this regime are no longer expected to be Gaussian, and hence the higher moments are not related to the variance (16) in any simple way. In particular, since the nonlinear term in (8) breaks the $h \to -h$ symmetry, odd moments may become nonzero. Nevertheless the higher moments are expected to satisfy scaling relations similar to (16). Under this assumption it follows that the general form of the transient amplitudes is

$$a_n = (|\lambda| A^2)^{n/3} c_n \tag{17}$$

and

$$a_v = (|\lambda| A^2)^{1/3} c_v , \tag{18}$$

where the absolute values of c_n and c_v are expected to be universal numbers. The *signs* of c_n (for $n>2$) and c_v are not fixed *a priori*, but it is clear from the symmetry of (8) that they have to be determined by the (model-dependent [25]) sign of λ. It has been shown previously [24] that the sign of c_v is opposite to the sign of λ [see also (14)].

Both c_2 and c_v can be related to the scaling function g of the variance (16). Going to the continuum limit in k one obtains

$$c_2 = \frac{1}{\pi} \int_0^\infty dx \frac{g(x)}{x^2} \tag{19}$$

and

$$|c_v| = \frac{1}{2\pi} \int_0^\infty dx [1-g(x)] \tag{20}$$

[recall that $\lim_{y\to\infty} g(y)=1$ by definition]. Assuming a Gaussian shape for the scaling function, $g(x)=1-e^{-\alpha x^2}$, leads to the simple relation

$$c_2 |c_v| = \frac{1}{4\pi} \approx 0.079\,58 \tag{21}$$

independent of the width α.

The main point of these considerations is that all amplitudes can be expressed in terms of only two model parameters, the spatial correlation function amplitude A and the KPZ coefficient λ. In the context of the KPZ equation (8), this implies that the parameters ν and D appear only in the combination D/ν. The nontrivial dynamic amplitudes (17) and (18) are governed by the single scaling parameter

$$\vartheta = A^2 |\lambda| . \tag{22}$$

In particular, the nth cumulant diverges as $(\vartheta t)^{n/3}$ in the transient regime, with a universal prefactor c_n.

It is instructive to rederive this result from a simple argument developed previously [7,29] to demonstrate the scaling relation $\zeta+z=2$. At a given time $t \ll L^{3/2}$ the interface is rough on all scales below the dynamic correlation length $\xi_\parallel(t)$. At smaller scales the height fluctuations are stationary, which implies that the asymptotic form (11) of the height-difference correlation function can be used to estimate the width as $\xi^2 \approx A \xi_\parallel$. We consider a typical interface fluctuation, which is a hump of width $\xi_\parallel$ and height ξ. It is readily shown [7] that such a hump widens, under the action of the nonlinear term in the KPZ equation (8), according to

$$\dot{\xi}_\parallel \approx |\lambda| (\xi/\xi_\parallel) \tag{23}$$

which leads to $\xi_\parallel \approx (A^{1/2}|\lambda| t)^{2/3}$ and $\xi \approx (A^2|\lambda| t)^{1/3}$. The same reasoning carries over to higher-dimensional interfaces, where the scaling exponents ζ and z are not known exactly. Defining the stationary amplitude A through $C_h(\mathbf{r}) = A|\mathbf{r}|^{2\zeta}$ we find $\xi_\parallel \approx (A^{1/2}|\lambda| t)^{1/z}$ with $z=2-\zeta$ and, using the scaling relation, $\xi \approx (A^{1/\zeta}|\lambda| t)^{\zeta/z}$. Hence the general expression for the scaling parameter is

$$\vartheta = A^{1/\zeta} |\lambda| . \tag{24}$$

We note, however, that the relation between A and the parameters in the KPZ equation is not as simple as (12) in higher dimensions. In particular, A is expected to depend on λ.

III. SINGLE-STEP MODELS

It is useful for our purposes to start out with a family of models for which the parameters A and λ can be obtained analytically. The nearest-neighbor height differences (step heights) $\sigma_x = h_{x+1} - h_x$, $x=1,\ldots,L$, in these models are restricted to the values $+1$ or -1, and hence can be conveniently thought of as "spins" [15,30]. Particles are added, $h_x \to h_x + 2$, at local minima where $(\sigma_{x-1}, \sigma_x) = (-1, 1)$, and the spins at sites $x-1$ and x are exchanged by the addition. The total magnetization is thus conserved by the dynamics. Periodic boundary conditions are used for the spins. Let $N = N_+ - N_-$ denote the excess number of $+$ spins, which is fixed by the initial configuration. The tilt of the interface is then $u = \langle \sigma_x \rangle = N/L$ and the height variables satisfy *helical* boundary conditions, $h_{L+1} = h_1 + N$. If the rate of adding particles is chosen to be equal at all eligible growth sites, it is straightforward to show [15] that all configurations with the prescribed value of N have the same weight in the steady state of the dynamics. This implies that

$$A = \langle \sigma_x^2 \rangle - \langle \sigma_x \rangle^2 = 1 - u^2 . \tag{25}$$

The density of growth sites is $(1-u^2)/4$ and, since the

addition of a particle increases the height by two, the inclination-dependent growth rate is given in units of the rate of particle addition by

$$v_\infty(u)=\tfrac{1}{2}(1-u^2) \tag{26}$$

so $\lambda=-1$ independent of u. Hence the simplest way to vary the scaling parameter ϑ is by tilting the surface.

Gates and Westcott [31] generalized the single-step model by allowing the growth rate at a given local minimum $(\sigma_{x-1},\sigma_x)=(-1,1)$ to depend on the neighboring spins σ_{x-2} and σ_{x+1}. Specifically, the rates corresponding to the various local spin configurations are given by

$$\begin{aligned} R(1,-1,1,-1)&=\min(1,e^{\beta}) \\ R(-1,-1,1,1)&=\min(1,e^{-\beta}) \\ R(-1,-1,1,-1)&=R(1,-1,1,1) \\ &=\tfrac{1}{2}[R(1,-1,1,-1) \\ &\quad +R(-1,-1,1,1)] . \end{aligned} \tag{27}$$

This choice of rates guarantees that the steady state of the spin system is the Gibbs state of the one-dimensional Ising model at reduced inverse temperature $|\beta|$ [31,32]. The Ising model is ferromagnetic for $\beta>0$ and antiferromagnetic for $\beta<0$. For large positive β the spins are strongly correlated and the interface consists of large stretches of constant slope, i.e., extended hills and valleys [Fig. 1(a)]. Similarly for large negative β the interaction makes the interface rather flat [Fig. 1(b)]. This is reflected in the simple result for the stationary correlation function amplitude at zero tilt [31]

$$A=e^{\beta/2} . \tag{28}$$

The growth rate at zero tilt is given by [31]

$$v_\infty=\frac{e^{-|\beta|/2}}{1+e^{\beta/2}} . \tag{29}$$

Using the Ising steady state the inclination dependence of both A and v_∞ can be worked out [33]. The resulting variation of λ with β is shown in Fig. 2. It should be noted that λ changes sign at $\beta=\beta_c=-2\ln(3)$. Similar behavior has been found in other growth models [34].

It is evident from Fig. 2 that the regimes of large positive and negative β are qualitatively different in the sense that $A\gg1\gg\lambda$ for $\beta\gg1$ while $A\ll1\ll\lambda$ for $\beta\ll-1$. On the other hand, the variation in the scaling parameter ϑ is rather modest for reasonable values of β. In the limit $\beta\to-\infty$ the dynamics reduces [31] to the polynuclear

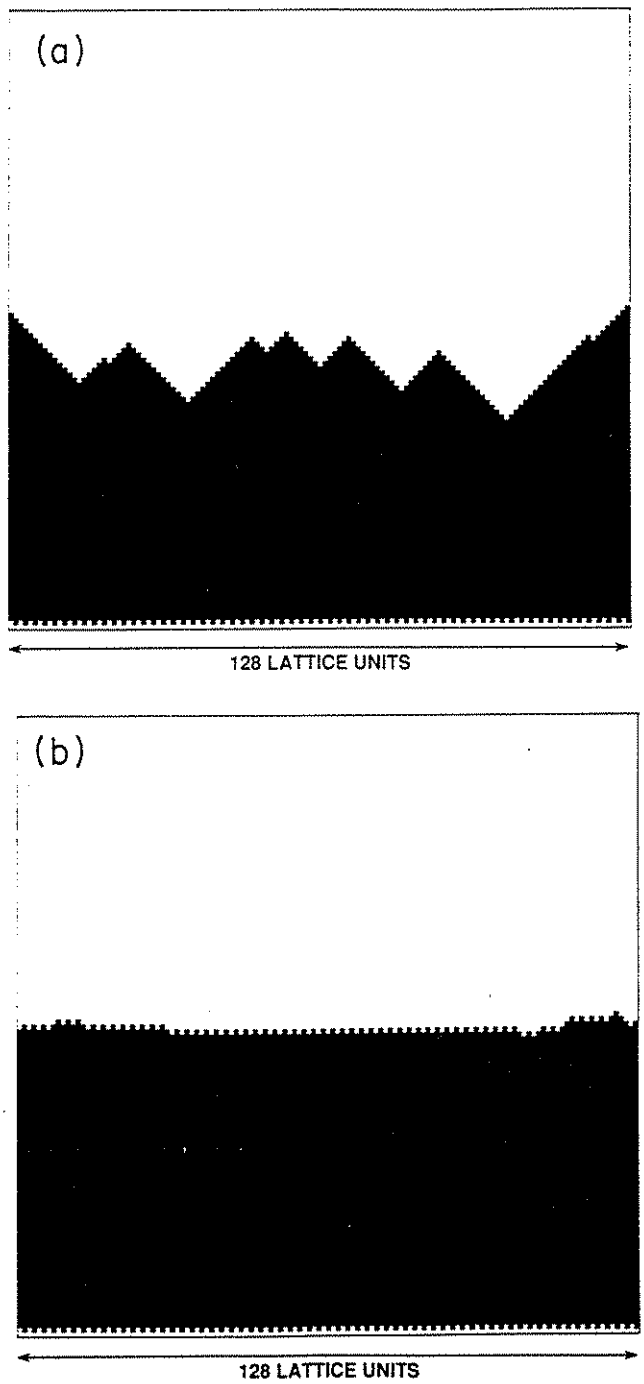

FIG. 1. Interface structures obtained from small-scale simulations carried out to illustrate the model of Gates and Westcott [31]. (a) The strongly ferromagnetic case ($\beta=4$) and (b) the strongly antiferromagnetic case ($\beta=-4$).

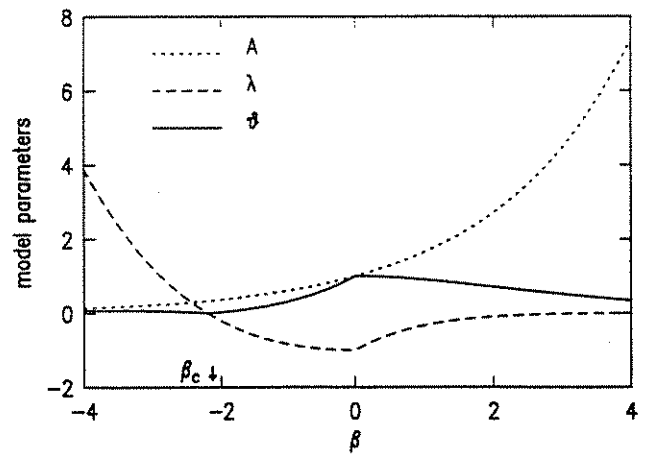

FIG. 2. Analytical results for the static correlation-function amplitude A, the KPZ coefficient λ and the scaling parameter $\vartheta=A^2|\lambda|$ of the Gates-Westcott model. The transition point β_c where λ goes through zero is indicated by an arrow.

growth (PNG) model [35], in which islands nucleate at a rate $p \approx e^{\beta} \ll 1$ and then grow sideways at unit speed. The regime of large negative β is therefore more efficiently accessed by directly simulating a discretized [36] PNG model. In the limit of small nucleation rate it can be shown [36] that $A = \sqrt{2p}$ and $\lambda = 1/\sqrt{2p}$, hence

$$\vartheta = \sqrt{2p} \ , \tag{30}$$

which can be made arbitrarily small. In practice, p is limited by the requirement that the average step spacing $l \approx 1/A$ remain small compared to the substrate size.

IV. NUMERICAL RESULTS FOR GROWTH MODELS

In addition to the models discussed in the preceding section, we have investigated the restricted solid-on-solid (RSOS) model of Kim and Kosterlitz [20], and square-lattice ballistic deposition with sticking at nearest-neighbor (NN), and nearest as well as next-nearest-neighbor (NNN) columns [15]. For these models A was determined numerically from the stationary height-difference correlation function (11), and λ was extracted from the stationary velocity-correction amplitude (14) using the numerically determined value of A, i.e., the scaling parameter (22) was defined through $\vartheta = 2A|b_v|$. Examples of the kind of data we have used are shown in Fig. 3. The results are summarized for future reference in Table I. We also include estimates of λ obtained by directly measuring the inclination dependence of the growth rate [25]. The value of A can alternatively be determined from the stationary width amplitude (13), which gives identical results within the statistical uncertainties.

These uncertainties vary substantially from model to model. Quite accurate values for A and λ, which are in excellent agreement with the analytical results presented in Sec. 3, can be obtained from the Gates-Westcott model for small values of β. For the RSOS model we estimate that the uncertainties in A and λ are less than $\pm 10\%$. For the NN and NNN ballistic deposition models it is much more difficult to approach the asymptotic ($t \to \infty, L \to \infty$) limit and the uncertainties are larger than $\pm 10\%$, even for simulations in which as many as 5×10^{10} particles are deposited.

There is a subtle time-scale effect involved in measuring the stationary velocity-correction amplitude for reaction limited models [25] (such as the single-step models and the RSOS model), which is discussed in the Appendix. In general, however, the choice of time scale (which is largely arbitrary for the models of interest here) does not affect the estimation of the amplitudes (3) and (6), as long as the choice is made consistently for *all* measurements on a given model. The reason is that time t appears in the combination λt in all observable quantities [cf. (17) and (18)]. Since λ is the second derivative of the growth rate with respect to inclination, cf. (15), any rescaling of time rescales the growth rate and hence λ as well, leaving λt invariant.

The cumulant amplitudes (3) were measured in simulations on very wide substrates (up to $L = 2^{21} = 2\,097\,152$) in order to avoid saturation effects. In some cases better scaling was achieved by using many (typically 200) independent runs on smaller substrates ($L = 10\,000$). The number of particles added during a simulation ranged from 2×10^9 for the PNG model up to 5×10^{10} for NNN ballistic deposition. We have taken care to only use data that were as far as possible within the asymptotic scaling region, since otherwise large uncertainties in the amplitudes result. In particular, this has prevented us from exploring the region close to the critical point $\beta = \beta_c$ of the Gates-Westcott model (cf. Sec. III), where λ vanishes and therefore the time required to reach the asymptotic regime diverges. An example of the data used to determine a_2 and a_3 is shown in Fig. 4(a). In determining the finite-size correction amplitude (6) we have used the fact that the asymptotic growth rate v_∞ is known exactly for the single-step models (cf. Sec. III). For the other models a_v is determined by adjusting the asymptotic growth rate v_∞ to optimize the expected scaling (5) of the correction [Fig. 4(c)]. Alternatively a linear fit of the time-averaged growth rate $\langle h \rangle / t$ versus $t^{-2/3}$ can be used [Fig. 4(b)].

Our results for the Gates-Westcott model are shown in Fig. 5. The second-cumulant amplitude was measured in

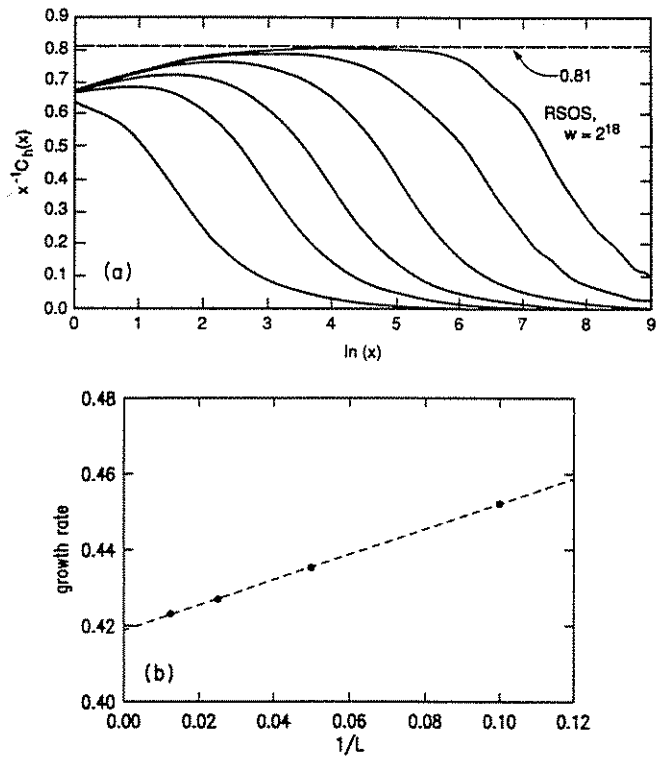

FIG. 3. Measurement of the static amplitude A and the coefficient λ for the restricted solid-on-solid model [20] with a maximal nearest-neighbor height difference of unity. (a) The determination of A from the height-difference correlation function $C_h(x)$ defined in Eq. (11), on a substrate of size $2^{18} = 262\,144$. The asymptotic behavior $C_h \sim x$ has been divided out. The correlation function is shown at six stages during the deposition process. The dashed horizontal line indicates the value estimated for A. (b) The stationary growth rate as a function of the inverse system size. The dashed line indicates a linear least-squares fit to the data, the slope of which yields our estimate for $b_v = -A\lambda/2$. Each data point corresponds to between 2×10^7 and 2×10^8 attempted depositions.

TABLE I. Numerical estimates of model parameters. A was determined from the stationary height-difference correlation function, $\lambda^{(1)}$ is an estimate using the stationary growth-rate correction amplitude, and $\lambda^{(2)}$ was obtained from the inclination dependence of the growth rate. v_∞ is the asymptotic growth rate at zero tilt, in units of one (attempted) deposition per substrate site.

Model	v_∞	A	$\lambda^{(1)}$	$\lambda^{(2)}$	ϑ
Restricted SOS	0.419	0.81	−0.81	−0.75	0.53
NN ballistic deposition	2.14	2.46	1.54	1.30	9.37
NNN ballistic deposition	4.06	6.76	1.21	1.36	55.4

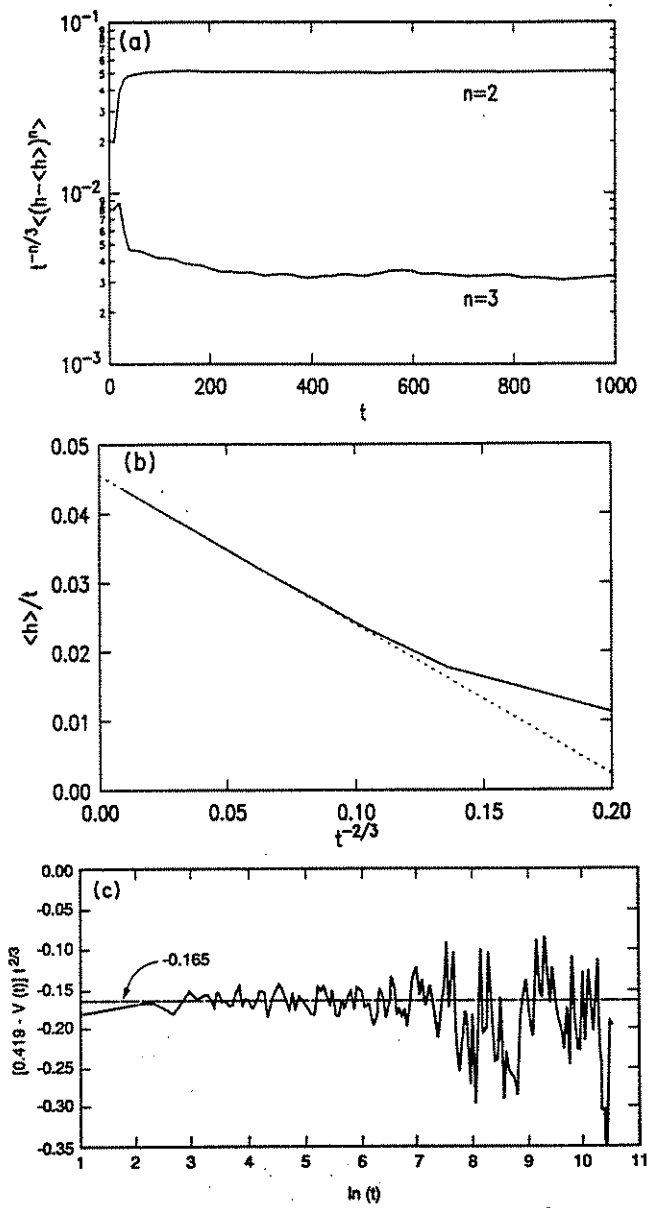

FIG. 4. Examples of simulation data used to estimate transient amplitudes. (a) Results for the second and third height fluctuation cumulant of the discrete time PNG model [36] with a nucleation probability of $p=0.001$. The predicted time dependence has been divided out. The data were obtained by averaging over 250 independent runs on a lattice of size 10 000. (b) The integrated growth rate $\langle h \rangle / t$ vs $1/t^{2/3}$, obtained from the same set of simulations. The dotted line indicates a linear least-squares fit used to estimate the amplitude a_v. (c) The momentary growth rate for the restricted solid-on-solid model on a lattice of size 2^{18}. The asymptotic growth rate v_∞ is adjusted to optimize the $t^{-2/3}$ scaling of the correction, and the estimate $a_v \approx 0.165$ is indicated by the dashed line.

the range $-4 \le \beta \le 4$, while reliable estimates for the correction amplitude a_v could be obtained only for $-1 \le \beta \le 1.5$. Figure 6 summarizes all our simulation results for c_2. We find strong evidence for universality over almost four decades in the scaling parameter $\vartheta = A^2|\lambda|$, and we estimate

$$c_2 = 0.404 \pm 0.013 \ . \tag{31}$$

Figure 7 shows the actually measured values of a_2, $|a_3|$, and $|a_v|$ in a log-log plot to demonstrate the scaling with θ predicted by (17) and (18). From the data shown we estimate

$$|c_v| = 0.193 \pm 0.013 \tag{32}$$

yielding $c_2|c_v| \approx 0.077$ in close, but possibly fortuitous, agreement with the approximate relation (21). The sign of c_3 is observed to be *equal* to the sign of λ in all cases, and the magnitude is

$$|c_3| = 0.071 \pm 0.005 \ . \tag{33}$$

Finally we quote an estimate of the fourth-cumulant amplitude obtained from a simulation of the single-step model at zero tilt,

$$c_4 = 0.02 \pm 0.002 \ . \tag{34}$$

Since $\lambda < 0$ for the single-step model, this implies that the sign of c_4 is the *opposite* of the sign of λ in general.

A useful measure of the asymmetry of the height fluctuation distribution is the *skewness* [37,38]

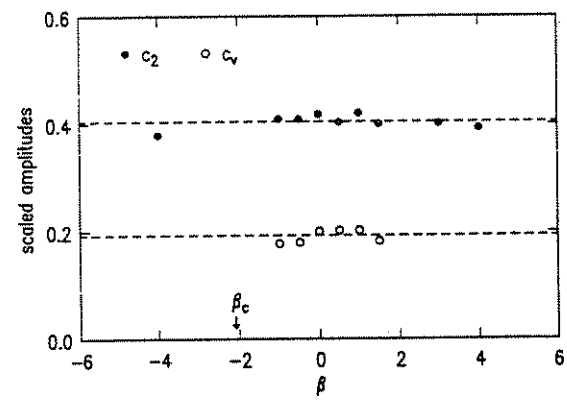

FIG. 5. Numerical results for the reduced amplitudes c_2 and c_v obtained from simulations of the Gates-Westcott model at various values of β. The dashed lines indicate our best estimates for the amplitudes, obtained by averaging the results from all models. We have not included data from the neighborhood of the transition point β_c due to the strong crossover effects observed there.

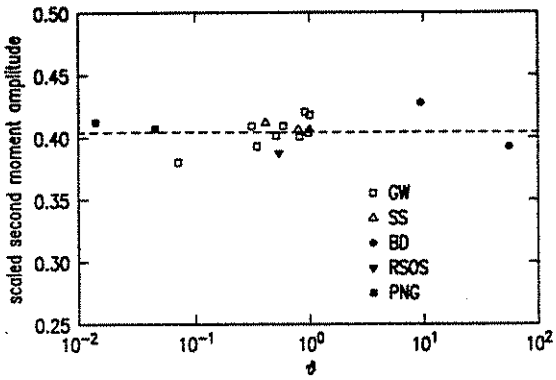

FIG. 6. Numerical results for the reduced amplitude of the second cumulant, obtained from simulations of the Gates-Westcott (GW) model, the single-step model at various values of the tilt u (SS), two versions [15] of ballistic deposition (BD), the restricted solid-on-solid model with unit maximal height difference (RSOS), and the discrete time PNG model with nucleation probability $p=0.001$ and 0.0001 (PNG). The dashed line is our best estimate for c_2.

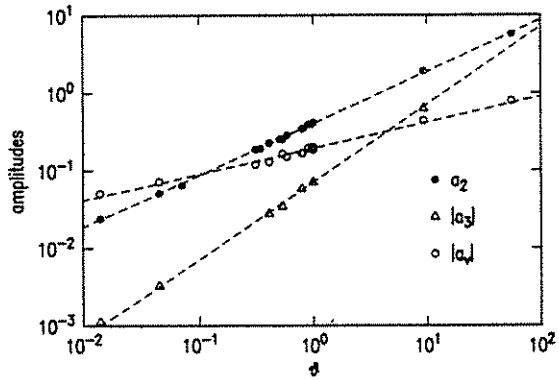

FIG. 7. Summary of numerical estimates for the cumulant amplitudes a_2 and $|a_3|$, and the finite-size correction amplitude $|a_v|$, plotted as a function of $\vartheta=A^2|\lambda|$. The dashed lines indicate the predicted power laws $a_n=c_n\vartheta^{n/3}$, $a_v=c_v\vartheta^{1/3}$ with our best values for c_n and c_v.

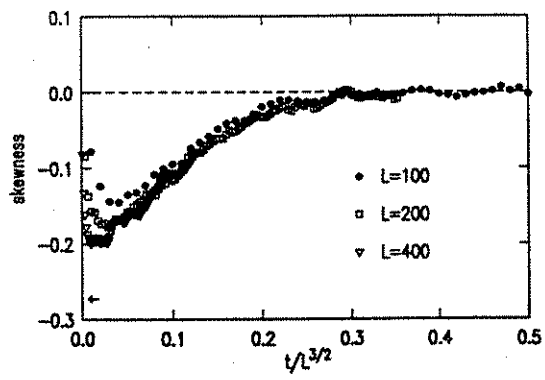

FIG. 8. Skewness of the height fluctuation distribution in the single-step model for small system sizes. The data constitute an average over 10 000 independent runs. The arrow indicates the value of the skewness in the limit $L\to\infty$.

$$s=\frac{\langle (h-\langle h\rangle)^3\rangle}{\langle (h-\langle h\rangle)^2\rangle^{3/2}} \tag{35}$$

which we estimate from (31) and (33) to take the value

$$|s|=0.28\pm0.04 \tag{36}$$

in the transient regime. We noted in Sec. II that the height fluctuations are Gaussian in the stationary regime, and hence the skewness (as well as all higher cumulants) is expected to vanish for $t\gg L^{3/2}$. It is then natural to conjecture a scaling form

$$s(t,L)=f_s(t/L^{3/2}) , \tag{37}$$

where $|f_s(0)|$ is given by (36) and $\lim_{y\to\infty}f_s(y)=0$. Similar behavior was found previously in a deterministic growth model [38]. In Fig. 8 we show numerical data for the skewness in small systems. In spite of severe finite-size effects which prevent the skewness from reaching the predicted short-time maximum value (36), there is clear indication of the dynamic-scaling form (37).

V. DIRECTED POLYMER AMPLITUDES

Closely related to the dynamic scaling properties of the stochastic-growth models discussed above are the equilibrium statistical mechanics features of finite-temperature directed polymers in random media (DPRM) [1,8]. In its discrete realization [39] for one transverse dimension ($d=1$), which we have used in the numerical simulations discussed below, the finite temperature DPRM involves a directed walk that commences at the origin of a square lattice and proceeds upwards into the half plane $t>0$, one step at a time. The vertical bonds have uncorrelated random energies $\mu(x,t)$ drawn from a uniform distribution of width Δ and variance $\sigma^2=\Delta^2/12$, while the horizontal bonds have a fixed energy cost E_0, with associated Boltzmann weight $\gamma=e^{-E_0}$ (both E_0 and μ are measured in units of kT). Consequently, a transverse step to the left or right to take advantage of a particularly favorable vertical random bond incurs a penalty $\gamma<1$. For reasons of numerical convenience, we operate under the assumption that the temperature, though finite, is relatively low so that only single steps are allowed. The transfer-matrix method permits us to investigate numerically the full partition function of the DPRM by calculating recursively the Boltzmann weight $Z(x,t)$ of paths running from the origin to the point (x,t) in the time slice t,

$$Z(x,t+1)=e^{-\mu(x,t)}[Z(x,t)+\gamma Z(x-1,t)+\gamma Z(x+1,t)] \tag{38}$$

assuming the initial condition $Z(x,0)=\delta_{x,0}$. The full partition function $Z(t)$ is then obtained by summing over x,

$$Z(t)=\sum_x Z(x,t) . \tag{39}$$

The quantities of immediate physical interest are the geometric and free-energy fluctuations. The former concern the disorder-induced transverse fluctuations exhibited by the directed paths as they meander through the

random energy landscape. These fluctuations are characterized by the wandering exponent [14] ζ_{DP}, through the relation

$$\langle x^2(t)\rangle^{1/2} \sim t^{\zeta_{DP}} . \tag{40}$$

Our convention here is that thermal averages with respect to the Boltzmann weights are implicit and done first, while angular brackets denote disorder averages taken over many realizations of randomness. It is well established [9,19] that $\zeta_{DP}=\frac{2}{3}$ for the case of one transverse dimension. The free-energy fluctuations, given by the disorder average of $\mathcal{F}=-\ln Z$, scale with a different exponent,

$$\langle [\mathcal{F}(t)-\langle \mathcal{F}(t)\rangle]^2\rangle^{1/2} \sim t^{\omega} , \tag{41}$$

where it is known [8,16,40] that $\omega=2\zeta_{DP}-1$. The rms fluctuations (40) and (41) were first studied numerically by Huse and Henley [40], as well as Kardar [39]. Recent work by Halpin-Healy [42] has addressed the much broader question of the full geometric and free-energy probability distributions responsible for these and higher moments. A surprising feature of this recent work was the uncovering of an asymmetric free-energy distribution [43] that underlies the unique third-cumulant scaling associated with the $d=1$ DPRM. Predicted by Kardar [9] and observed by Halpin-Healy [42], this third-cumulant scaling lies at the heart of the matter, fixing the free-energy fluctuation exponent at $\omega=\frac{1}{3}$. In an effort to test the predictions made by Kardar [9] and more recently by Bouchaud and Orland [41] (BO), to be discussed in detail in Sec. VII, and to explore issues of amplitude universality, we have performed a series of finite-temperature simulations for various values of γ and Δ, studying paths of length 500 steps and typically averaging over 10^4 realizations of the random-energy landscape.

In contrast to the discrete microscopic model just delineated, the continuum formulation of the DPRM centers on the path-integral statement of the partition function,

$$Z(x,t)=\int_{y(0)=0}^{y(t)=x}\mathcal{D}y(s)\exp\left[-\int_0^t ds\left[\frac{1}{4\Gamma}\dot{y}^2 - \mathcal{V}(y(s),s)\right]\right] , \tag{42}$$

where one sums explicitly over all directed paths emanating from the origin and ending at the point (x,t). The pinning potential $\mathcal{V}$ has zero mean and variance

$$\langle \mathcal{V}(x,t)\mathcal{V}(x',t')\rangle = V^2\delta(x-x')\delta(t-t') . \tag{43}$$

Here Γ is a macroscopic diffusion constant and V^2 measures the strength of the quenched randomness. In a sense to be made clear below, these parameters are renormalized versions of γ and σ^2, respectively. The partial unraveling of the precise relationship between these renormalized and microscopic parameters was a secondary interest of the present work. To establish the connection to the KPZ equation, recall that the restricted partition function $Z(x,t)$ obeys a Euclidean-time Schrödinger equation with a time-dependent random potential $\mathcal{V}$. A simple substitution [1,19] then reveals that it is the restricted free energy $F(x,t)=-\ln Z(x,t)$ that satisfies the KPZ equation (8), with the parameters

$$\nu=\Gamma , \quad \lambda=-2\Gamma , \quad D=V^2 , \tag{44}$$

and the exponents defined in (40) and (41) are related to those of the interface (cf. Sec. I) by $\zeta_{DP}=1/z$, $\omega=\zeta/z$. Note that the sign of λ is fixed to be *negative* for the DPRM. The central scaling parameter (22) is given by

$$\vartheta=\frac{V^4}{2\Gamma} , \tag{45}$$

a result derived by BO directly from the partition function (42).

The major difference between the height $h(x,t)$ of the growing interfaces discussed in the preceding sections and the restricted free energy $F(x,t)$ lies in the initial condition $Z(x,0)=\delta(x)$ for the DPRM, which corresponds to a deep narrow groove in the interface [44]. Conversely, the substrate initial condition $h(x,0)=0$ corresponds, in the context of the DPRM, to an ensemble of paths emanating from *all* points x rather than just from the origin [45]. Let $\tilde{Z}(x,t)=\exp[-h(x,t)]$ denote the restricted partition function for the DPRM with substrate initial condition. $\tilde{Z}(x,t)$ gives the total weight of all paths with end point (x,t) and *arbitrary* starting point. Clearly this quantity is identical, in a statistical sense, to the weight of all paths with arbitrary end points and fixed origin, i.e., the full partition function $\tilde{Z}(t)$ [Eq. (39)]. Hence we conclude that the height fluctuations studied earlier in this paper should correspond *quantitatively* to the fluctuations of the full free energy $\mathcal{F}$ of the DPRM [46]. In particular, we expect a finite-size correction to the average free energy per unit length (cf. Sec. II)

$$\langle \mathcal{F}(t)\rangle/t = f_0 + \frac{3c_v\vartheta^{1/3}}{t^{2/3}} \tag{46}$$

with $c_v>0$. A similar correction, however with the opposite sign, was derived by BO [41,47].

The difficulty that forces itself upon the simulator desiring to test the concept of amplitude universality in the DPRM concerns the "correct" values of V^2 and Γ to substitute into (45). BO were, of course, aware of this subtlety, but they assumed a very simple relationship between these renormalized quantities and the microscopic input parameters of the numerical simulation, viz., $\Gamma=\gamma/3$ and $V^2=\sigma^2$, which gave, rather fortuitously in retrospect, very heartening results for some early simulations. Nevertheless, it is clear that such an assumption, though perhaps natural, is unlikely to be correct—a fact that is made apparent in the more extensive simulations that we have done.

The *proper* extrication of the renormalized diffusion constant Γ and disorder strength V^2 necessitates numeri-

cal scrutiny of the logarithm of the positional probability distribution

$$P(x,t)=\frac{Z(x,t)}{Z(t)} . \tag{47}$$

As pointed out by Parisi [48], and then by BO, this distribution has the properties that

$$\langle \ln[P(x,t)/P(0,t)] \rangle = -\frac{x^2}{4\Gamma t} \tag{48}$$

and

$$\langle \{\ln[P(x,t)/P(0,t)]\}^2 \rangle - \langle \ln[P(x,t)/P(0,t)] \rangle^2 = \frac{V^2}{2\Gamma}|x| . \tag{49}$$

In fact, these relations follow rather naturally from the mapping to the KPZ equation. Recall that $\ln[P(x,t)/P(0,t)]=-[F(x,t)-F(0,t)]$, where the restricted free energy F can be viewed as an interface evolving according to (8). The "groove" initial condition $P(x,t)=\delta(x)$ evolves, under the action of (8) with a *negative* value of λ, into a parabola given precisely by (48) [50]. Moreover, since $F(x,t)-F(0,t)$ is constrained to vanish at $x=0$, its fluctuations increase linearly with x, as predicted by the KPZ height-difference correlation function (11) [note that $V^2/2\Gamma=D/2\nu=A$ according to (44)]. It is also clear from the scaling properties of the interface [2] that the linear increase of (49) only persists on length scales less than the dynamic correlation length, $x \ll t^{2/3}$, a fact that was noticed numerically by Mézard [49], who has already provided qualitative confirmation of relations (48) and (49). Here we will rely upon them in a *quantitative* sense to determine the macroscopic parameters of the continuum model.

Consider, for example, the finite-temperature DPRM numerical experiment that we performed with input microscopic parameters $\gamma=0.1, \sigma^2=0.833$. In Fig. 9, we collect the plots which allow us to ascertain the renormalized quantities Γ and V^2, the latter being the more stubborn of the two to pin down precisely. Figure 9(a) shows data collapse to a parabola for the time slices $t=100$, 200, and 500, as expected, where we have used the scaled variable $x/2t^{1/2}$ as the abscissa. With this choice, it is a simple matter to bracket the collapsed data by appropriately scaled curves. The inner parabola corresponds to a value of $\Gamma=0.09$, while the outer has 0.10. Thus, we estimate $\Gamma(\gamma=0.1,\sigma^2=0.833)=0.095\pm0.005$, in rather strong disagreement with the BO assumption that $\Gamma=\gamma/3$. In fact, our simulations show a distinct dependence of Γ on σ^2 at fixed γ (cf. Table II), indicating that no such simple proportionality holds. Figure 9(b) examines the second moment for the same three time slices. From Eq. (49) we see that the anticipated behavior is that of the absolute-value function. For values of x that are not too large, the data conform to this notion, and the tangent line yields the slope $A=3.0$, so that $V^2=2\Gamma A\approx 0.57$. With the renormalized parameters thus determined for our particular simulation, we find that the scaling parameter has the value $\vartheta=V^4/2\Gamma\approx 1.71$. This number in hand, we can now discuss properly the issue of free-energy amplitude universality in the one-dimensional DPRM.

In Fig. 10, we plot $\langle \mathcal{F} \rangle/t$ versus $t^{-2/3}$, which shows the effects of finite size upon the free energy per unit length, cf. Eq. (46). In the thermodynamic limit we observe $f_0=-0.49$ for $\gamma=0.1$ and $\sigma^2=0.833$. Kardar [9] has invoked the replica trick to compute the quenched averaged free energy from the continuum partition function (42). He finds

$$f_0=\langle \mu \rangle - 2\Gamma - \frac{V^2}{2}+\frac{V^4}{48\Gamma} , \tag{50}$$

leading to $f_0\approx -0.40$ for the case of Fig. 10. A look at the results for other parameter values collected in Table II reveals no correlation between the numerical estimates for f_0 and the formula (50). This is not entirely surprising, as the replica calculation involves [41,48,49] renormalizing the free energy by a cutoff-dependent, additive constant which arises from the self-interaction of replicas. While f_0, therefore, does not carry any universal information, the data shown in Table II do provide some insight into its general parameter dependence.

Returning to Fig. 10, we note that the free energy approaches its thermodynamic limit from *above*, consistent with the fact that $\lambda<0$ in the equivalent KPZ equation but in disagreement with the prediction of BO. The drawn tangent has slope 0.60 ± 0.01, providing us with an estimate of the amplitude of the finite-size correction. Similar data collected in Table II reveal that this amplitude is universal for a broad range of microscopic input parameters (ϑ varies from 0.17 to 179), with a value which we estimate to be

$$c_v^{\mathrm{DP}}=0.180\pm0.014 \tag{51}$$

in rather nice agreement with the numerical value (32) obtained from the growth-model simulations.

Figure 11 monitors the behavior of the amplitudes of the second and third cumulants of the free energy as a function of path length for the numerical simulation discussed above, with $\gamma=0.1$ and $\sigma^2=0.833$. As is evident from the figure, the quality of the data is such that it is possible to estimate these coefficients with rather high precision. For example, we find that asymptotically $\langle (\mathcal{F}-\langle \mathcal{F} \rangle)^2 \rangle / t^{2/3}=0.581\pm0.002$. Since this amplitude is to be identified with $a_2=\vartheta^{2/3}c_2$, while $\vartheta\approx 1.71$, we have $c_2\approx 0.406$ for this particular set of microscopic input parameters. A glance at Table II shows that runs made for other values of γ and σ^2 yield values consistent with these, leading us to estimate

$$c_2^{\mathrm{DP}}=0.400\pm0.057 \tag{52}$$

for the universal amplitude of the second cumulant, in

TABLE II. Numerical results from finite-temperature DPRM simulations. See text for explanations.

γ	σ^2	Γ	V^2	ϑ	f_0	c_v	c_2	s
0.0125	0.833	0.026	0.395	3.00	−0.27	0.20	0.50	−0.32
	3.33	0.046	1.84	36.8	−0.94	0.17	0.35	−0.29
	8.93	0.053	2.86	77.2	−1.60	0.18	0.37	−0.32
	13.33	0.056	4.48	179	−2.68	0.19	0.35	−0.28
0.1	0.208	0.086	0.17	0.168	−0.28	0.16	0.45	−0.27
	0.833	0.095	0.57	1.71	−0.49	0.17	0.41	−0.33
	3.33	0.105	1.68	13.44	−1.16	0.19	0.37	−0.26

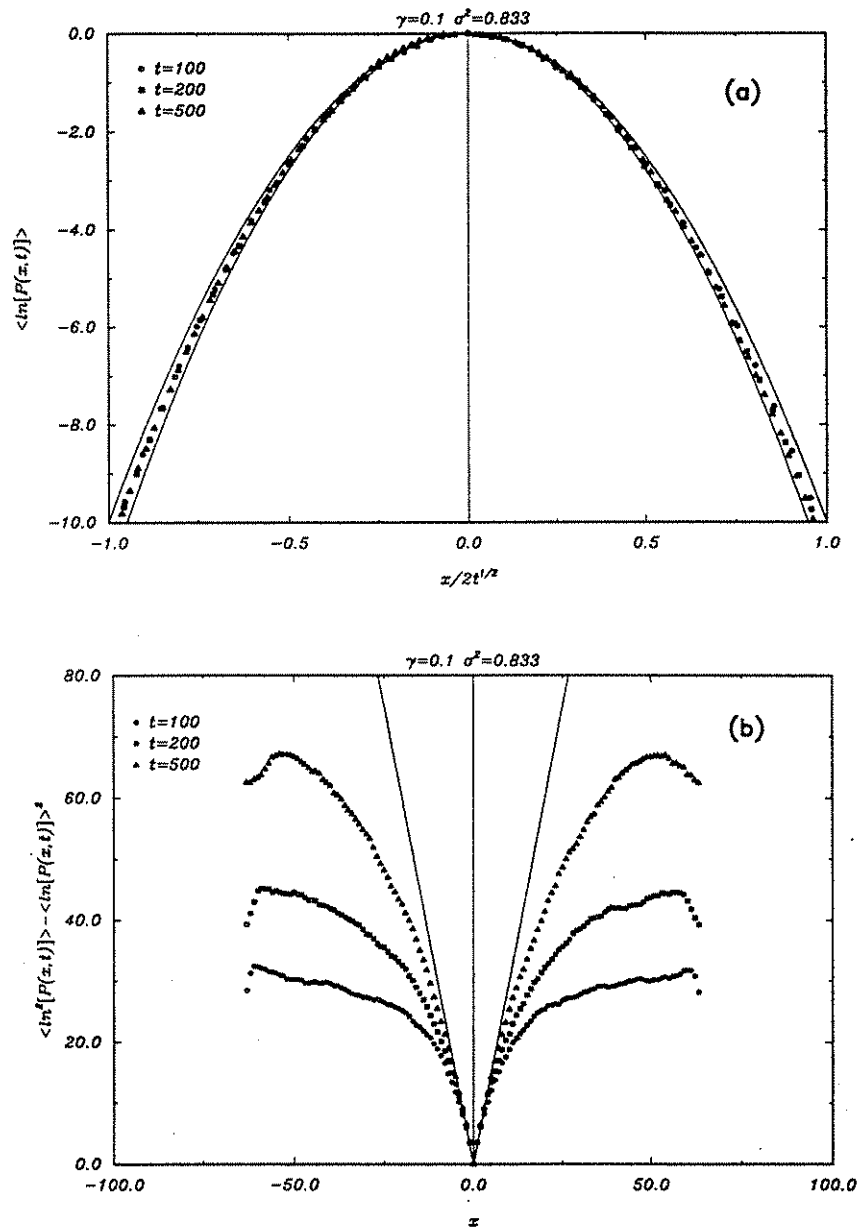

FIG. 9. (a) Disorder average of the logarithm of the spatial probability distribution $P(x,t)$ for the DPRM in $d=1$ (500 steps, 10^4 realizations of the random-energy landscape) with microscopic parameters $\gamma=0.1$ and $\sigma^2=0.833$; data collapse for the three time slices $t=100$, 200, and 500. The inner parabola corresponds to $\Gamma=0.090$, while the outer has $\Gamma=0.10$. We estimate $\Gamma(\gamma=0.1,\sigma^2=0.833)=0.095\pm0.005$. (b) Second cumulant of $\ln P(x,t)$ for the same time slices. The solid line corresponds to the function $3|x|$, which implies $A=3.0$, so that $V^2=0.57$. Together, the figures permit us to estimate $\vartheta=(V^4/2\Gamma)\approx1.71$ for the given microscopic input parameters.

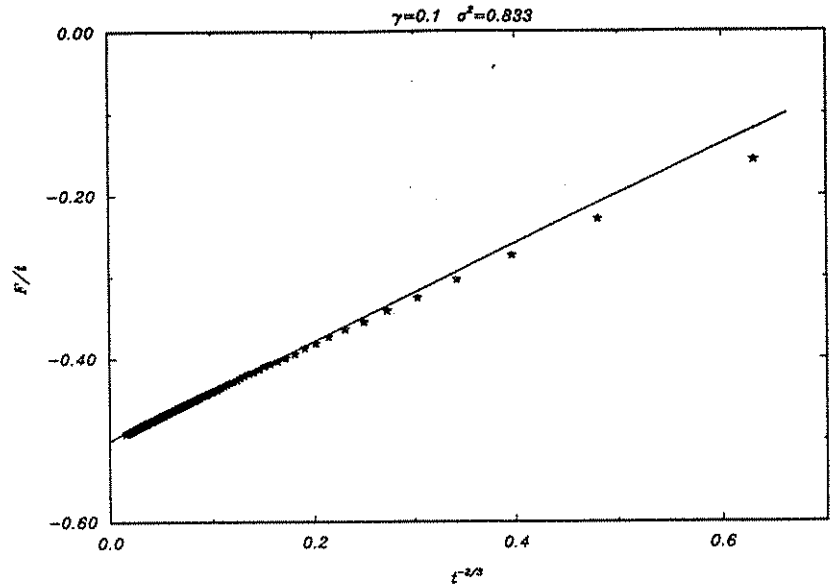

FIG. 10. Finite-size correction to the free energy per unit length of the one-dimensional DPRM vanishes as $t^{-2/3}$. The slope of the asymptotic tangent line is our estimate of the *finite-size effect* amplitude a_v for the particular simulation done here, with $\gamma=0.1$ and $\sigma^2=0.833$.

good agreement with the growth-model result (31).

Returning to Fig. 11, we note that the third cumulant is negative, in accord with the general relation between the sign of c_3 and the sign of the KPZ coefficient λ found for the growth models. The data for the third cumulant are a bit noisier than for the second. Nevertheless, we find that for large t, $\langle(\mathcal{F}-\langle\mathcal{F}\rangle)^3\rangle/t\approx-0.145\pm0.005$, which yields the estimates $c_3\approx-0.085$ and $s\approx-0.33$ for the skewness (35) of the free-energy probability distribution. In the final column of Table II, we collect our results for this skewness parameter. Figure 12 actually illustrates the behavior of this quantity as a function of path length for these runs as well as some additional ones that we made for the express purpose of pinning down s. Overall, our estimate for the skewness is

$$s^{\mathrm{DP}}=-0.296\pm0.028\ . \tag{53}$$

We have also included in Fig. 12 data for a typical zero-temperature simulation of the DPRM, which exhibits a skewness of similar magnitude in the distribution of the ground-state energy.

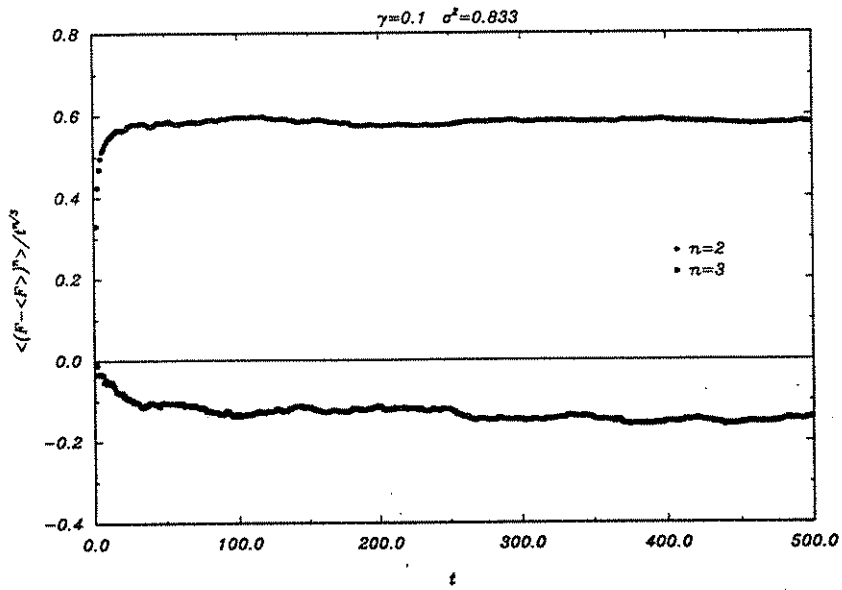

FIG. 11. Amplitudes of the second- and third-order cumulants of the free energy as a function of path length for the DPRM. Same microscopic input parameters as in previous figures. Asymptotically, $\langle(\mathcal{F}-\langle\mathcal{F}\rangle)^2\rangle/t^{2/3}$ goes to 0.581 ± 0.002, which is our estimate for a_2. Dividing by $\vartheta^{2/3}$ gives ≈0.406, which is our estimate for the *second-cumulant* universal amplitude c_2. Note that the third-order cumulant has a smaller amplitude, with $\langle(\mathcal{F}-\langle\mathcal{F}\rangle)^3\rangle/t$ approaching -0.145 ± 0.005 for large times. The relative sizes of the cumulants provide a measure for the skewness of the free-energy probability distribution.

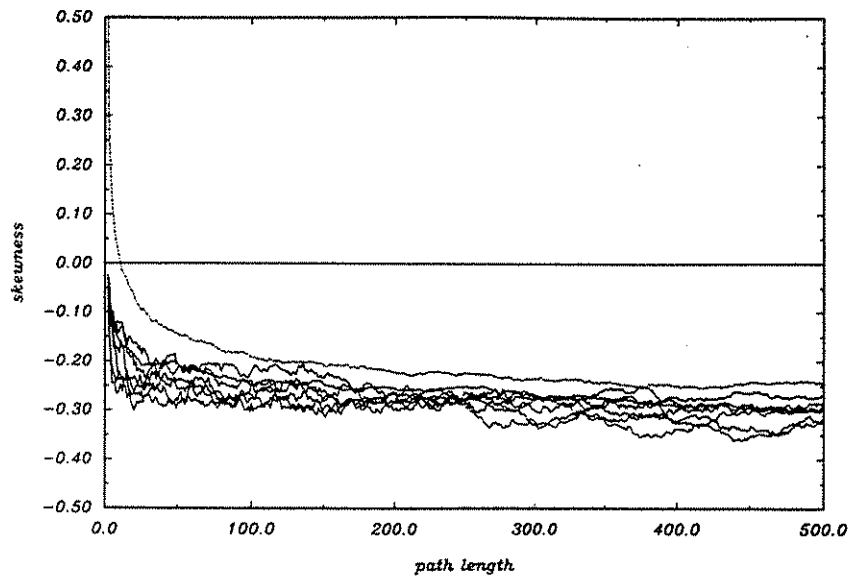

FIG. 12. *Skewness* of the free-energy probability distribution for the finite-temperature DPRM as measured by the parameter $s=\langle(\mathcal{F}-\langle\mathcal{F}\rangle)^3\rangle/\langle(\mathcal{F}-\langle\mathcal{F}\rangle)^2\rangle^{3/2}$, for simulations done with various values of γ and σ^2. We estimate $s=-0.296\pm0.028$. The uppermost curve, which is dot-dashed, shows data for the zero-temperature version of the model [8].

VI. DYNAMIC CORRELATIONS IN THE STEADY STATE

The nontrivial scaling properties of the KPZ equation (8) manifest themselves both in the roughening of an initially flat interface and in the dynamic correlations of an interface with fully developed roughness which has been growing for a time $t \gg L^z$. This latter case has received much less attention, mainly due to the numerical difficulties associated with reaching the stationary regime for large systems; it may also be of somewhat questionable physical relevance. However, the dynamic correlations in the stationary state are more easily accessible to analytic approaches starting from (8) than transient correlations involving the flat initial state, and some nontrivial amplitudes can be predicted by mode-coupling and renormalization-group calculations [27,28,51]. We have therefore performed simulations of stationary interfaces using the single-step model [15,30], where the generation of stationary configurations is trivial: Indeed, since the height differences are independent in the stationary state it is sufficient to randomly distribute spins $\sigma_i=\pm1$ on the lattice such that the total magnetization takes on a prescribed value (cf. Sec. III). There is no need to actually simulate the relaxation into the steady state.

The objects of interest are height fluctuation cumulants of the form

$$C_n(t)=\lim_{s\to\infty}\langle[h(x,t+s)-h(x,s) -\langle h(x,t+s)-h(x,s)\rangle]^n\rangle_c \tag{54}$$

and in particular their reduced amplitudes

$$\bar{c}_n=\lim_{t\to\infty}\lim_{L\to\infty}(A^2|\lambda|t)^{-n/3}C_n(t)\ , \tag{55}$$

cf. (3) and (17). Obviously, the growth-rate corrections (5) are absent here. We have determined $\bar{c}_2$ and $\bar{\zeta}_3$ from 200 runs in which a single-step interface of length $L=10\,000$, at zero tilt, was grown for 1000 time steps, and we estimate

$$\bar{c}_2=0.712\pm0.003 \tag{56}$$

and

$$\bar{c}_3=-0.199\pm0.004 \tag{57}$$

(recall that $\lambda=-1$ for this model). The skewness of the distribution is thus close to the value found in the transient case, $|s|\approx0.33$. The fact that $\bar{c}_2>c_2$ is easily understood: The stationary average includes fluctuations in the initial conditions in addition to those generated in the growth process, and therefore the distribution of height fluctuations is expected to be broader. For the linearized KPZ equation a simple calculation shows that the ratio of the stationary to the transient amplitude equals $\sqrt{2}$.

The presence of fluctuations in the initial conditions has dramatic consequences if the interface is tilted. The gradient expansion of the inclination-dependent growth rate $v_\infty(u)$ leading to the KPZ equation (8) gives, in general, a linear term $v'_\infty(u)\nabla h$ where $v'_\infty(u)=-u$ for the single-step model. This term causes slope fluctuations to drift laterally along the interface. It is irrelevant, and therefore commonly transformed away, in the transient situation, but in the stationary case the drift allows the initial fluctuations to completely swamp those generated by the growth process [52]. As a consequence the second moment grows *linearly* in time,

$$C_2(t)=|v'_\infty|At+\mathcal{O}(t^{2/3}) \tag{58}$$

and the nontrivial scaling behavior appears only as a subleading correction. The leading behavior of (58) in fact does not depend on the presence of the nonlinearity in the KPZ equation (note that the amplitude is indepen-

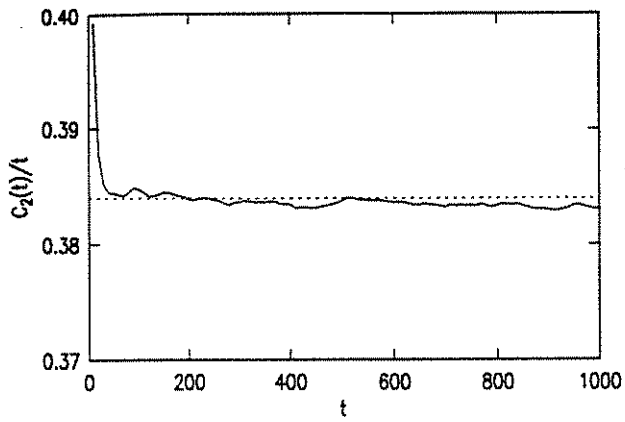

FIG. 13. Height fluctuations in the stationary state for the single-step model on an inclined substrate. The squared fluctuations increase *linearly* in time. The system size was $L=100\,000$, the tilt $u=0.6$, and the data are an average over 20 runs. The dotted line is the prediction (58) for the prefactor.

dent of λ), and can easily be derived from the linearized theory. We have checked the prediction (58) in a simulation at $u=0.6$ (Fig. 13).

VII. DISCUSSION AND CONCLUSION

The central result of this paper is the demonstration of amplitude universality for a large class of stochastic models of interface growth and directed polymers in random media. We reemphasize that the same values of the appropriately normalized amplitudes where found for *all* models we investigated. In this last section we summarize the current state of affairs regarding quantitative predictions of these amplitudes. Before doing so we discuss related numerical work on the subject.

In a study of crossover behavior in kinetic roughening, Guo, Grossmann, and Grant (GGG) [53] measured the λ dependence of the width prefactor, a_2, for a discretized version of the KPZ equation. They found $a_2 \sim \lambda^{0.46\pm0.04}$ in contrast with the scaling result $a_2 \sim \lambda^{2/3}$. Our results, displayed in Fig. 7, clearly support the scaling prediction (17). For comparison it should be noted that GGG varied λ by a factor of 2, while our work covers four orders of magnitude in the scaling parameter. Moreover, GGG used the bare value of λ, neglecting a possible renormalization due to the discretization scheme. Hence we expect that subsequent studies of the discretized KPZ equation will find agreement with our results.

Several very recent papers address questions concerning the probability distribution of height fluctuations, or free-energy fluctuations for the directed polymer [42,54–56]. Havlin *et al.* [54] presented numerical results for height fluctuations in ballistic deposition, and claimed the scaled distribution to be Gaussian *both* in the stationary ($t \gg L^z$) and the transient ($t \ll L^z$) regime. It is clear from our work that this can be true only in an approximate sense, for the simple reason that the transient distribution is skewed, as was observed by Halpin-Healy [42] and previously noted by Nattermann and Renz [43]. Kim, Moore, and Bray [55] studied the distribution of the ground-state energy in a zero-temperature directed-polymer simulation. They estimate the skewness $s=-0.29\pm0.02$ and the ratio $c_4/c_2^2 \approx 0.16$, both in good agreement with our estimates. Amar and Family [56] obtained $c_2=0.45\pm0.05$ from simulations of various growth models and $c_2 \approx 0.37$ from a numerical solution of the KPZ equation, both consistent with our results. They also estimated the static amplitude ratio $b_v/(\lambda b_2)=6.5\pm0.2$, in reasonable agreement with the exact value $b_v/(\lambda b_2)=6$ [cf. (13) and (14)].

Summarizing these remarks, we conclude that a coherent picture appears to be emerging on the numerical side. The theoretical situation is much less clear. In the context of the KPZ theory of kinetic roughening the only analytic amplitude predictions were made for the steady-state dynamic correlations discussed in Sec. VI [57]. Van Beijeren, Kutner, and Spohn (BKS) [27] derived a self-consistent integro-differential equation for the two-point correlation function within the mode-coupling approximation. Assuming a Gaussian shape for the universal scaling function, this leads to the prediction [36,29] $\bar{c}_2=\sqrt{2/\pi w}^{-1}$, where w is the width of the Gaussian. A self-consistent determination of w gives $\bar{c}_2=0.686$, while a perturbative calculation of the scaling function for small arguments [28] gives $\bar{c}_2=0.74\pm0.01$, both rather close to our numerical estimate (56) [58]. Very recently Hwa and Frey [51] have argued that the BKS equation is an *exact* consequence of the dynamic renormalization group. They solved the equation numerically and obtained the estimate $\bar{c}_2=0.69\pm0.01$, in good agreement with the earlier predictions [27,28] and our numerical value.

A different calculation of the stationary dynamic correlations was presented by Yakhot and She [59]. Their result implies $\bar{c}_2=(2/\pi^2)^{2/3}\Gamma(\frac{1}{3}) \approx 0.924$, which is clearly ruled out by our numerics. This is not surprising, as the proposed form of the scaling function [59] is singular at the origin and hence is expected to be valid only for sufficiently large arguments.

A number of predictions for the universal amplitudes arise from the work of Kardar [9] and Bouchaud and Orland [41] in the context of directed polymers. These authors employ the replica trick, which means that averaged moments $\langle Z^n \rangle$ of the polymer partition function (42) are evaluated and then analytically continued to $n=0$. $\langle Z^n \rangle$ is related to the propagator of a quantum-mechanical system of n particles interacting through a pair potential given by the noise correlator (43). As the length of the polymer (the time t in the interface model) becomes large, the propagator is dominated by the ground-state energy, which takes a simple form for δ-function interactions. Expanding the asymptotic form for $\langle Z^n \rangle$ in n then yields expressions for the cumulants of the free energy, $-\ln Z$.

Proceeding along these lines, Kardar [9] found that the *third* cumulant is extensive (proportional to t), and concluded therefore that the free-energy exponent $\omega=\zeta/z=\frac{1}{3}$, in agreement with the KPZ result [1]. His prediction for the reduced amplitude of the third cumulant, in our units, is $c_3=-\frac{1}{4}$, which is clearly inconsistent

with our numerical estimates (though it does predict the correct sign). Moreover, the replica calculation implies that all higher cumulants vanish in the thermodynamic limit, $c_n=0$ for $n>3$, whereas we (as well as Kim, Moore, and Bray [55]) find evidence that $c_4>0$.

Bouchaud and Orland [41] (BO) refined Kardar's treatment by including the center-of-mass motion of the particle system in the evaluation of the quantum-mechanical propagator. Following a transformation to an equivalent toy model [60] of a Hookian spring subject to potential energy of Gaussian random slope, which is readily simulated, they arrive at the predictions $c_2=0.28$ and $c_v=-0.32$. Again, these values are nowhere near our numerical estimates. Halpin-Healy [42] found similarly poor agreement with the predictions [41] concerning the positional fluctuations of the polymer. Thus the claim of BO that their toy model "contains the full physics of the original problem" does not hold up to closer scrutiny.

While we hope that these discrepancies will be clarified by future work, we may tentatively attribute them to the breaking of replica symmetry [12,61] in the disordered polymer problem. It should be clear from our previous remarks that the replica calculations imply a nontrivial exchange of the limits $t\to\infty$ and $n\to 0$. Parisi [48] has recently argued that these limits do not commute in general, and that their failure to do so may change the values of amplitudes. Hence the amplitudes that we have determined could be useful in uncovering rather deep notions in the statistical mechanics of disordered systems. In that sense, they seem to carry much more information than the scaling exponents themselves, which appear to be rather robust with respect to such subtleties.

ACKNOWLEDGMENTS

We thank T. Hwa, M. Kardar, and H. Spohn for useful discussions, and T. Hwa, J. M. Kim, and J. G. Amar for making their work available to us prior to publication. This work was supported in part by grants from the Research Corporation and the Petroleum Research Fund, the latter being administered by the American Chemical Society.

APPENDIX: TIME-SCALE FLUCTUATIONS AND FINITE-SIZE EFFECTS

The following considerations apply to models in which the inclination dependence of the growth rate is due to a variation of the density of growth sites with inclination [25]. If the eligible growth sites are filled independently at unit rate, the growth rate is then proportional to the number of growth sites per projected substrate area. We use the single-step model [15,30] as an illustration, but we have observed similar effects in simulations of the restricted solid-on-solid model [20] and we expect them to occur in, e.g., the Eden model [62] as well.

We have shown in Sec. III that the density ρ of growth sites in the single-step model at zero tilt ($u=0$) equals $\frac{1}{4}$ in the thermodynamic limit. Here we are concerned with the leading correction to this value for a system of L sites with periodic boundary conditions. We will argue that the correction depends on the ensemble in which the average growth rate is evaluated, an effect which is important to take into account in numerical simulations. For simplicity we restrict ourselves to the case $u=0$. In terms of the spin representation introduced in Sec. III,

$$\rho=\tfrac{1}{4}(1-\langle\sigma_{x-1}\sigma_x\rangle) \tag{A1}$$

and the result $\rho=\frac{1}{4}$ follows from the independence of spins in the thermodynamic limit. In a finite system it is still true that all configurations with fixed magnetization (tilt) have the same weight in the stationary state [15]. For $u=0$ there are $L/2$ spin of each sign to be distributed on the lattice. A growth site is given by a pair $(\sigma_{x-1},\sigma_x)=(-1,1)$. For the first spin $\sigma_{x-1}=-1$, there are L positions available. However, once the first spin is fixed, there are only $L-1$ positions available to place one of the $L/2+$spins. This implies a negative correlation

$$\langle\sigma_x\sigma_y\rangle=-\frac{1}{(L-1)} \tag{A2}$$

for $x\neq y$, which is in fact *independent* of the distance between the spins. Thus

$$\rho=\tfrac{1}{4}\left[1+\frac{1}{L-1}\right]. \tag{A3}$$

Using (25) and (26) this is verified to agree, to leading order in $1/L$, with the general expression (14) [24].

To correctly generate the stationary state of the continuous time stochastic process which defines the single-step model, it is important that *time* in a simulation be counted as the number of *attempted depositions* per site. In an elementary simulation step a site is picked at random, deposition is attempted, and time is increased by $1/L$ independent of the success of the attempt. On this time scale the deposit thickness (number of successful depositions per substrate site) becomes a fluctuating quantity. From the point of view of computational efficiency it is natural to avoid unsuccessful attempts by keeping a *list* of eligible growth sites and making a random choice only among these. Time is then equal to the deposit thickness which does *not* fluctuate. A moments thought reveals that this procedure, referred to as the *list algorithm* in the following, defines a new dynamical ensemble in which configurations with many growth sites carry more weight [63]. To investigate this effect quantitatively we introduce the number $C(L,M)$ of configurations with zero tilt and M growth sites in a system of size L [64]. Here $M=1,\ldots,L/2$ and the total number of configurations is

$$\mathcal{C}(L)=\sum_{M=1}^{L/2}C(L,M)=\binom{L}{L/2} \tag{A4}$$

In the ensemble where each configuration has the same weight the probability distribution for the number of growth sites is simply $P(M)=C(L,M)/\mathcal{C}(L)$, the first moment of which is $\langle M\rangle=\rho L$. In contrast, the dynamic ensemble generated by the list algorithm is readily seen to give rise to the distribution

$$\tilde{P}(M)=\frac{M}{\langle M\rangle}P(M)\ , \tag{A5}$$

i.e., the probability to find M growth sites is multiplied by M. While we have not been able to explicitly calculate the $C(L,M)$, we observe by exact numerical enumeration up to $L=16$ that the distribution (A5) is *symmetric* for all L. Its first moment is therefore $(L/2+1)/2$, and the density of growth sites evaluated in this ensemble is

$$\tilde{\rho}=\tfrac{1}{4}\left[1+\frac{2}{L}\right] \tag{A6}$$

with a leading correction term that differs from (A3). We note that it is possible to incorporate the correct time-scale fluctuations into the list algorithm by increasing time by the inverse of the actual number of growth sites at each deposition step [65]. The growth rate measured in such a way is

$$v=\frac{2}{L\langle 1/M\rangle_{\sim}}=\frac{2\langle M\rangle}{L}=2\rho\ , \tag{A7}$$

where $\langle\ \rangle$ and $\langle\ \rangle_{\sim}$ denote averages obtained using the distribution P and $\tilde{P}$, respectively.

[1] M. Kardar, G. Parisi, and Y. C. Zhang, Phys. Rev. Lett. **56**, 889 (1986).

[2] Some recent reviews are J. Krug and H. Spohn, in *Solids Far From Equilibrium: Growth, Morphology and Defects*, edited by C. Godrèche (Cambridge University Press, Cambridge, 1991); J. Krug, *Die Entstehung fraktaler Oberflächen* (Harri Deutsch, Frankfurt, 1990); F. Family, Physica A **168**, 561 (1991); *Dynamics of Fractal Surfaces*, edited by F. Family and T. Vicsek (World Scientific, Singapore, 1991).

[3] T. Vicsek, *Fractal Growth Phenomena* (World Scientific, Singapore, 1989).

[4] J. Villain, J. Phys. Fr. I **1**, 19 (1991).

[5] P. Meakin, CRC Crit. Rev. Solid State Mater. Sci. **13**, 143 (1987).

[6] M. A. Rubio, C. A. Edwards, A. Dougherty, and J. P. Gollub, Phys. Rev. Lett. **63**, 1685 (1989); V. K. Horváth, F. Family, and T. Vicsek, J. Phys. A **24**, L25 (1991); J. Krug and P. Meakin, Phys. Rev. Lett. **66**, 703 (1991).

[7] J. Krug and P. Meakin, Phys. Rev. A **40**, 2064 (1989), and references therein.

[8] M. Kardar and Y. C. Zhang, Phys. Rev. Lett. **58**, 2087 (1987).

[9] M. Kardar, Nucl. Phys. B **290**, 582 (1987).

[10] B. Derrida, Physica A **163**, 71 (1990), and references therein.

[11] T. Halpin-Healy, Phys. Rev. A **42**, 711 (1990).

[12] M. Mézard and G. Parisi, J. Phys. Fr. I **1**, 809 (1991).

[13] F. Family and T. Vicsek, J. Phys. A **18**, L75 (1985); R. Jullien and R. Botet, *ibid.* **18**, 2279 (1985).

[14] R. Lipowsky, in *Fundamental Problems in Statistical Mechanics VII*, edited by H. van Beijeren (North-Holland, Amsterdam, 1990).

[15] P. Meakin, P. Ramanlal, L. M. Sander, and R. C. Ball, Phys. Rev. A **34**, 5091 (1986).

[16] J. Krug, Phys. Rev. A **36**, 5465 (1987).

[17] E. Medina, T. Hwa, M. Kardar, and Y. C. Zhang, Phys. Rev. A **39**, 3053 (1989).

[18] D. Forster, D. R. Nelson, and M. J. Stephen, Phys. Rev. A **16**, 732 (1977).

[19] D. A. Huse, C. L. Henley, and D. S. Fisher, Phys. Rev. Lett. **55**, 2924 (1985).

[20] J. M. Kim and J. M. Kosterlitz, Phys. Rev. Lett. **62**, 2289 (1989).

[21] B. M. Forrest and L.-H. Tang, Phys. Rev. Lett. **64**, 1405 (1990).

[22] T. Hwa (private communication).

[23] For a random variable with zero mean the first three cumulants are equal to the moments $\langle X^n\rangle_c=\langle X^n\rangle$ for $n=1,2,3$, and the fourth cumulant is $\langle X^4\rangle_c=\langle X^4\rangle-3\langle X^2\rangle^2$.

[24] J. Krug and P. Meakin, J. Phys. A **23**, L987 (1990).

[25] J. Krug, J. Phys. A **22**, L769 (1989).

[26] M. Plischke and Z. Rácz, Phys. Rev. A **32**, 3825 (1985).

[27] H. van Beijeren, R. Kutner, and H. Spohn, Phys. Rev. Lett. **54**, 2026 (1985).

[28] H. K. Janssen and B. Schmittmann, Z. Phys. B **63**, 517 (1986).

[29] See also J. Krug in Ref. [2].

[30] M. Plischke, Z. Rácz, and D. Liu, Phys. Rev. B **35**, 3485 (1987).

[31] D. J. Gates and M. Westcott, Proc. R. Soc. London Ser. A **416**, 443 (1988); **416**, 463 (1988); D. J. Gates, J. Stat. Phys. **52**, 245 (1988).

[32] S. Katz, J. L. Lebowitz, and H. Spohn, J. Stat. Phys. **34**, 497 (1984).

[33] H. Brandstetter, Diploma thesis, University of Munich 1990 (unpublished).

[34] J. G. Amar and F. Family, Phys. Rev. Lett. **64**, 543 (1990); J. Krug and H. Spohn, *ibid.* **64**, 2232 (1990).

[35] W. van Saarloos and G. H. Gilmer, Phys. Rev. B **33**, 4927 (1986), and references therein.

[36] J. Krug and H. Spohn, Europhys. Lett. **8**, 219 (1988).

[37] D. E Wolf, J. Phys. A **20**, 1251 (1987).

[38] J. Krug and H. Spohn, Phys. Rev. A **38**, 4271 (1988).

[39] M. Kardar, Phys. Rev. Lett. **55**, 2923 (1985).

[40] D. A. Huse and C. L. Henley, Phys. Rev. Lett. **54**, 2708 (1985).

[41] J. P. Bouchaud and H. Orland, J. Stat. Phys. **61**, 877 (1990).

[42] T. Halpin-Healy, Phys. Rev. A **44**, R3415 (1991).

[43] T. Nattermann and W. Renz, Phys. Rev. B **38**, 5184 (1988).

[44] In the growth model context the natural analog of this initial condition is the growth from a point seed rather than from a substrate.

[45] This geometry was employed in the recent zero-temperature DPRM simulations of Kim, Bray, and Moore [55].

[46] In the terminology of first-passage percolation, which is an equivalent formulation of the zero-temperature DPRM (see H. Kesten, Ann. Prob. **15**, 1231 (1987) for a review, and J. Krug and H. Spohn in [2] for a brief discussion of the relation to growth models and DPRM), $Z(x,t)$ is a

point-to-point partition function (all paths share the same starting *and* end point), while $Z(t)$ is a *point-to-line* quantity. Though it can be shown that the averages of $F=-\ln Z$ and $\mathcal{F}=-\ln Z$ agree to leading order in t, the finite-size corrections and fluctuations may be expected to differ in the two cases. Our preliminary numerical results indicate that F and $\mathcal{F}$ are characterized by the same scaling exponents but *different* amplitudes.

[47] J. Cook and B. Derrida, J. Stat. Phys. **63**, 505 (1991), compute finite-size corrections for the mean-field version of the DPRM.

[48] G. Parisi, J. Phys. Fr. **51**, 1595 (1990).

[49] M. Mézard, J. Phys. Fr. **51**, 1831 (1990).

[50] In the context of growth models the use of inhomogeneous macroscopic profiles to extract parameters like λ was proposed by D. E. Wolf and L.-H. Tang, Phys. Rev. Lett. **65**, 1591 (1990).

[51] T. Hwa and E. Frey (unpublished).

[52] H. van Beijeren, J. Stat. Phys. **63**, 47 (1991) investigated the relative importance of initial and kinetically generated fluctuations in the equivalent [36] case of one-dimensional driven diffusive systems [27,28]. For a brief discussion in the interface context see Chap. 6 of the review article by J. Krug and H. Spohn in [2].

[53] Hong Guo, B. Grossmann, and M. Grant, Phys. Rev. A **41**, 7082 (1990).

[54] S. Havlin, S. V. Buldyrev, H. E. Stanley, and G. H. Weiss, J. Phys. A **24**, L925 (1991).

[55] J. M. Kim, M. A. Moore, and A. J. Bray, Phys. Rev. A **44**, 2345 (1991).

[56] J. G. Amar and F. Family (unpublished).

[57] Amar and Family [56] quote a result obtained from the one-loop renormalization calculation of KPZ [1], $c_2 \approx 0.57$, which presumably also refers to the steady-state situation.

[58] In [36] this result was erroneously applied to the transient case.

[59] V. Yakhot and Z. S. She, Phys. Rev. Lett. **60**, 1840 (1988).

[60] J. Villain, B. Semeria, F. Lanon, and L. Billard, J. Phys. C **16**, 2588 (1983); U. Schultz, J. Villain, E. Brézin, and H. Orland, J. Stat. Phys. **51**, 1 (1988).

[61] The applicability of the concept of replica symmetry breaking in this context (and in general) was recently challenged by D. S. Fisher and D. A. Huse, Phys. Rev. B **43**, 10 728 (1991).

[62] R. Hirsch and D. E. Wolf, J. Phys. A **19**, L251 (1986).

[63] This observation was independently made by H. C. Kang and J. W. Evans, Phys. Rev. A **44**, 2335 (1991).

[64] In the spin language, $C(L,M)$ is the number of Ising configurations with fixed magnetization *and* fixed energy.

[65] A similar definition of time is used in simulations of diffusion-limited reaction kinetics; see, e.g., D. Ben-Avraham, J. Stat. Phys. **48**, 315 (1987).

* 1+1 DPRM ~ VARIATIONS ON A THEME:

a) CORRELATED, GAUSSIAN NOISE

see also M. Kardar, J. Appl. Phys. 61, 3601 (1987).

between sites — on each individual site

■ pinning impurities possess correlator

$$\langle V(z,x)V(0,0)\rangle = \delta(x)R(z)$$

where $R(z) \sim z^{\alpha}$

$\alpha = 1 \rightarrow$ RF case ($\zeta_{RF} = 1$)

$\alpha = -1 \rightarrow$ RB case ($\zeta_{RB} = \frac{2}{3}$)

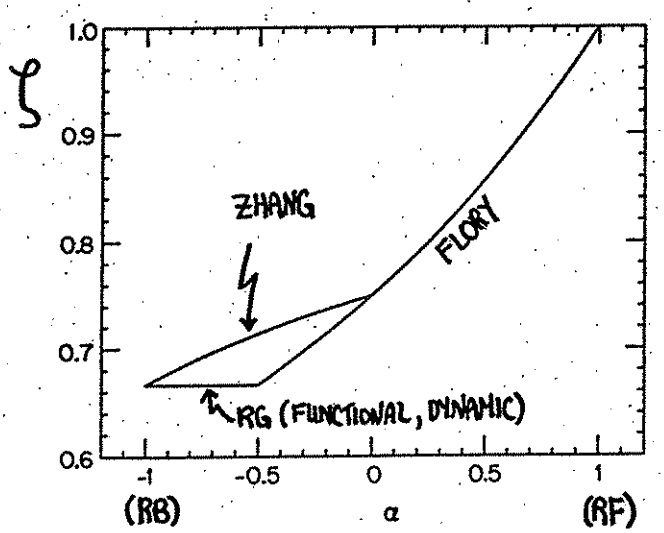

see

THEORY:

* DYNAMIC RG – Medina, et al PRA 39, 3053 (1989).
* FUNCTIONAL RG – Halpin-Healy, PRL 62, 442 (1989).
* REPLICA SCALING – Zhang, PRB 42, 4897 (1990).

NUMERICAL EXPT: done in growth model context –

* J. Amar, P.-M. Lam, + F. Family, PRA 43, 4548 RC (1991)
* Stanley, et al., PRA 44, 2239 AC (1991).

b) UNCORRELATED, POWER-LAW NOISE

■ interesting new model proposed by Zhang – bond/site energies uncorrelated, but nongaussian, distributed according to

$$P(\varepsilon) \sim \varepsilon^{-(\mu+1)}$$

so-called "POWER-LAW" noise.

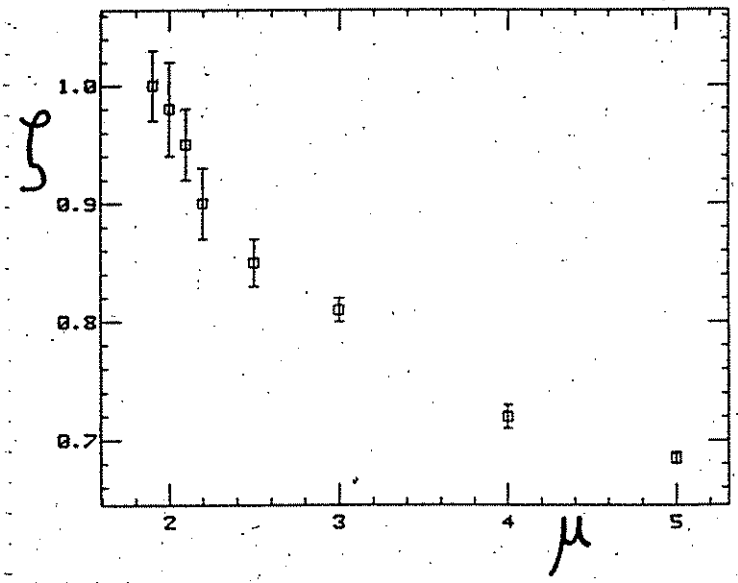

+ DPRM → ENHANCED WANDERING

* Moreno + Zhang, J. Stat. Phys. 61, 885 (1990)

+ STOCHASTIC GROWTH MODELS (EDEN, BALLISTIC DEPOSITS) → "ANOMALOUS" KINETIC ROUGHENING

* Y.-C. Zhang, J. Physique 51, 2129 (1990).
* Y.-C. Zhang, Physica A170, 1 (1990).
* J. Amar + F. Family, J. Phys. A24, L79 (1991).
* S. Buldyrev et al., PRA 43, 7113 (1991).

for Flory estimate of wandering exponent see Zhang, as well as

* J. Krug, J. Phys (FRANCE) I 1, 9, (1991).

$$\zeta_{FLORY} = \frac{\mu+1}{2\mu-1}$$

DOES WELL FOR $\mu \geq 2$, BUT INCORRECTLY PREDICTS $\mu_c = 5$

GAUSSIAN NOISE

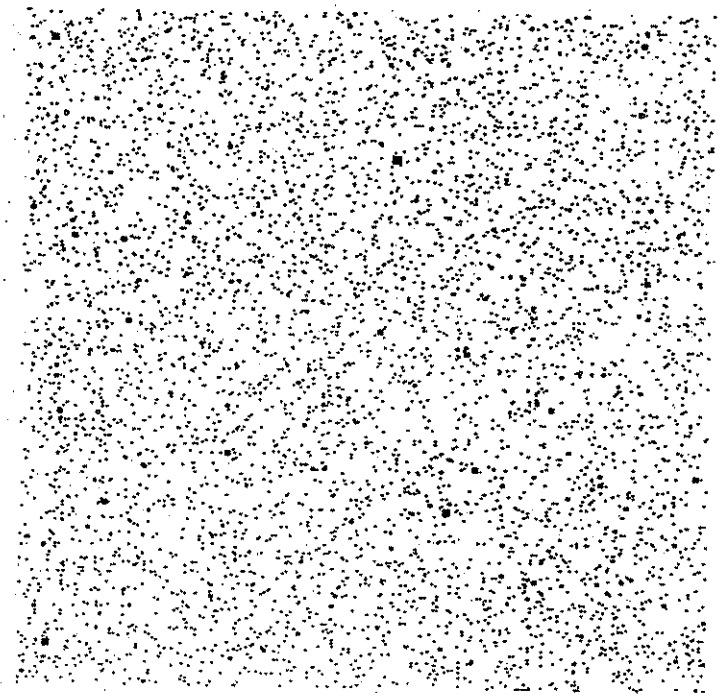

compared to

$\mu = 3$ POWER LAW NOISE

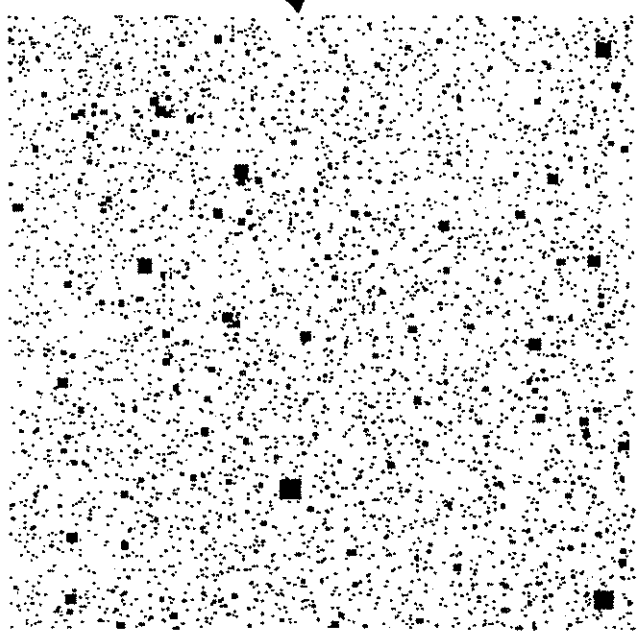

BUT,

$\mu = 2$ POWER LAW NOISE

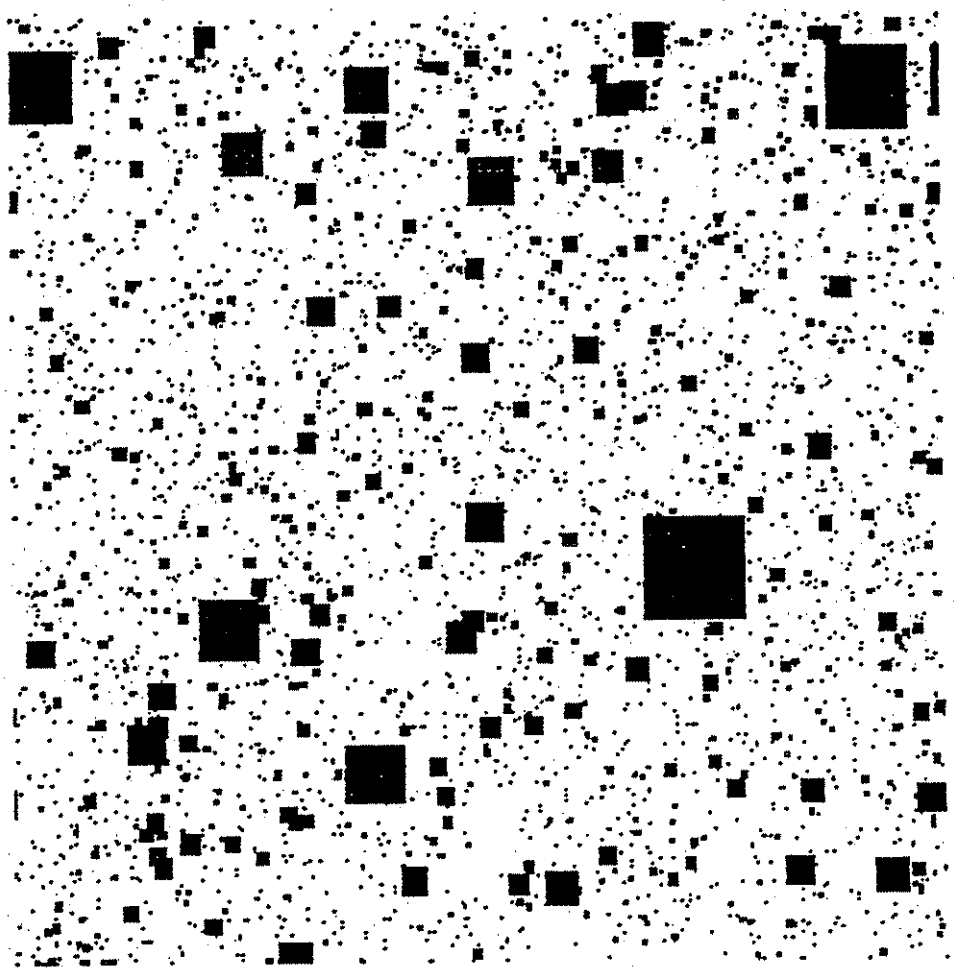

which corresponds to the marginal case ($\mu < 2 \Rightarrow$ Levy distribution), appears noticeably different...

1+1 DPRM RIVER BASIN DELTAS

↳ "POWER-LAW" NOISE

$\mu = 1$

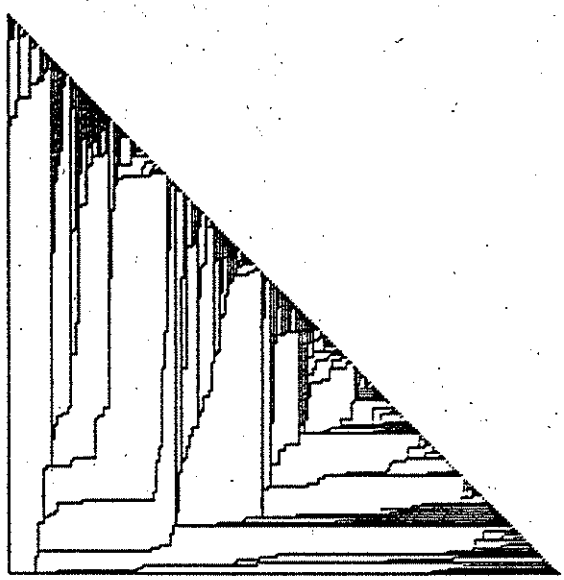

$\mu = 3$

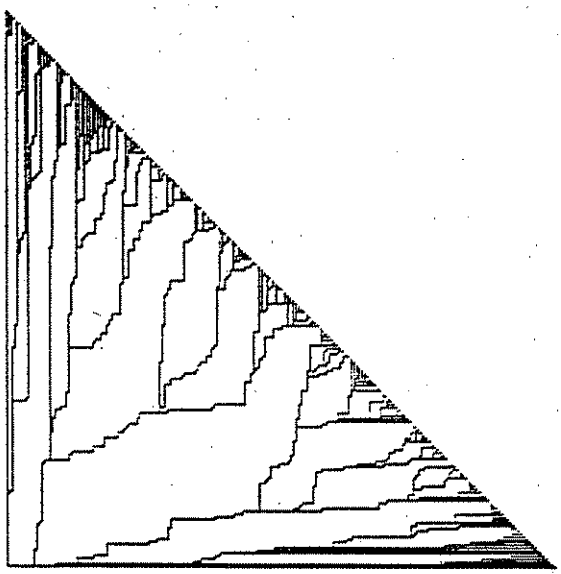

$\mu_c = 7$

(power law with sufficiently fast fall off → Gaussian case)

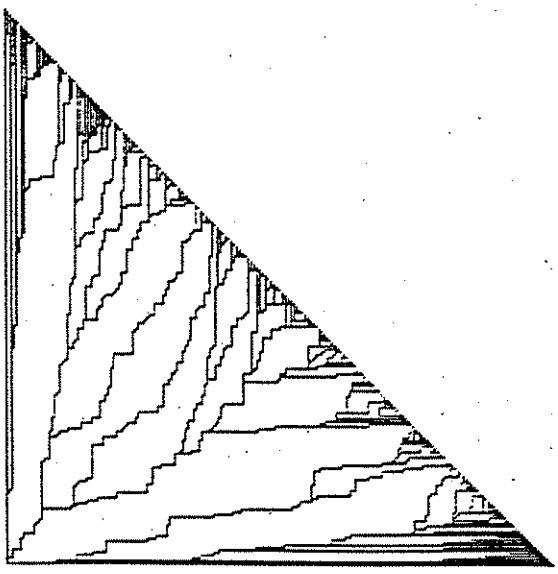

see R. Bourbonnais, H. Hermann, + S. Vicsek, Int. J. Mod. Phys. C 2, 719 (1991).

✸ ANOMALOUS KINETIC ROUGHENING ⟵ POWER-LAW NOISE

Y.-C. Zhang, J. Physique 51, 2129 (1990).

STEADY-STATE ROUGHNESS EXPONENT (characterizes saturation width)

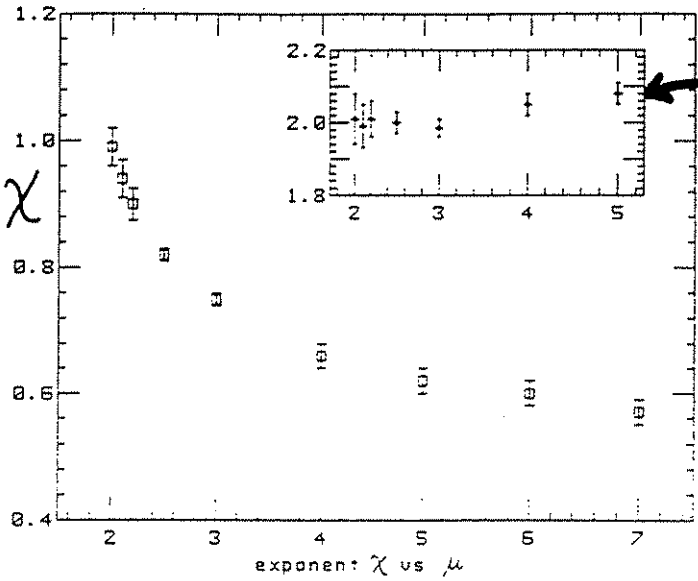

$\chi + z = 2$

EXPONENT IDENTITY REMAINS SATISFIED FOR ALL μ

⇓

STILL KPZ

■ EXAMPLE #1: "SELF-AFFINE FIRE FRONTS ~ PAPER BURNING"

les frères pyrotechniques, J. Zhang & Y.C. Zhang, Physica A (to appear)

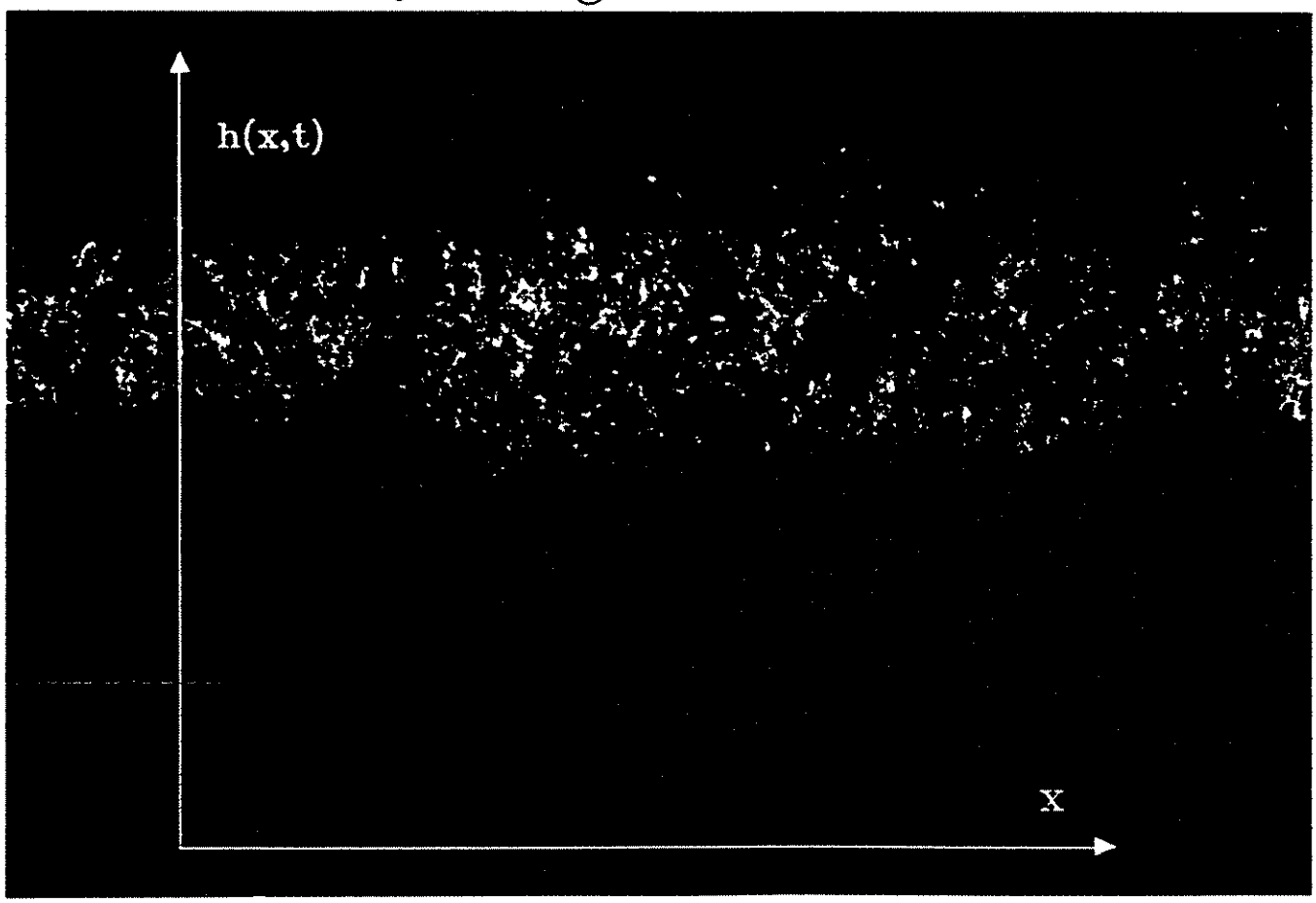

- material = optical lens cleaning tissue (Whatman Paper Ltd, UK), 110 × 46 cm □, very thin 45 μm treated with a solution of KNO_3, a common oxydization aid used in many explosives,
  ⇒ FLAMELESS, RELATIVELY SLOW BURNING
- fire ~ ignited from bottom side by straight electric heating wire. Typical propagation speed ≈ 6.8 mm/sec

high resolution photography records fire front propagation → pictures are then captured by video camera into a 512 × 750 pixel buffer with multi-level grey scale. Images then undergo digital analysis.

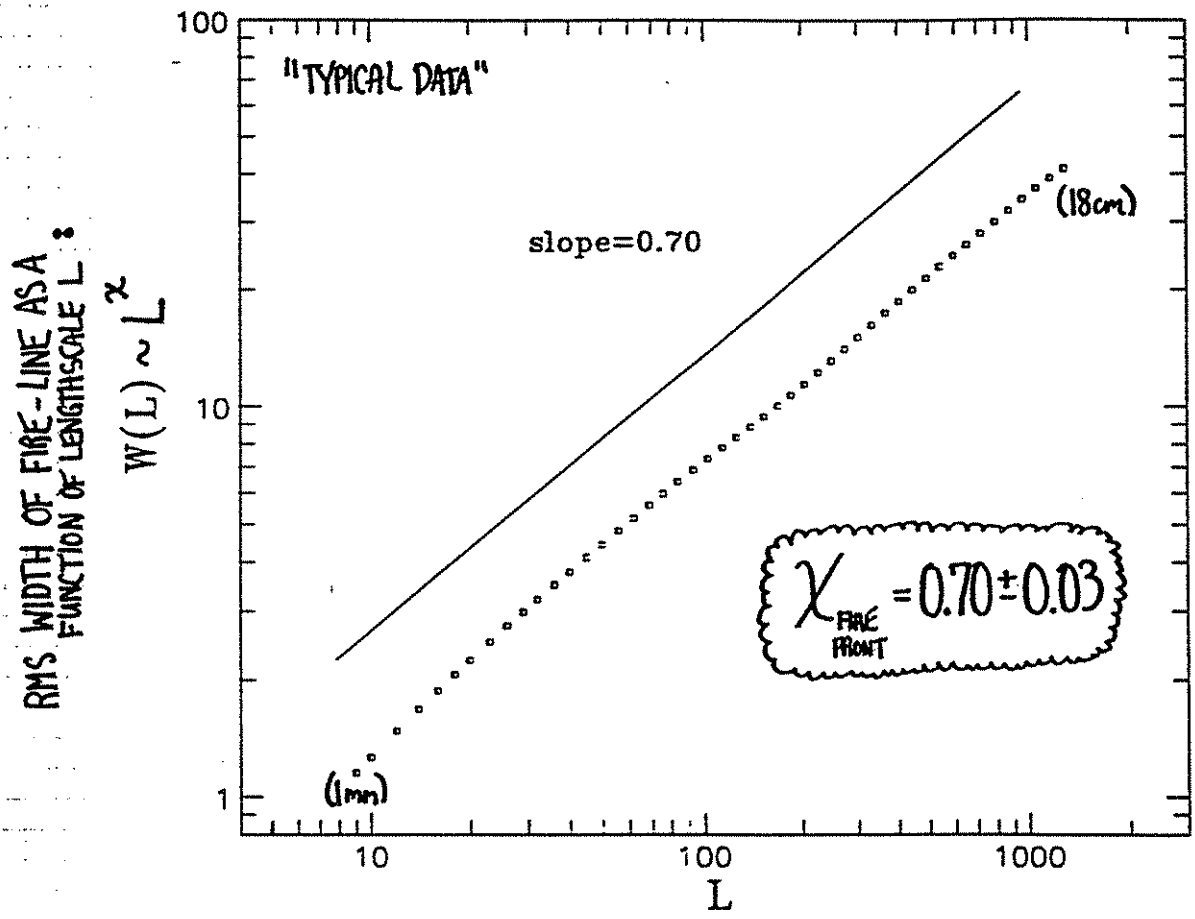

noise is due to unavoidable local irregularities in the random fiber network, porosity, chemical composition & other factors

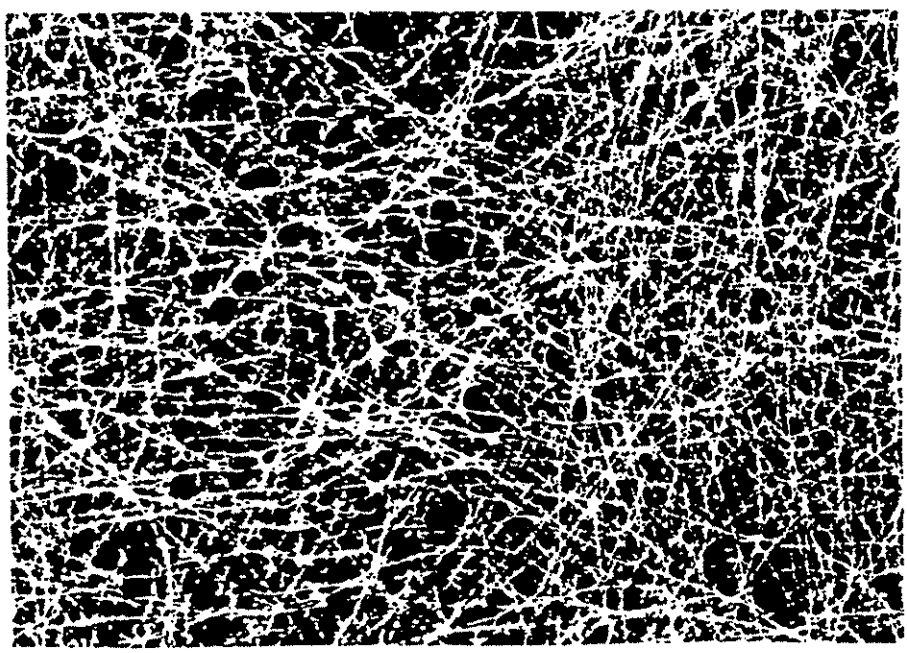

20X MAGNIFICATION

■ EX#2: "SELF-AFFINE BACTERIA COLONIES"

references :- J. Vicsek, M. Cserzö, & V. Horvath, Physica 167, 315 (1990).
H. Diratzouian, B. Tanminga, & J. Halpin-Healy, work in progress.

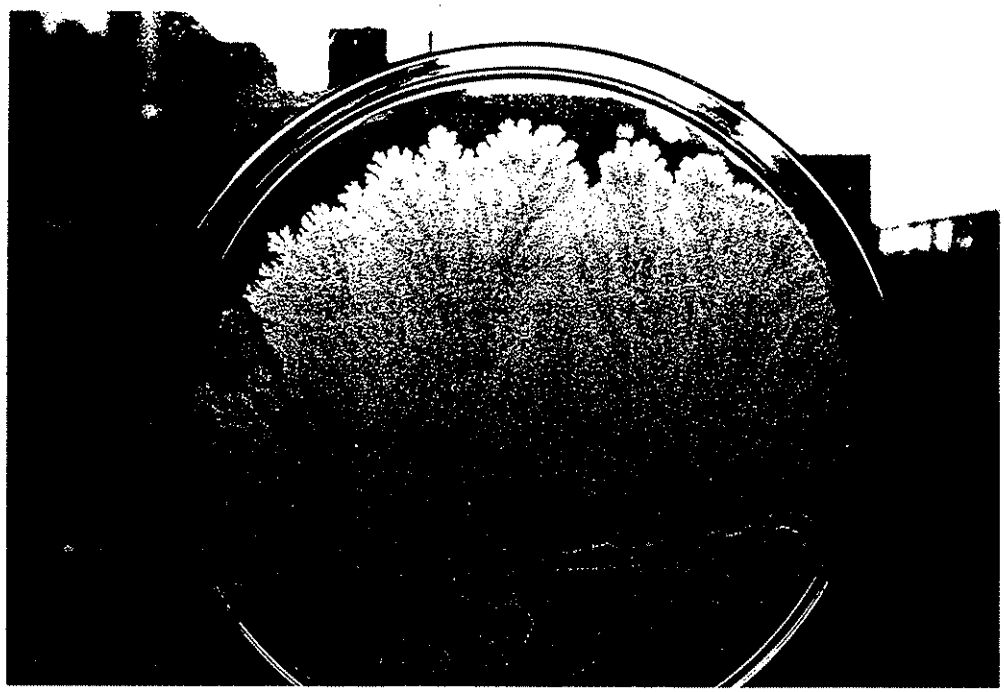

Bacillus subtilus
inoculated from a
LINE SOURCE
- nutrient rich agar
- grown for 2 weeks

* work of Vicsek, etal:

COMPUTER SIMULATION
vs.
"REAL LIFE"

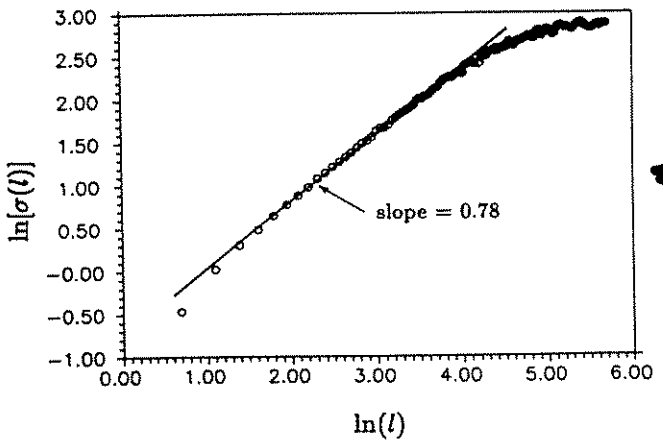

$\chi = 0.78 \pm 0.07$
BACTERIAL COLONY

ROUGHNESS EXPONENT

■ EX #3: "FLUID-FLOW IN POROUS MEDIA"

reference: Rubio, et al, PRL 63, 1585 (1989).

VOLUME 63, NUMBER 16 PHYSICAL REVIEW LETTERS 16 OCTOBER 1989

Self-Affine Fractal Interfaces from Immiscible Displacement in Porous Media

M. A. Rubio,[1,2] C. A. Edwards,[1] A. Dougherty,[1] and J. P. Gollub[1,3]
[1]*Department of Physics, Haverford College, Haverford, Pennsylvania 19041*
[2]*Departamento de Física Fundamental, Universidad Nacional de Educación a Distancia, Apartado Correos 60141, Madrid 28080, Spain*
[3]*Department of Physics, University of Pennsylvania, Philadelphia, Pennsylvania 19104*
(Received 5 June 1989)

Wetting immiscible displacement of one fluid by another in a porous medium yields self-affine (anisotropic) fractal interfaces between the two fluids. Water-air interfaces are characterized experimentally by a scale-dependent roughness $w(L) = AL^{\chi}$, with $\chi = 0.73 \pm 0.03$, independent of the capillary number Ca, and $A \propto \mathrm{Ca}^{-0.47 \pm 0.06}$. The exponent χ is related to the "box" and "divider" dimensions by $D_b = 2 - \chi$ and $D_d = 1/\chi$, respectively.

INTERFACE PROFILES

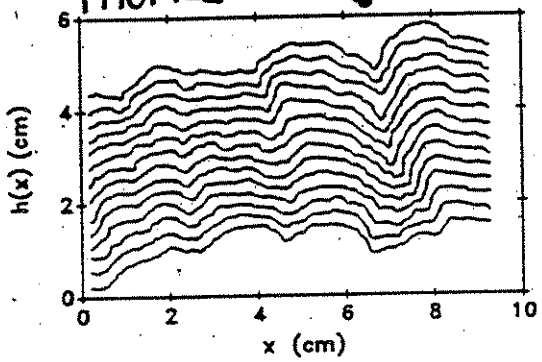

FIG. 1. Plot of fourteen successive interfaces at Ca = 4.93×10^{-3}. The time interval between single interfaces is 30 s.

SCALING PLOT

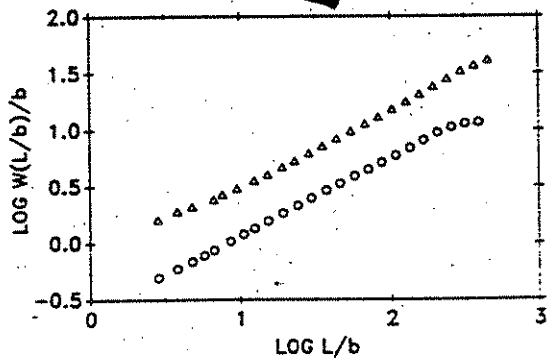

FIG. 2. Plot of roughness vs length scale at two different values of Ca for bead size $b = 200$ μm. Ca = 2.47×10^{-3} (△) and 9.78×10^{-3} (○).

STEADY STATE ROUGHNESS EXPONENT

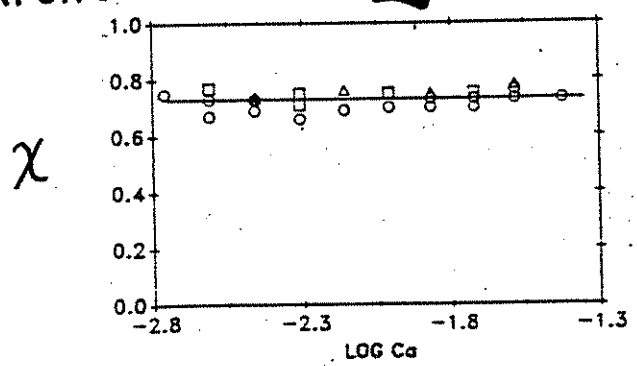

$\chi_{\text{FLUID FLOW}} = 0.73 \pm 0.03$

FIG. 3. Roughness exponent vs Ca for $b = 100$ (□), 200 (○), and 350 μm (△). The uncertainties are comparable to the size of the symbols. The line corresponds to the average value of $\chi = 0.73 \pm 0.03$.

* for more recent expt'l work plus possible corroborative evidence for experimental relevance of power law noise distributions, see → V. Horvath, F. Family, & J. Vicsek, PRL 67, 3207 (1991).

** ALTERNATIVE EXPLANATION: Jang & Leschorn, PRA 45, 8309 RC (1992); Stanley et al, PRA 45, 8313 RC (1992).

* MANY-DIMENSIONAL DPRM ⇝ FINITE TEMPERATURE

references ↳ B. Derrida & O. Golinelli, Phys. Rev. A 41, 4160 (1990).
J. Cook & B. Derrida, J. Stat. Phys. 57, 89 (1989).

It is known from various arguments (probability, QM, RG) that the 1+1 DPRM is governed at all times by T=0 fixed pt. Even if one simulates the model at high temperatures, it is true that at sufficiently long lengthscales, the wandering will not be entropic, but rather exhibit superdiffusive behavior. This state of affairs is summarized as follows –

1+1 DPRM

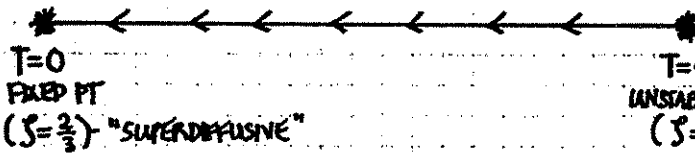

PHASE DIAGRAM + RG FLOWS

Note that the infinite temperature, thermal fixed pt is unstable to disorder ⇒ simplest phase diagram topology has NO FINITE TEMP PHASE TRANSITION. In fact it is known that the 2+1 DPRM possesses this very same phase diagram topology (with ζ≈5/8, however, at T=0), though the T=∞ FP is only "MARGINALLY" unstable in this difficult dimensionality, leading to excruciatingly slow crossover effects to the strong disorder, T=0 FP ⇝ see Kim, Bray & Moore, Phys. Rev. A 44, 4782 RC (1991). Nevertheless, the 3+1 DPRM does possess a finite temp fixed pt separating phases of disorder-induced and entropic wandering:

3+1 DPRM

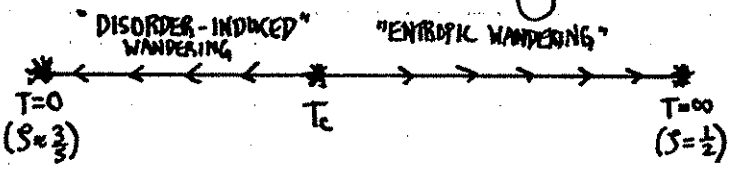

PHASE TRANSITION!

Derrida and Golinelli have used transfer matrix techniques to study the SPECIFIC HEAT of the finite temperature many-dimensional DPRM, finding evidence for the transition in d=3+1 (see figures that follow). Indeed, with probability arguments, they can even set bounds on the transition temperature. For d>2+1, there exists a temperature beyond which the free energy/length of the DPRM is given by the ANNEALED, rather than QUENCHED average (⇒ existence of high temperature phase!), so

$$\frac{\ln Z_L}{L} = \frac{\ln \langle Z_L \rangle}{L} = \ln\left(2d \langle \exp(-\varepsilon/T) \rangle\right) = \ln 2d + \frac{\beta^2}{2}$$

assuming the bond energies, ε, are uncorrelated & gaussian distributed. They estimate the upper bound on T_c by calculating the ratio $\langle Z_L^2 \rangle / \langle Z_L \rangle^2$ and showing that it is finite as $L \to \infty$ for $T > T_2(d=3+1) = 0.790$.

* DIRECTED POLYMERS - FINITE TEMPERATURE

Derrida & Golinelli
PRA 41, 4160 (1990).

$C_n(T) = \frac{d}{dT}\left(T^2 \frac{d}{dT} \frac{\ln Z_L}{L}\right)$

$a_n(T) = \frac{d^3}{d\beta^3}\left(\frac{\ln Z_L}{L}\right)$

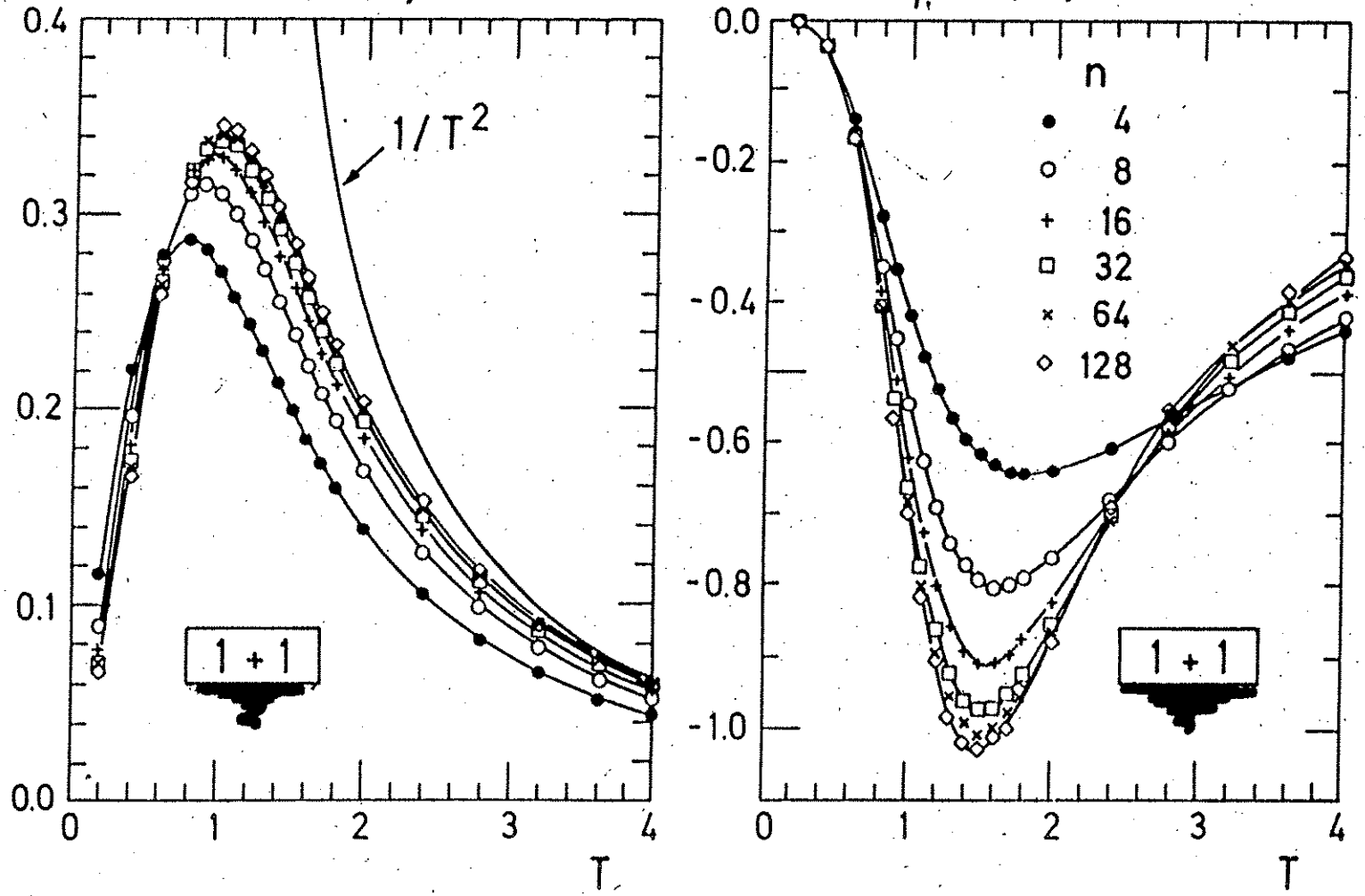

would vanish in high temperature phase when free energy is given by ANNEALED AVERAGE
$\Rightarrow \frac{\ln Z_L}{L} = \text{cst} + \frac{1}{2}\beta^2$

$\Rightarrow$ NO PHASE TRANSITION - 1+1 DPRM

3+1 DPRM:

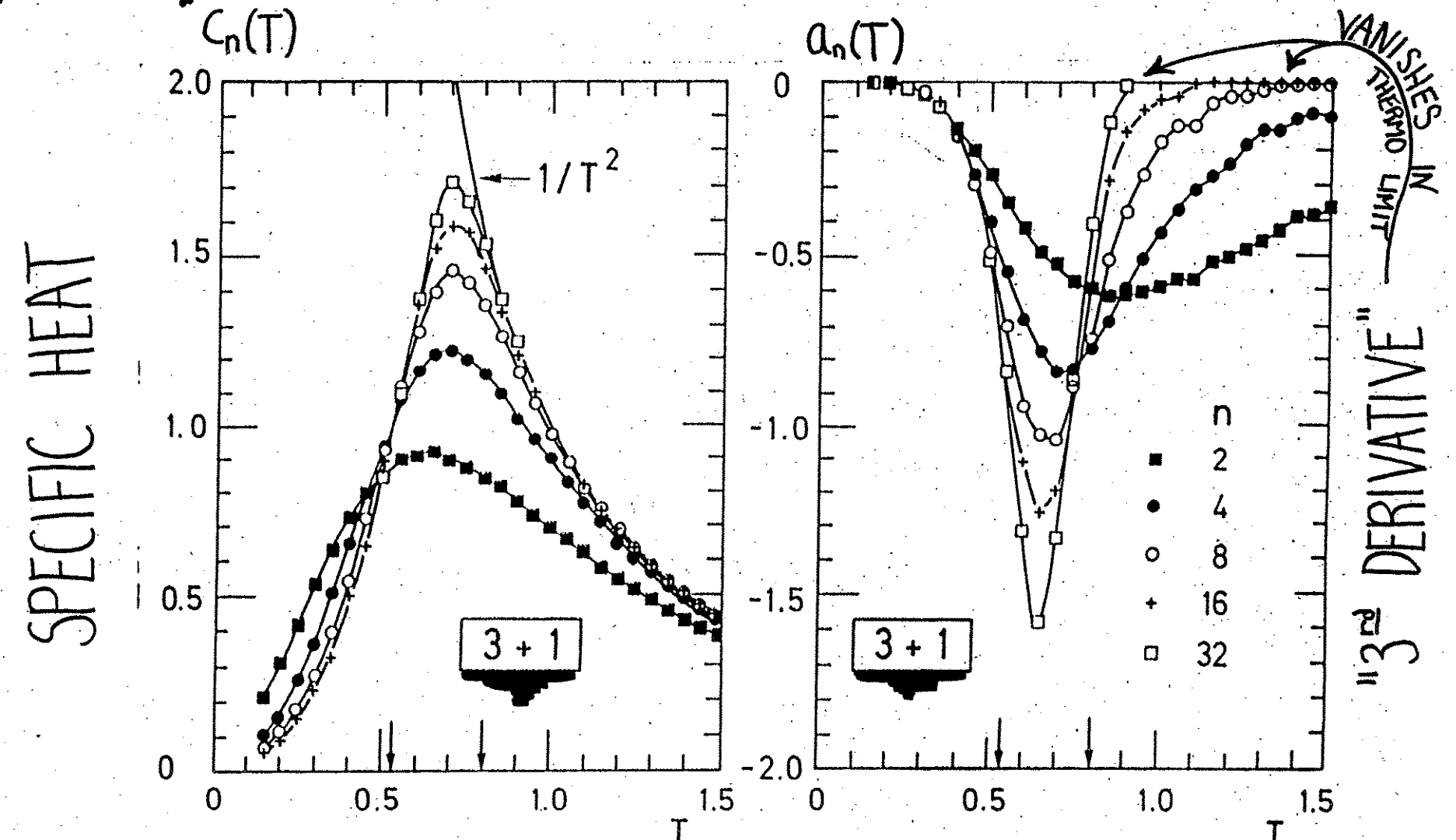

PHASE TRANSITION !

2+1 DPRM ~ MARGINAL CASE:

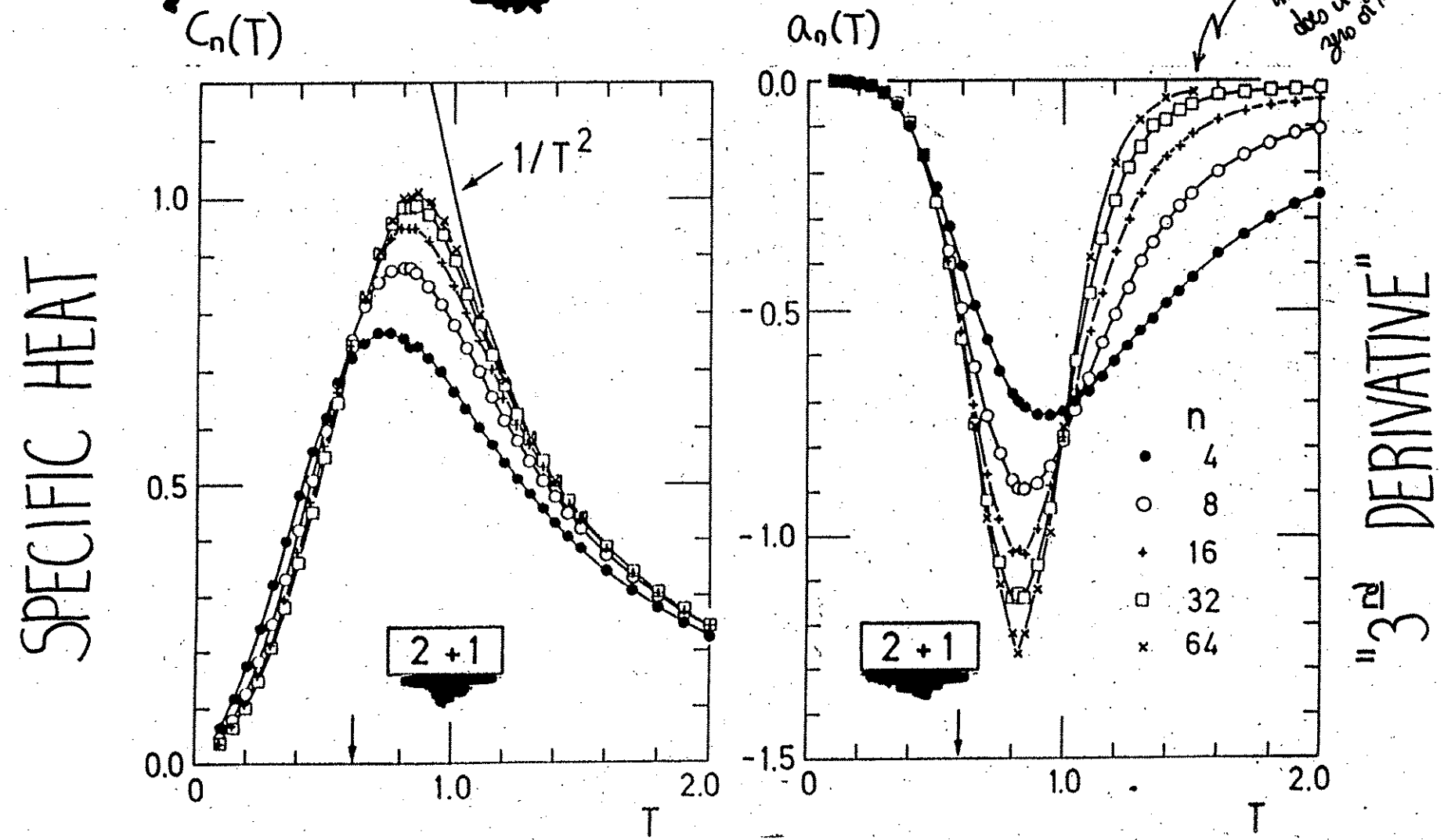

???!!

(IN FACT, LATER WORK RULES OUT POSSIBILITY OF PHASE TRANSITION, SEE – Kim, Bray, & Moore, PRA 44, 4782 RC (1991) ALSO ~ Jang, Matteuwann, & Fornet, PRL 65, 2422 (1990).)

* To be published in the Proceedings of the Les Houches Winter School on "Surfaces Rugueuses: Croissance, Désordre et Transitions de Phase" March 31 - April 9, 1992

DISTURBING THE RANDOM ENERGY LANDSCAPE*

Timothy Halpin-Healy and Devorah Herbert

Physics Department, Barnard College, Columbia University, New York NY 10027-6598

Abstract. We examine the effects of correlated perturbations upon globally optimal paths through a random energy landscape. Motivated by Zhang's early numerical investigations into ground state instabilities of disordered systems as well as the work of Shapir on random perturbations of roughened manifolds, we have studied the specific case of random bond interfaces unsettled by small random fields, confirming recent predictions for the instability exponents. Implications for disordered magnets and growing surfaces are discussed.

1. Introduction

Much of the present interest in kinetic roughening phenomena [1] can be traced to the tremendous outpouring of research on the dynamic scaling properties of Eden clusters and ballistic deposits [2], following the introduction of a noisy Burgers' equation by Kardar, Parisi and Zhang [3]. In the past five years, we have discovered the extraordinary richness of this intriguing equation; within the realm of KPZ can be found a wonderfully varied collection of apparently unrelated physical problems which, beyond the stochastic growth models mentioned above, include long time tails of randomly stirred fluids, the asymptotics of flame front propagation, as well as the roughening of vortex flux lines in ceramic superconductors. This last system [4], which in a different guise concerns the meandering of a directed polymer in a random medium (DPRM) [5-6], is essentially a baby version of the very difficult spin-glass problem [7] that has plagued the statistical physics community for the last decade, replete with an ultrametric free energy landscape and potentially severe replica symmetry breaking [8], though blessed by a number of simplifying features that make it one of the few tractable problems of ill-condensed matter. Controlled by a strong disorder zero temperature fixed point, the DPRM is a classic global optimization problem in which one seeks to minimize the total energy of a directed path through a random environment. Performing averages of many realizations of the random energy landscape yields highly nontrivial geometric and thermodynamic properties that characterize the ensemble of optimal paths. The present paper, motivated initially by the work of Zhang [9], and later influenced by the efforts of Shapir [10] and Mezard [11], investigates the resistance of these optimal paths to random disturbances of the disordered landscape. Our results address specifically the role of correlated drifts in the DPRM random energy landscape and confirms important predictions for random field (RF) perturbations of random bond (RB) domain walls in disordered two-dimensional magnets.

2. The Model

Our starting point is Zhang's formulation of the zero-temperature DPRM, which is most amenable to extensive numerical simulation. One considers a directed walker who, starting at the origin of a square lattice, has the option of making an immediate step diagonally left or right to $(x,t) = (\pm 1, 1)$. These and succeeding diagonal bonds have random energies drawn uniformly between 0 and 1. Neighboring bonds are uncorrelated. At the time slice t there are t+1 possible endpoints to the 2^t paths emanating from (0,0). As discussed earlier, the zero temperature DPRM is simply a matter of global optimization which, for a given realization of the random energy landscape (i.e., collection of random bonds on the lattice), entails finding the path of overall least energy, where the total energy of a path is given by the sum of the random bonds visited along the way. Many essential features of the 1+1 dimensional DPRM were established early on; in particular, it is known that its geometric properties are controlled by transverse fluctuations off the central axis that scale as $x_{rms} \sim t^{\zeta=2/3}$, while sample to sample fluctuations in the energy of the globally optimal trajectory scale as $e_{rms} \sim t^{\omega=1/3}$, there being an index relation, $\omega = 2\zeta - 1$, connecting the energy and wandering exponents.

As stressed by Zhang [9], the globally optimal path through a given realization of the random energy landscape is, however, quite susceptible to small changes in that random environment, there being many neighboring paths whose energies are very close to that of the ground state, but whose configurations differ considerably. These concerns have great physical import, of course, since true physical systems often possess quenched disorders that are actually dynamical variables, albeit on rather long timescales and very small amplitudes. In his own numerical investigation into these issues, Zhang concentrated on the effects of an uncorrelated slow drift in the random energies of the bonds; that is, he considered adding to each random bond energy an uncorrelated perturbation drawn with uniform probability between 0 and δ, with $\delta << 1$. In the context of disordered two-dimensional magnets, this corresponds to uncorrelated RB perturbations upon a RB interface. In the DPRM global optimization problem, this procedure yields two realizations of the random energy landscape that are different, though produced from similar distributions and possessing substantial overlap. Because of the work of Shapir [10], one knows that there exists a crossover length scale $t^* \sim \delta^{-1/\varphi}$, where $\varphi_{RB} = 1/6$ for random bond perturbations and $\varphi_{RF} = 1/2$ for random field perturbations, beyond which the small differences between the

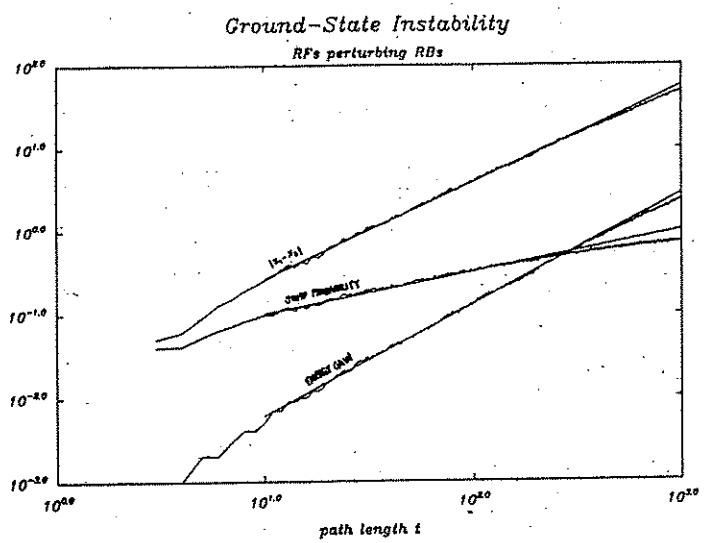

Figure 1. RF perturbations of the DPRM. From the left- Top curve: mean jump distance. Middle curve: jump probability. Bottom curve: energy advantage of new best path over old best path.

perturbed and unperturbed realizations of the random energy landscape manifest themselves in an asymptotic fashion. There are, however, a number of interesting scaling properties associated with ground-state instabilities of this disordered system that reveal themselves immediately. We focus our attention upon them first.

3. The Numerical Data

Consider, for example, the fact that the two globally optimal paths in the two different, but highly correlated random environments, are typically quite distinct. If x_1, x_2 denote the tranverse positions of these two best paths, then we find for RFs perturbing RB interfaces that the mean jump scales with path length as, see Fig. 1, $\mid x_1 - x_2 \mid \sim t^{\alpha=1.16\pm0.02}$, entirely consistent with Shapir's prediction that

$$\alpha_{RF} = \varphi_{RF} + \zeta_{RB} = 1/2 + 2/3 = 7/6$$

Our own data for the case of RBs perturbing RBs, which Zhang considered in his original work and is presented here for sake of comparison, is shown in Fig.2, corroborating the mean jump exponent $\alpha_{RB} = \varphi_{RB} + \zeta_{RB} = 1/6 + 2/3 = 5/6$. In both instances, we have used $\delta = 0.1$ and performed disorder averages over 4000 realizations of the random energy landscape. Furthermore, it is apparent that in the case of RFs perturbing RBs, where the crossover length scale $t^*_{RF} \sim \delta^{-2} \sim 100$, the data begin to pull away from the straight line fit. By contrast, for RBs perturbing RBs, the data

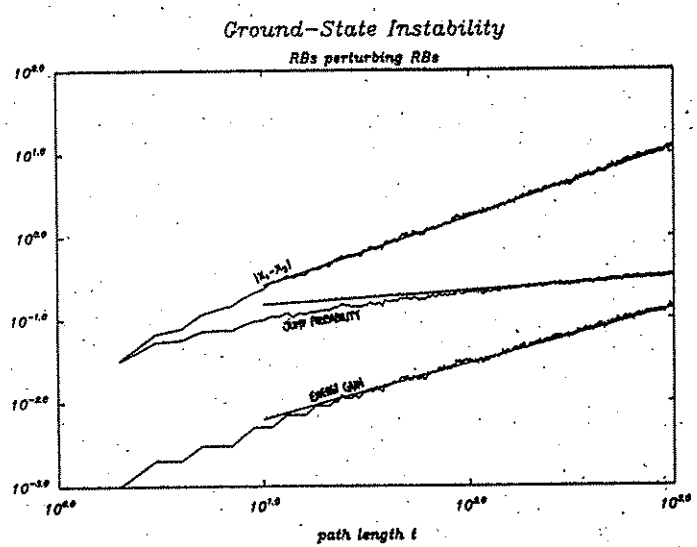

Figure 2. Same as previous figure, but for RB perturbations of the DPRM- the case considered by Zhang.

follows the line well beyond accessible system sizes since $t^*_{RB} \sim \delta^{-6} \sim$ million steps in this case.

Note that this mean jump scaling index is quite large because of the ultrametric structure of the ensemble of locally optimal paths. The very best path in a given realization of randomness is stable with respect to its immediate family thanks to the substantial ancestry they have in common. Hence, there is an intrinsic resistance to change, which Zhang alludes to as a Hopfield memory effect. Nevertheless, because of the random perturbations upon the original disordered landscape, a distant relative of the original best path can accumulate enough energy gains to become the globally optimal trajectory in the perturbed landscape, incurring a large transverse jump in the process. Since the triumphant neighbor is rarely a local relative, the jumps make important contributions to the statistical averages.

In addition to the mean jump size, we have also studied the probability that a jump actually happens ($x_1 \neq x_2$) for the case of RF perturbations of the random energy landscape. A glance at Fig. 1 reveals that for paths shorter than the crossover lengthscale, the data are well fit by a line of slope 1/2. For RBs perturbing RBs, the data fall along a line of slope 1/6, as explained by Feigel'man and Vinokur [12]. Again, for the RB case, there is no indication, whatsoever, of incipient crossover phenomena. Note that, while there are geometric arguments [12-14] that predict these jump probability exponents, for both RFs and RBs, they coincide with the crossover index φ.

All this is easily understood on the basis of Shapir's scaling ansatz for the interfacial roughness $| x(t) |$,

$$| x_\delta(t) | = | x_o(t) | g(\delta t^\varphi) = | x_o(t) | \{1 + g'(0)\delta t^\varphi + ...\}$$

from which it follows that the displacement in the perturbed environment is given by

$$\Delta x(t) = | x_\delta(t) | - | x_o(t) | \sim | x_o(t) | g'(0)\delta t^\varphi \sim \delta t^{\varphi+\zeta}$$

whence the mean jump exponent, while

$$P(jump) \sim \Delta x(t) / | x_o(t) | \sim \delta t^\varphi$$

For reasons that are unclear, the energy-based derivation of Feigel'man and Vinokur[12] for the jump probability exponent appears not to carry through for RF perturbations of the RB landscape. Nonetheless, the linear dependence of both the mean jump distance and the jump probability on the strength of the perturbation were manifest in the RF simulations we performed for other values of δ [15]. Zhang had pointed out similar behavior in the RB case.

Given the quickly growing jump probability, it is natural to wonder whether the old best path in the original random energy landscape retains some honor by remaining a locally optimal path in the new disordered environment. In our numerical studies, we found that the energy change of the old best path in the different energy environments had an exponent of unity for RFs, which suggests that the new locally optimal path does indeed overlap substantially with the old best path. Finally, we investigated the energy advantage, in the new environment, that motivated the jump away from the old optimal path. See Figs. 1 and 2. It scales with an exponent $\omega'_{RF} = 4/3$ for RF perturbations, $\omega'_{RB} = 2/3$ for RB perturbations. The latter index had been noted of course, by Zhang. Nevertheless, our RF simulation provides additional support to the conjecture that the instability exponents obey a scaling relation, $\omega' = 2\alpha - 1$, analogous to that of the unperturbed problem.

Finally, in Fig. 3, we illustrate the long term implications of RF perturbations upon the RB landscape. Whereas the data for geometric and free energy fluctuations in the original unperturbed random energy landscape scale nicely and are consistent with the exponents $\zeta_{RB} = 2/3$ and $\omega_{RB} = 1/3$, in the new environment RF perturbations incur crossover to the stronger fluctuations characteristic of correlated roughening, the exponents $\zeta_{RF} = \omega_{RF} = 1$ in agreement with the those predicted by Imry-Ma type arguments [16] for the 2d RF Ising model. Note that, while deviations manifest themselves first for the sample to sample fluctuations of the energy, the march to asymptotic scaling is well under way for both quantities once the length scale $t^*_{RF} \sim 100$ is crossed.

It is clear from our numerical studies that correlated random perturbations can incur severe ground-state instabilities in uncorrelated disordered systems. In the case of the DPRM, a RF perturbation upon the RB landscape can have increasingly drastic consequences for the configuration of globally optimal paths, causing large jumps to distant relatives beyond the immediate family. Ultimately, of course, the scaling is

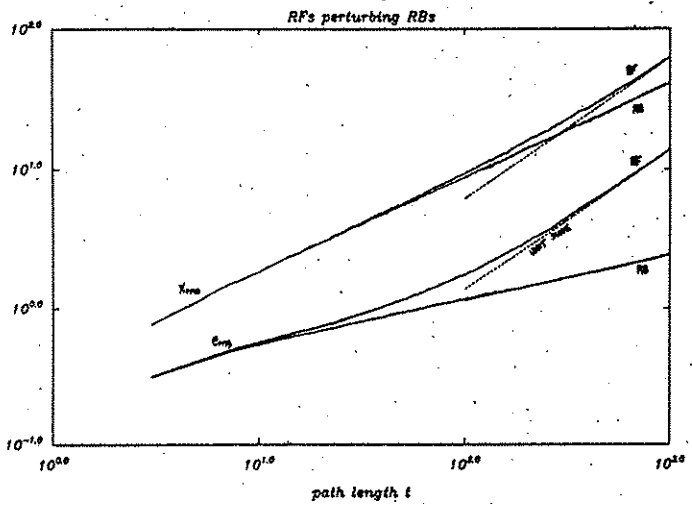

Figure 3. Position (top pair) and energy (bottom pair) fluctuations of the globally optimal path. Upper curves within each pair correspond to the best path in the disordered environment perturbed by random fields. For RFs perturbing RBs, both the position and energy fluctuations eventually scale with unit slope, in agreement with Imry-Ma predictions for the 2d RF Ising model. Lower curves, associated with the original unperturbed energy landscape, exhibit standard 1+1 DPRM exponents, $\zeta_{RB} = 2/3, \omega_{RB} = 1/3$.

controlled entirely by the RF fixed point, characterized by exponents quite different from those of the RB problem. These effects are presumably observable in 2d RB magnets that are subject to a very weak external magnetic field, giving rise to small perturbing RFs within the sample [17]. Thermally activated jumps of domain walls to minimal energy configurations might manifest themselves as large observable noises in measurements of the magnetization, susceptibility, etc. For the kinetic roughening of stochastically grown surfaces, the importance of a spatially correlated perturbation in the atomic beam would be dramatic, leading to radically different surface morphologies with substantially different scaling properties.

Acknowledgment

We tip our hat to Y.-C. Zhang for writing the nice PRL that inspired this work. THH was supported by grants from the Research Corporation and the Petroleum Research Fund, while DH was a participant in the Undergraduate Research Program of the Pew Charitable Trust.

References

[1] J. Krug and H. Spohn, *Solids far from Equilibrium*, (G. Godreche, ed.)Cambridge University Press, Cambridge 1991.

[2] F. Family and T. Vicsek, eds., *Dynamics of Fractal Surfaces*, World Scientific, Singapore 1991.

[3] M. Kardar, G. Parisi and Y.-C. Zhang, *Phys. Rev. Lett.* **56** 889 1986.

[4] T. Nattermann and R. Lipowsky, *Phys. Rev. Lett.* **61** 2508 1988.

[5] M. Kardar and Y.-C. Zhang, *Phys. Rev. Lett.* **58** 2087 1987.

[6] M. Kardar, *J. Appl. Phys.* **61** 3601 1987.

[7] M. Mezard, G. Parisi and M.A. Virasoro, *Spin glass theory and beyond*, World Scientific, Singapore 1987.

[8] M. Mezard and G. Parisi, *J. de Physique* **I1** 809 1991.

[9] Y.-C. Zhang, *Phys. Rev. Lett.* **59** 2125 1987.

[10] Y. Shapir, *Phys. Rev. Lett.* **66** 1473 1991.

[11] M. Mezard, *J. de Physique* **51** 1831 1990.

[12] M.V. Feigel'man and V.M. Vinokur, *Phys. Rev. Lett.* **61** 1139 1988.

[13] T. Nattermann, *Phys. Rev. Lett.* **60** 2701 1988.

[14] Y.-C. Zhang, *Phys. Rev. Lett.* **60** 2702 1988.

[15] T. Halpin-Healy and D. Herbert, *unpublished*

[16] T. Halpin-Healy, *Phys. Rev.* **A42** 711 1990.

[17] S. Fishman and A. Aharony, *J.Phys.* **C12** L729 1979.

the finite-temp phase transition of the 3+1 DPRM manifests itself via KPZ in the stochastic growth model context:

* NEW ROUGHENING TRANSITION ~ BALLISTIC DEPOSITION

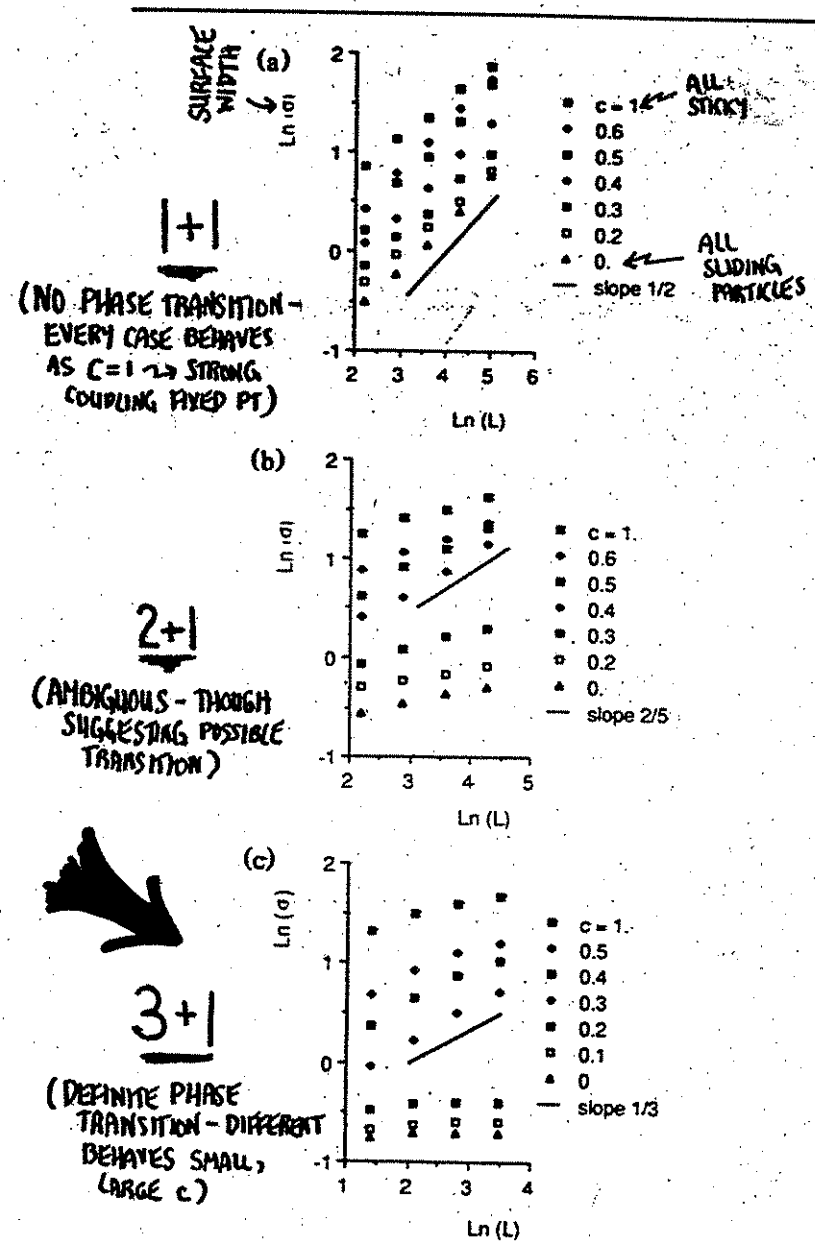

FIG. 1. Large-h saturated value of σ vs L (log-log plot) for different values of c. Cases (a), (b), and (c) correspond to $d=2$, 3, and 4, respectively.

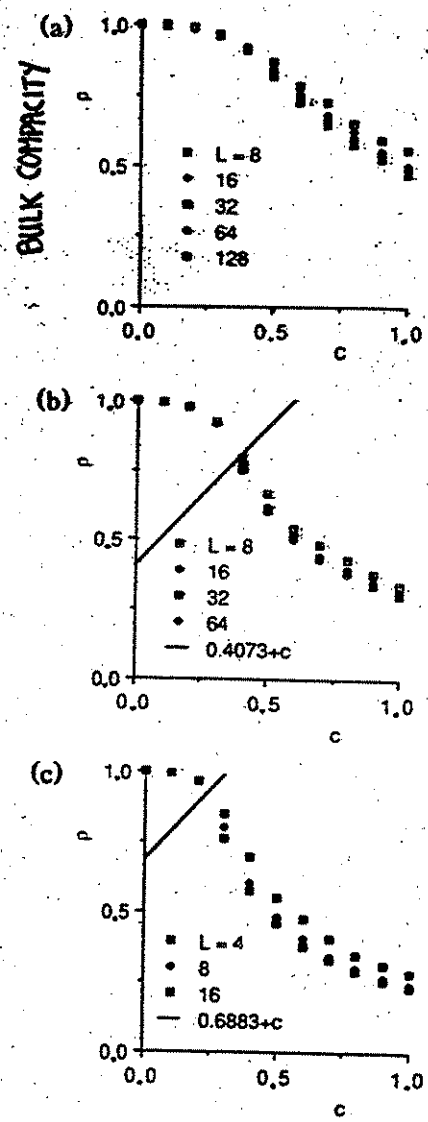

FIG. 2. Large-L saturated value of the bulk compacity, ρ, as a function of c. Cases (a), (b), and (c) correspond to $d=2$, 3, and 4, respectively. The line corresponds to the equation $\rho = c + 1 - c_p$, where c_p is the concentration threshold for site percolation on a $(d-1)$-hypercubic lattice ($c_p = 0.5927$ and 0.3117, for $d-1=2$ and 3, respectively).

SEE ↳ Pellegrini & Jullien, Phys. Rev. Lett 64, 1745 (1990).
Phys. Rev. A43, 920 (1991).

(Yan, Kessler & Sander, Phys. Rev. Lett 64, 926 (1990) ~ related work)

* ULTRAMETRIC TREE STRUCTURE: 1+1 DPRM

references:

M. Kardar & Y.C. Zhang, PRL 58, 2087 (1987).
Y.C. Zhang, PRL 59, 2125 (1987).
E. Perlsman & M. Schwartz, Europhys. Lett. 17, 11 (1992).
} RB case only → $\zeta = 2/3$

M.M. Pang & I. Halpin-Healy, attached preprint ← RF case & $\mu = 2$ POWER LAW NOISE

Motivated by the work of Zhang who examined the geometric properties of the 1+1 DPRM river basin delta in terms of the familial ancestry of the GLOBALLY OPTIMAL PATH, Perlsman and Schwartz initiated a quantitative transfer matrix analysis for the RB case (uncorrelated, gaussian noise). Their most important findings concern:

i) CROSS-SECTION (of globally optimal path)

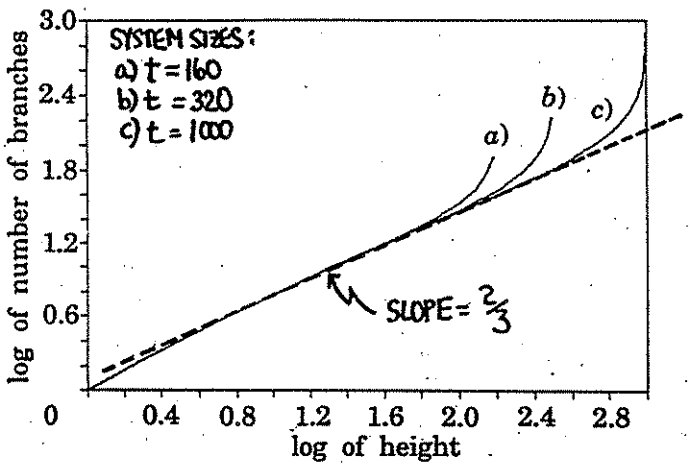

# of branches emanating from globally optimal path

$$W = f(H/t)\, t^{2/3}$$

where H is the height above the base of a t size tree/delta. For a relatively large range of $0 < X < \frac{1}{2}$, the scaling function $f(X) \approx X^{2/3}$.

ii) BRANCHING PROBABILITY (globally optimal path)

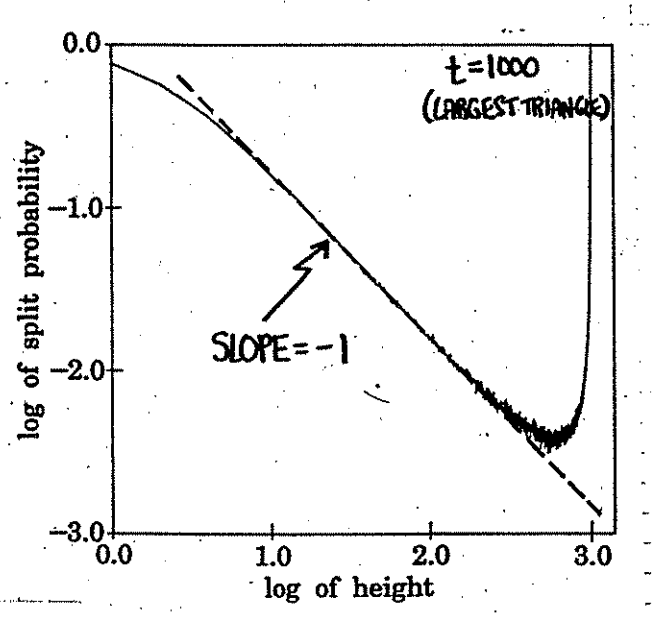

Width of branch at height H, W(H), is just the sum of the widths of the branches that split from it at lower heights

$$W(H) = \int_1^H P(h) W(h)\, dh$$

where P(h) dh is the probability that the branch splits between h and h+dh. Since W(H) is a power law in H, we must have

$$\boxed{P(h) \sim \frac{1}{h}}$$

■ MORAL: in the end, all geometric properties of the RB DPRM delta ride on the wandering exponent 2/3.

*1+1 DPRM RIVER BASIN DELTA

NOISE DRAWN FROM FLAT DISTRIBUTION

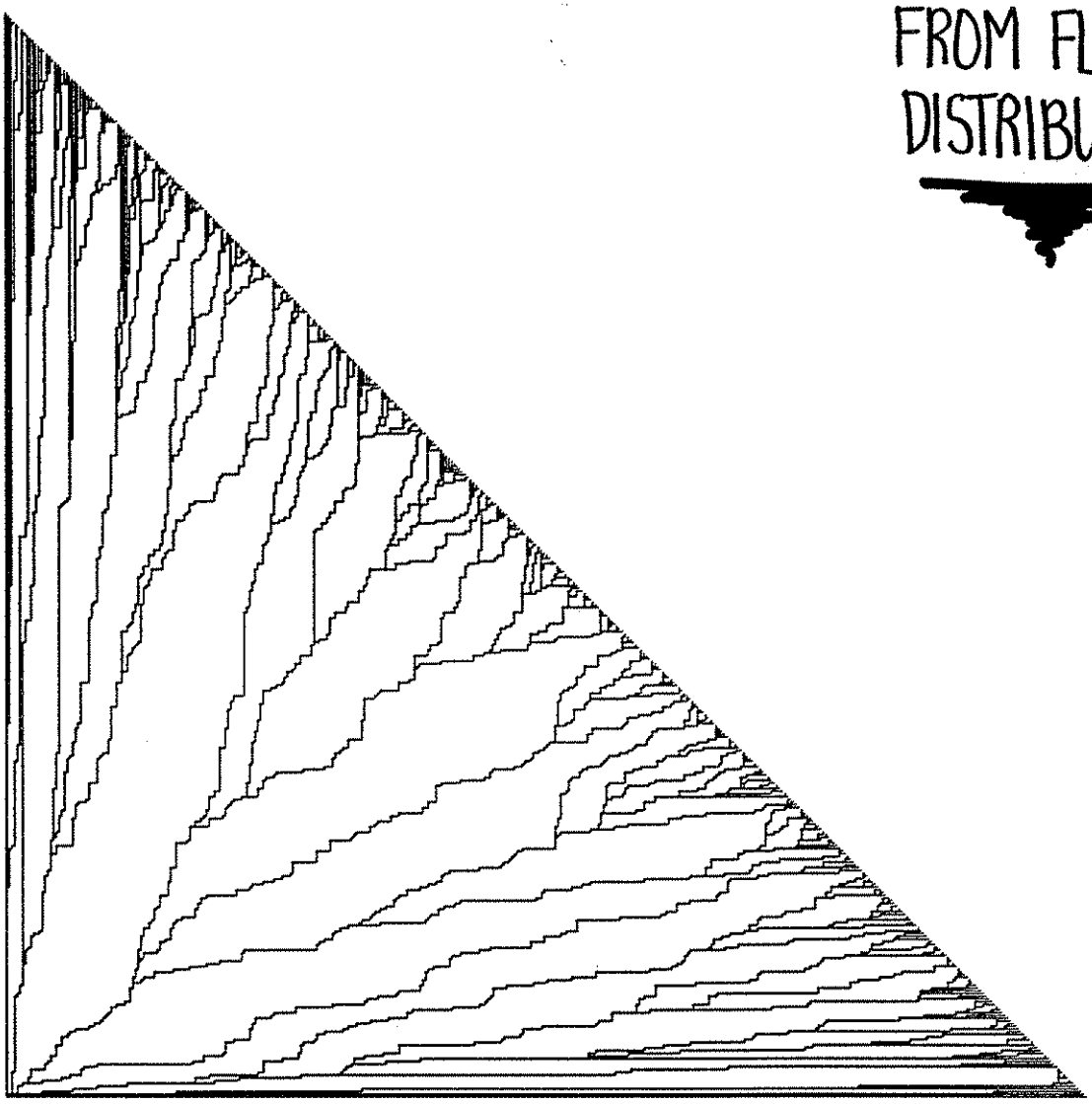

NILE DELTA ?

- for a recent attempt at a complete treatment of the evolution of more general river networks, including effects of erosion, turbulent diffusion, and redistribution of soil, see → S. KRAMER & M. MARDER, PRL 68, 205 (1992).

Discerning Differences amongst Anomalous Wanderers

Ning-Ning Pang[1] and Timothy Halpin-Healy[2]

[1]Physics Department, Columbia University, NY, NY 10027
[2]Physics Department, Barnard College, Columbia University, NY, NY 10027-6598

Abstract: We contrast the effects of uncorrelated, power-law noise and linearly correlated, gaussian noise upon the anomalous wandering of directed polymers in random media. In the first instance, we explore the role of the noise on the morphology of the ultrametric tree structure of the ensemble of locally optimal paths, and then, motivated by the work of Zhang [Phys. Rev. Lett. 59, 2125 (1987)] and more recently by Perlsman and Schwartz [Europhys. Lett. 17, 11 (1992)], provide strong evidence for universality of the model's river basin patterns. Lastly, we discuss those precise features of the positional and energy fluctuations that could permit a resourceful experimentalist to discern the noise distribution underlying anomalous roughening recently observed in fire fronts, bacterial growth, and fluid flow through porous media.

PACS numbers: 2.50.+s, 5.40.+j, 61.50.Cj

submitted to Physical Review A

Because of its immediate and varied connections to a broad collection of outstanding, difficult questions in the statistical mechanics of ill-condensed matter,[1] the problem of directed polymers in a random medium (DPRM) has achieved a well-deserved notoriety, capturing the attention of many practitioners in the field. In its initial guise, the 1+1 dimensional DPRM appeared in the context of impurity-induced domain-wall roughening in disordered 2d magnets.[2] More recently, the many-dimensional DPRM has surfaced in discussions of Abrikosov vortices in high-T_c superconductors,[3] dislocation lines in disordered solids,[4] as well as the possible conformations of a polyelectrolyte in a gel matrix. Kardar and Zhang,[5] who introduced the DPRM and noted its important connection to the noisy Burgers equation, made the crucial observation that the physics of the low-dimensional DPRM was controlled by a zero-temperature fixed point, implying that the finite-temperature properties of the polymer would be identical to those at T=0. These same authors, with assistance of the Europeans,[6] soon came to appreciate the DPRM as a more manageable, but equally rich version of the very stubborn spin glass problem, complete with issues of replica-symmetry breaking (RSB), and structural matters associated with an ultrametric free energy landscape. Indeed, at T=0, the DPRM becomes a matter of global optimization, an amusing variant of the travelling salesman problem in which, fittingly enough, maximization of commission, rather than minimization of path length, becomes the goal at hand. Finally, as stressed by Kardar and Zhang, the ultrametric properties of the DPRM ensemble of locally optimal paths bears a striking resemblence to patterns produced by Nature herself, including river basin deltas, capillary networks in the circulatory system, and neuronal arrays in the brain.

It is the purpose of this paper to concentrate on these geometric properties; not so much with an eye to test their legitimacy as models of Nature's pattern formation, but rather on the role of the noise distribution on their structure. In

particular, we concern ourselves with power-law noise distributions which, within the realm of KPZ,[7] have recently been proposed[8] to account for *anomalous scaling* observed in fire fronts,[9] bacterial colonies,[10] and fluid fronts in porous media.[11] In the present context, the freedom associated with the fall-off of the tail permits us an interesting laboratory in which to study the changing morphology of the random energy landscape, to make connections to the apparently unrelated case of correlated, gaussian noise,[12] to comment on recent findings[13] regarding DPRM ultrametricity, and lastly to discuss, precisely, what are the discernable differences between anomalous wanderers.

Let us first recall the T=0 formulation of the 1+1 DPRM. It is conveniently visualized[14] by considering the first quadrant of the square lattice, upon which quenched random energies (drawn from a variety of probability distributions- uniform, gaussian, power-law) are placed on all the bonds. Neighboring bonds are assumed, momentarily, to be uncorrelated. It is in this manner that we create a single realization of the random energy landscape. Our interest is in the collection of paths emanating from the origin, that proceed forward by single steps in the vertical (y-) or horizontal (x-) directions. As these paths are directed (backtracking not permitted), we naturally identify the diagonal (y=x) as the longitudinal or time direction. The energy of a given path of n steps is given by the algebraic sum of the bonds visited along the way. There are 2^n paths reaching the endpoints of the n^{th} time slice and of these, n+1 constitute the ensemble of locally optimal paths of maximal energy with endpoint specified. Geometrically, this set (see Fig. 1, for example) gives rise to the DPRM *river basin deltas* mentioned earlier. Note, however, that the details of the pattern are very much sample-dependent, though interesting statistical information can be had, and furthermore, even for a single random energy landscape, configurations undergo drastic revision from one time slice to the next. Within a locally optimal ensemble, the path of absolute greatest

energy is referred to as *globally optimal*. The statistical properties of this sole path, obtained by averaging over many realizations of the random energy landscape, are well-known for the 1+1 DPRM. Its transverse positional fluctuations about the symmetry axis are governed by the wandering exponent ζ, which, for uncorrelated gaussian noise,[2] has the superdiffusive value 2/3.

Our interest at this point is in power-law random bond energies distributed as $P(\varepsilon)=\varepsilon^{-(\mu+1)}$ for $\varepsilon>1$, zero otherwise, as first proposed by Zhang.[8,15] We generated the power-law tails by drawing a random number uniformly from the unit interval [0,1] and raising it to the power $-1/\mu$, being careful to be aware of the graininess of the *Numerical Recipes* supplied subroutine RAN3. This is especially important for the power-law DPRM because it is the rare event, buried deep in the tail, that fixes the scaling properties, both energy and geometric. Our main purpose, initially, was to understand the effect of varying μ on the nature of the random energy landscape and, in particular, its role in determining the geometric structure of the DPRM delta. As is well known, the case $\mu=2$ is marginal (the 2nd moment of the bare probability distribution is logarithmically divergent), with $\mu<2$ corresponding to Levy flights, while $\mu\approx 2\text{-}3$ has become the focus of attention of the kinetic roughening community as the most physically relevant range, providing a possible explanation for the anomalous scaling[9-11] observed in propagating fire fronts, bacterial colonies, and fluid fronts in porous media. It should be stressed that, in sharp contrast to the DPRM with gaussian noise (both correlated and not), there has been precious little analytical progress in the context of power-law distributions, aside from a novel Flory argument proposed independently by Krug[16] and Zhang[17] that is based on the occurrence of rare, but dominant fluctuations inherent in power-law tails. These authors predict $\zeta(\mu)=(\mu+1)/(2\mu-1)$ for the power-law DPRM wandering exponent- a formula which is entirely consistent with numerical simulations for small values of $\mu>2$, but incorrectly predicts a $\mu_c=5$. Indeed, recent work of Bourbonnais *et al*[18] has

convincingly established that it is for μ_c=7 that the power-law tail drops sufficiently fast for the wandering exponent to fall to its uncorrelated, gaussian noise value.

In Fig. 1, we plot the DPRM deltas for μ=1,3, and 7. Please note that each of the deltas was generated using the same seed to initialize the random number generator, so that the figure truly illustrates the evolution of the river basin morphology as the power law tail is changed. We observe the following features- For μ=1, which corresponds to an extreme Levy flight case, there is a predominance of straight line segments and persistence of right angle vertices on *macroscopic scales* that appears lost, or at least greatly weakened, as μ is increased beyond 2 to 3. This substantive qualitative change is also manifest as $\mu \rightarrow 3$ in an increased jaggedness of the trajectories and an enhanced meandering in the middle of the delta. By contrast, a comparison of the deltas for μ=3 and 7 reveals a morphological shift that is much more modest, being one of degree rather than kind. In other words, the important geometric characteristics gleaned from the μ=3 delta are maintained, and merely amplified, as the range of the power-law tail is decreased. Finally, there is a growing ratio of black to white (indication of an increasing fractal dimension), while the persistence of linearity is for the most part relegated to the border paths and its immediate neighbors.

In Fig. 2, we have paired together the DPRM delta corresponding to power-law noise with μ=2, for which numerical studies strongly suggest that $\zeta \approx 1$, and the river basin pattern generated by linearly correlated, gaussian noise. For the latter, the globally optimal path through the random energy landscape is identical to the 1d interface in a 2d random-field (RF) Ising model, a problem[19] with a long, colorful and contentious history which is, nevertheless, characterized by the very same wandering exponent as μ=2 power-law noise. That ζ_{RF}=1 was established numerically by Fernandez, et al.,[20] then analytically by Zhang[21] via the stochastic Burgers equation, and finally rigorously by Imbrie,[22] who settled once and for all the

lower critical dimension of the model. Unfortunately, the fact that two grossly different noise distributions can give rise to the same anomalous wandering exponent has muddied the waters somewhat within the kinetic roughening community, though the presently prevailing sentiment is to attribute the anomalous scaling seen in the experiments[9-11] to uncorrelated power-law noise distributions. From a materials science point of view, it is plausible, though not entirely obvious why this should be so but, in an effort to categorize what, if any, are the discernible differences between the RF and μ=2 distributions upon the scaling properties of anomalous wanderers, we felt obliged to address this matter, both at the geometric level of the DPRM deltas, as well as the fully renormalized probability distributions.

With regard to delta ultrametricity, our findings strongly support the notion of universality first proposed by Zhang,[14] who phrased the discussion of basin geometry in terms of ancestry and progeny of the network, as well as the more recent efforts of Perlsman and Schwartz,[13] who addressed this issue quantitatively by examining the cross-section and branching probability of the globally optimal path. For the special case of uncorrelated, gaussian noise, these authors provide quite convincing numerical evidence that all geometric properties of the basin pattern are dictated by the wandering exponent ζ. Our new findings are in complete agreement with this idea- Fig. 3 reveals that the large sample-dependent differences evident in the deltas of the previous figure are statistically irrelevant, so that upon averaging over many realizations of the random energy landscape, an important geometrical property of the delta, such as the width of the globally optimal path, scales the same for both the μ=2 and RF distributions. The curves have slopes identical to our numerically determined wandering exponents, both near unity. Note that the cross-section, defined as the total number of paths emanating from the globally optimal path, scales properly only over a limited range, as first observed by

Perlsman and Schwartz.[13] The abrupt saturation that occurs at large heights is easily understood[23] in a quantitative fashion as a manifestation of a (non-)interference effect seen by Mezard[6] in a related context. Additional evidence in favor of universality is given in Fig. 4 which shows that the branching probability of the globally optimal path is apparently the same regardless of the distribution! Thus, our own conclusion is clear- at the level of the DPRM delta, there are no discernible differences, since the important statistical properties of the basin geometry are dictated entirely by the value of wandering exponent, not the underlying, bare probability distribution.

Dramatic differences between RF and μ=2 anomalous wandering are easily perceived, however, when we ask appropriate questions at the level of probability distributions[24] and amplitudes[25] that *completely* characterize the fluctuations of the globally optimal path. For example, the relative amplitudes of the first four even moments of positional probability distribution are in the ratio 1.00:1.30:1.52:1.70 for the μ=2 case, but 1.00:1.24:1.40:1.53 for the RF DPRM. This rather impressive distinction appears to arise from the distinction between correlated and uncorrelated noise, since the ratios for various power-law DPRM all tended to be quite close, somewhat surprisingly, to the RB DPRM.[24] We are presently investigating this matter in greater detail.[23] Differences are even more explicit for the renormalized energy probability distributions, see Fig. 5, where we note a narrow, statistically smooth, but highly skewed distribution for RF roughening (skewness s=-0.43, compared to s=-0.29 for the gaussian RB DPRM[25]) . By contrast, though still asymmetric, the renormalized energy distribution resulting from a μ=2 power-law tail is very noisy, with an ill-defined third cumulant, and much, much broader than that of the RF DPRM. As the fluctuations of the DPRM are closely tied to those of a stochastically evolving KPZ surface, we suggest the experimental relevance of these features in identifying the underlying noise distribution responsible for recently

observed anomalous kinetic roughening. It is our expectation that the matter will soon be settled at this level of inquiry.

This work was supported by the Research Corporation, NSF DMR92-11240, and the Petroleum Research Fund, the last being administered by the American Chemical Society.

References

[1] See, e.g., *Surfaces Rugeuses*, Proceedings of the 1992 Les Houches Winter School, ed. J. Kertesz and D. Wolf, (to be published); also, T. Halpin-Healy, Phys. Rev. A42, 711 (1990).

[2] D. A. Huse and C. Henley, Phys. Rev. Lett. 54, 2708 (1985).

[3] T. Nattermann and R. Lipowsky, Phys. Rev. Lett. 61, 2508 (1988).

[4] L. B. Ioffe and V. M. Vinokur, J. Phys. C 20, 6149 (1987).

[5] M. Kardar and Y.-C. Zhang, Phys. Rev. Lett. 58, 2087 (1987).

[6] G. Parisi, J. Physique 51, 1595, (1990); M. Mezard, ibid 51, 1831 (1990), and refs to the work of B. Derrida therein.

[7] M. Kardar, G. Parisi and Y.-C. Zhang, Phys. Rev. Lett. 56, 889 (1986).

[8] Y.-C. Zhang, J. Phys. (France) 51, 2129 (1990).

[9] J. Zhang, Y.-C. Zhang, P. Alstrom and M.T. Levinson (preprint).

[10] T. Vicsek, M. Cserzo and V.K. Horvath, Physica A167, 315 (1990).

[11] V. K. Horvath, F. Family, and T. Vicsek, Phys. Rev. Lett. 67, 3207 (1991); see also J. Amar and F. Family, J. Phys. A 24, L79 (1991).

[12] M. Kardar, J. Applied Phys. 61, 3601 (1987).

[13] E. Perlsman and M. Schwartz, Europhys. Lett. 17, 11 (1992)

[14] Y.-C. Zhang, Phys. Rev. Lett. 59, 2125 (1987).

[15] U. M. B. Marconi and Y.-C. Zhang, J. Stat. Phys. 61, 885 (1990).

[16] J. Krug, J. Physique. I 1, 9 (1991).

[17] Y.-C. Zhang, Physica A170, 1 (1990).

[18] R. Bourbonnais, H. J. Herrmann, and T. Vicsek, Int. J. Mod. Phys. C 2, 719 (1991).

[19] G. Grinstein, J. Appl. Phys. 55, 2371 (1984).

[20] J. F. Fernandez, G. Grinstein, Y. Imry, and S. Kirkpatrick, Phys. Rev. Lett. 51, 203 (1983).

[21] Y.-C. Zhang, J. Phys. A 19, L941 (1986).

[22] J. Z. Imbrie, Phys. Rev. Lett. 53, 1747 (1984).

[23] N.-N. Pang and T. Halpin-Healy, work in progress.

[24] T. Halpin-Healy, Phys. Rev. A44, 3415RC (1991).

[25] J. Krug, P. Meakin, and T. Halpin-Healy, Phys. Rev. A45, 638 (1992); see also J. Amar and F. Family, ibid.

Figure Captions

Fig. 1- River basin deltas associated with the power-law DPRM: a)μ=1, b)μ=3, and c)μ=7. The patterns were all generated from the same seed, but evolve differently when the tail of the distribution is changed.

Fig. 2- River basin deltas resulting from two very different bare noise distributions that, nevertheless, produce identical DPRM wandering exponents. a) linearly correlated, gaussian noise, b) uncorrelated, μ=2 power-law noise. Distinct random number generator seeds; apparently quite different patterns.

Fig. 3- *Cross-section* of the globally optimal path as a function of height from the base of the river basin delta; 5000 realizations of the random energy landscape. The RF and μ=2 cases scale in the same manner, with slopes identical to our independently extracted wandering exponents, as predicted by Schwarz and Perlsman [13]. Lower curve offset -0.5 for visibility.

Fig. 4- *Branching probability* of the globally optimal path for RF and μ=2 DPRM. Again, because of nearly perfect coincidence, the lower curve has been offset. The straight lines have slope -1, providing strong evidence that, aside from crossover and saturation effects, the probability falls inversely with height, independent of the underlying noise distribution. Perlsman and Schwartz [13] had previously noted this behavior for the uncorrelated, gaussian DPRM. Our work establishes the universality of their discovery.

Fig. 5- Very different disorder-averaged energy probability distributions for the RF and μ=2 DPRM. 50,000 realizations, path length 500 steps. Rescaled data collapse for time slices t=300,400,500. The energy fluctuation exponent ω is near unity for both cases, while *e* is the average energy per step.

Fig. 1

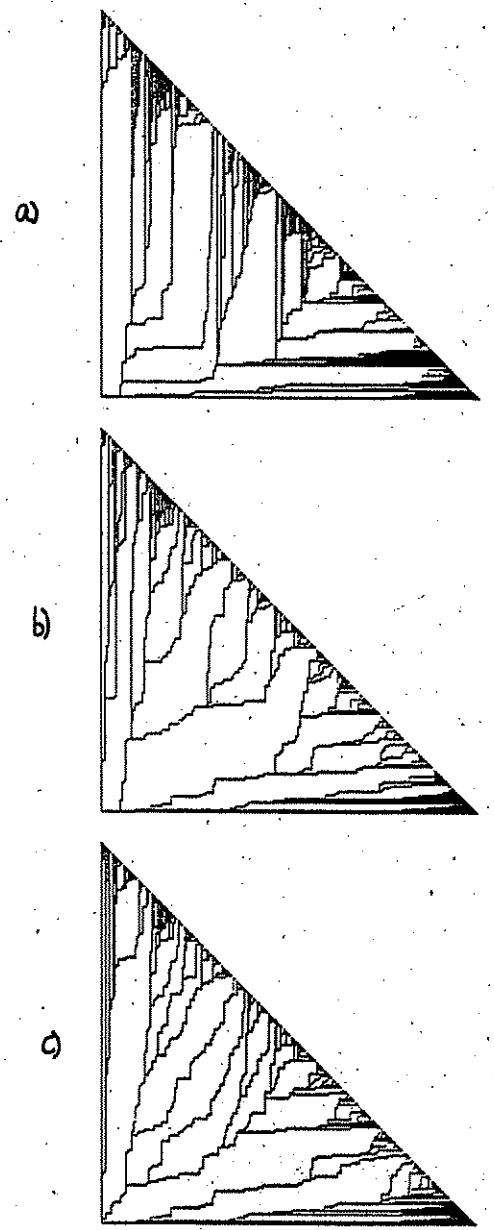

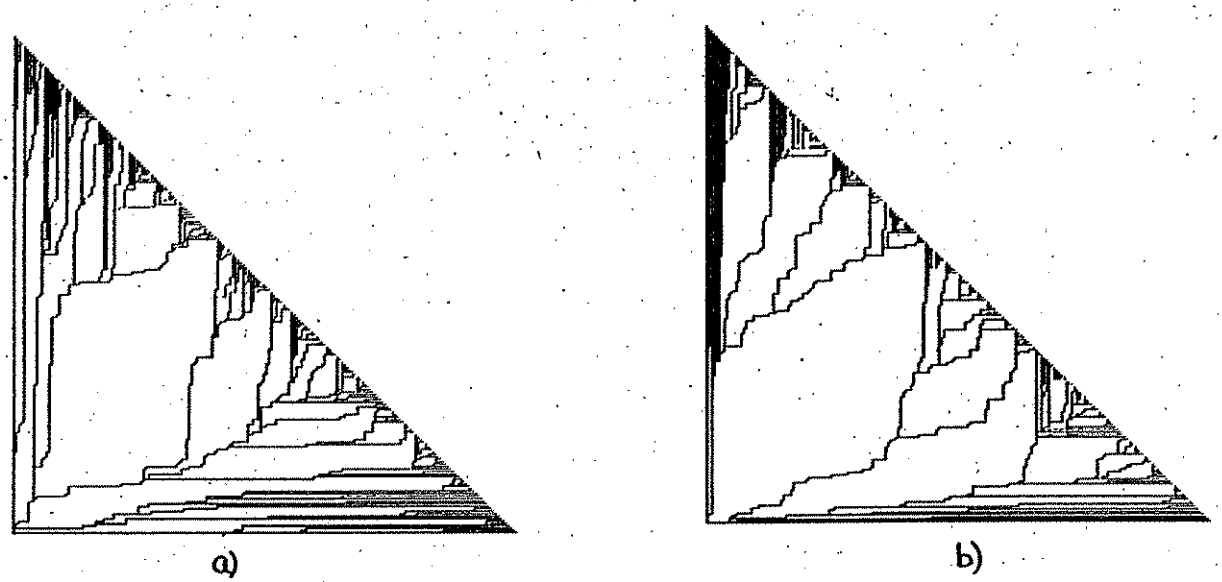
a)
b)

Fig. 2

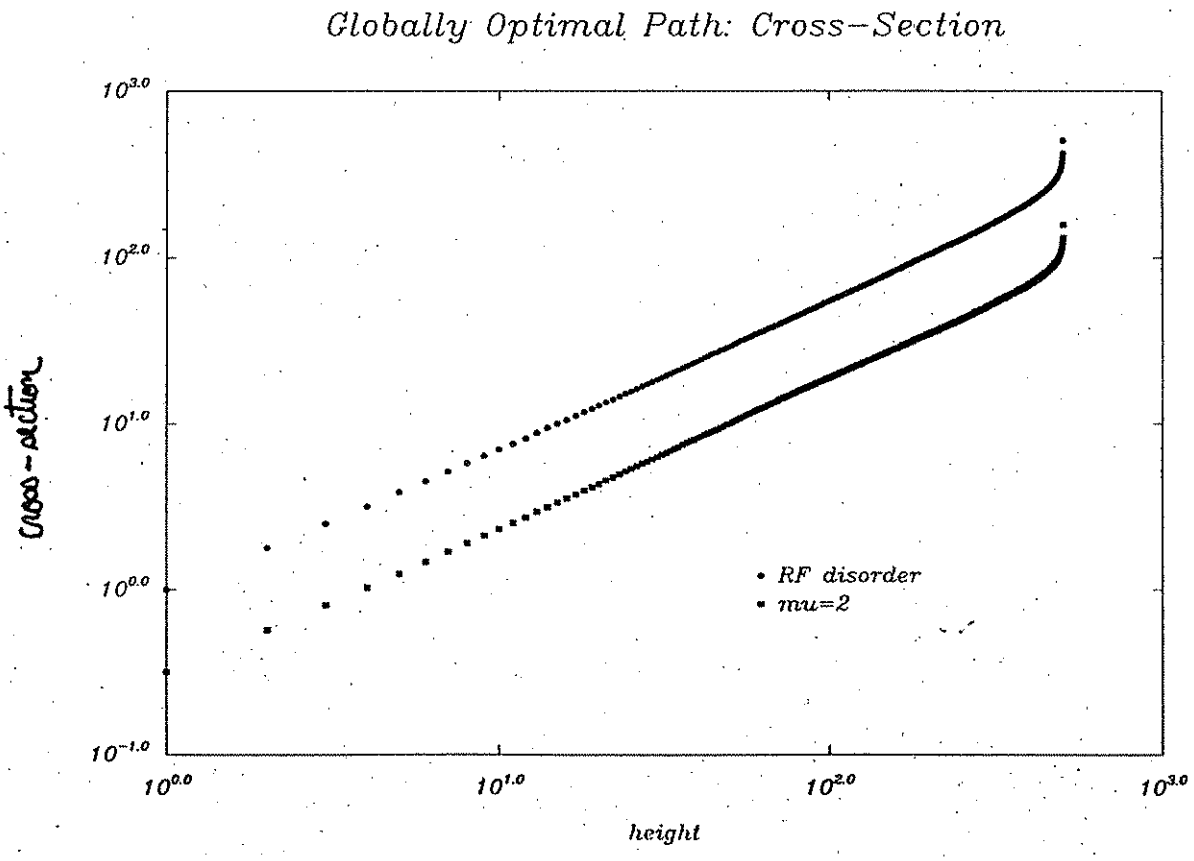
Globally Optimal Path: Cross-Section
cross-section
height
RF disorder
mu=2
10^3.0
10^2.0
10^1.0
10^0.0
10^-1.0
10^0.0
10^1.0
10^2.0
10^3.0

Fig. 3

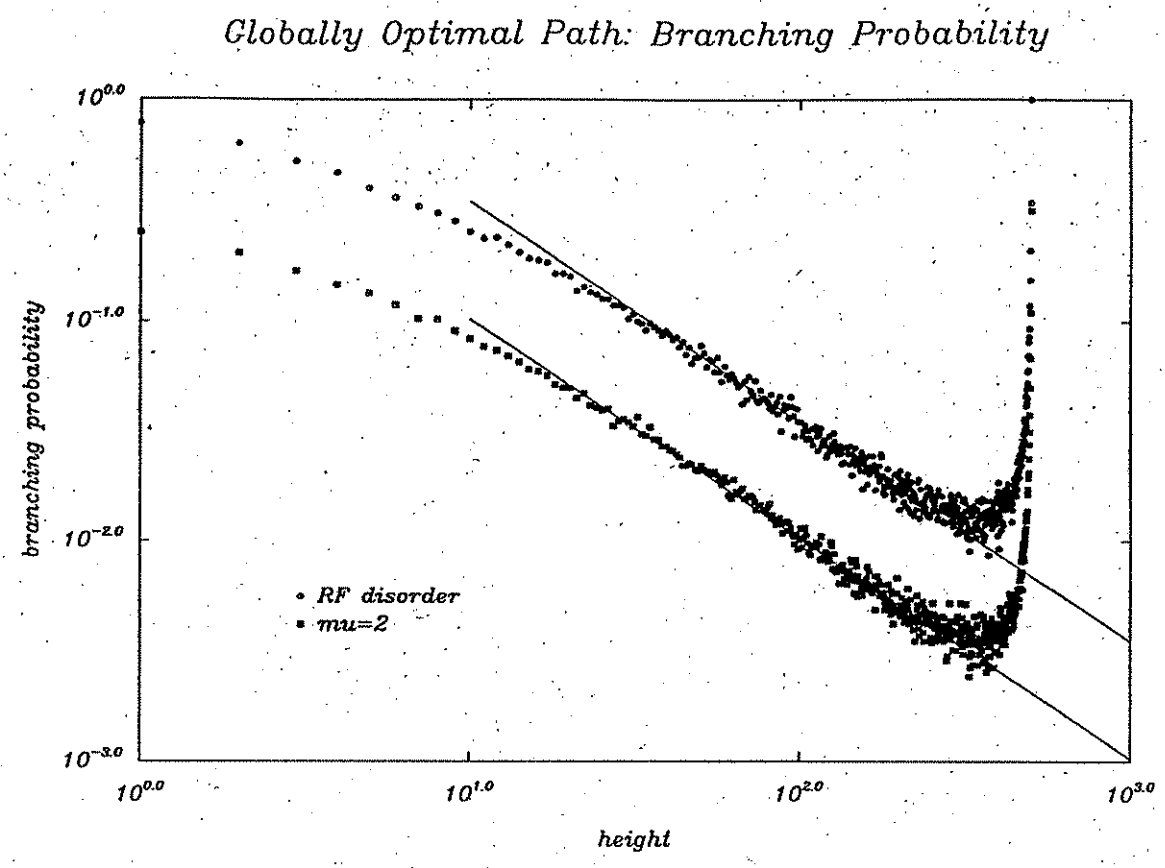
Globally Optimal Path: Branching Probability
branching probability
height
RF disorder
mu=2
10^0.0
10^-1.0
10^-2.0
10^-3.0
10^0.0
10^1.0
10^2.0
10^3.0

Fig. 4

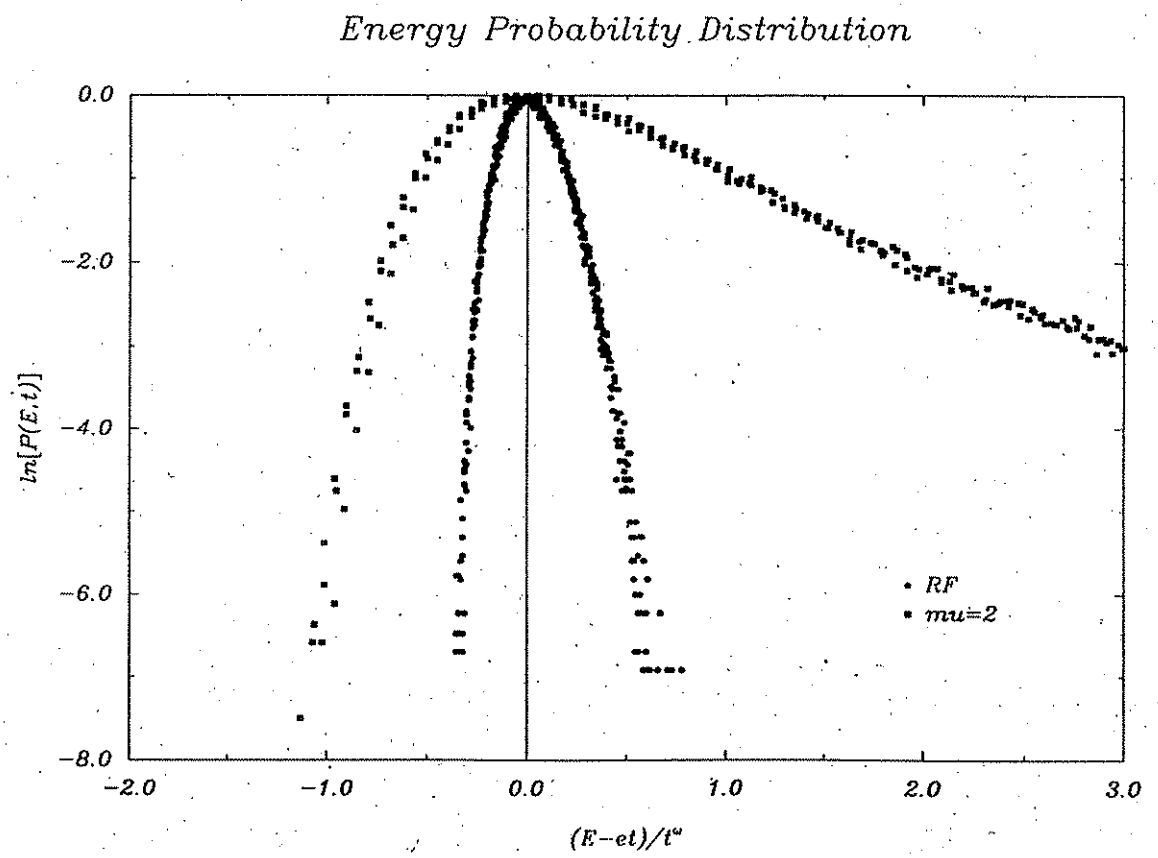
Energy Probability Distribution
ln[P(E,t)]
(E-et)/t^w
RF
mu=2
0.0
-2.0
-4.0
-6.0
-8.0
-2.0
-1.0
0.0
1.0
2.0
3.0

Fig. 5

* DEPINNING BY QUENCHED RANDOMNESS ~ M. Kardar, PRL 55, 2235 (1985)

Recall 2d critical wetting geometry ~ at zero temperature, my 1d interface runs straight thru the column of weak bonds along the edge of the sample (see lecture #1). As the temperature is raised, however, thermal fluctuations eventually liberate the interface, the associated delocalization transition restoring broken translational symmetry. Here we play a different game – we keep $T=0$, but allow the bonds in the bulk to be random variables, chosen from a gaussian distribution of variance σ^2. Our interface, now a RB interface or DPRM, wanders from the edge in search of OPTIMAL ENERGY CONFIGURATIONS. Since we are at $T=0$, entropy is irrelevant; it is purely a matter of energetics. The wandering of the DP is "disorder-induced" rather than thermally driven. As we increase the strength of the disorder in the bulk, the DP will eventually be freed from the (uniform) column of weak bonds along the edge. We'd like to know the nature of the singularities (FREE ENERGY, LOCALIZATION LENGTH) at the delocalization transition, when one has reached the critical value of the bulk disorder strength. For depinning by quenched randomness, we are lead to the replicated Hamiltonian

$$\tilde{\mathcal{H}}_n = -\gamma \sum_{\alpha=1}^{n} \frac{\partial^2}{\partial x_\alpha^2} - \sigma^2 \sum_{\alpha<\beta} \delta(x_\alpha - x_\beta) + \sum_{\alpha=1}^{n} V_S(x_\alpha)$$

"FAMILIAR PIECES"

SHORT-RANGED EDGE POTENTIAL DUE TO WEAK SURFACE BONDS (ATTRACTIVE PART + IMPENETRABLE CORE)

Need Bethe ansatz solution of interacting particles in an external potential! Educated guess $\Rightarrow$ $\tilde{\Psi}_0 \sim e^{-\sum k_i x_i}$ with $k_i = \lambda + 2(i-1)\kappa$ is a wise choice because it insures proper derivative discontinuities when two particles are exchanged and also gives fall off $e^{-\lambda x_1}$ for particle nearest the edge, which is sitting in the well. Here $\lambda \propto (T_W - T)$ is the quantity that VANISHES at the transition for purely thermal 2d critical wetting, where the binding energy goes to zero as λ^2 ($\Rightarrow$ discontinuity in the SPECIFIC HEAT) and the localization length diverges as λ^{-1}. Naively, since $\tilde{\Psi}_0$ has NO NODES, we expect that it represents the GROUND-

STATE of the Hamiltonian $\tilde{\mathcal{H}}_n$. Clearly, the set of momenta $\{k_i\}$ is the same regardless of the ordering of the particles $\Rightarrow$ the kinetic energy is $\gamma \sum k_i^2$. Evaluation of the total energy of the n-particle bound state yields

$$\tilde{E}_n = -\gamma\left[(\lambda^2 - 2\lambda\kappa + \tfrac{2}{3}\kappa^2)n + 2\kappa(\lambda-\kappa)n^2 + \tfrac{1}{3}\kappa^2 n^3\right]$$

Recall for pure, thermal critical wetting we were interested in the energy difference between bound and unbound states. For disorder-induced depinning, SAME STORY - though we need to keep in mind that the quench-averaged free energy $[\tilde{f}]$ of the pinned interface is given by the $n \to 0$ limit of $\tilde{E}_n/n$, so

$$[\tilde{f}] - [f] = \lim_{n\to 0} \frac{\tilde{E}_n - E_n}{n} = -\gamma(\lambda-\kappa)^2$$

← DISCONTINUOUS SPECIFIC HEAT - JUST LIKE THERMAL DEPINNING!

where we used the Bethe ansatz solution from the 1+1 DRRM that $E_n = -\frac{1}{3}\gamma\kappa^2(n^3-n)$, see earlier. One can also calculate the quench-averaged localization length $[\ell_p] = [\langle x\rangle]$. Assuming unbroken replica symmetry, one has $[\langle x\rangle] = \lim_{N\to 0} \sum_\alpha \langle x_\alpha\rangle / N$. Since $\tilde{\Psi}_0$ determines the asymptotic distribution probabilities of replicated polymers:

$$\langle \sum x_\alpha \rangle = \int_0^\infty dx_1 \cdots dx_n \left(\sum x_\alpha\right) \tilde{\Psi}_0 \Big/ \mathcal{N}(\lambda)$$

← "THERMAL AVERAGE"; $\mathcal{N}(\lambda)$: "NORMALIZATION FACTOR"

$\mathcal{N}(\lambda)$ is the sum of $n!$ equal contributions from different orderings $\Rightarrow$

$$\mathcal{N}(\lambda) = n! \int_0^\infty dx_1\, e^{-\lambda x_1} \int_{x_1}^\infty dx_2\, e^{-(\lambda+2\kappa)x_2} \cdots \int_{x_{n-1}}^\infty dx\; e^{-(\lambda+2(n-1)\kappa)x_n}$$

integration regions result from ordering $0 < x_1 < x_2 < \cdots < x_n$. Performing the integrals, right to left:

$$\mathcal{N}(\lambda) = n! \prod_{\alpha=1}^{n} \{\alpha\lambda + [2\alpha n - \alpha(\alpha+1)]\kappa\}^{-1} = \prod_{\alpha=1}^{n} \{\lambda + [2n-\alpha-1]\kappa\}^{-1}$$

Note that for all particle orderings a factor $-\lambda\sum x_\alpha$ appears in the exponent for $\tilde{\Psi}_0 \Rightarrow$ we can calculate the expectation value as

$$\langle \sum_\alpha x_\alpha \rangle = -\frac{\partial}{\partial\lambda} \ln \mathcal{N}(\lambda) = \sum_\alpha \frac{1}{\lambda + (2n-\alpha-1)\kappa}$$

$$= \sum_\alpha \int_0^\infty dy\, e^{-(\lambda+[2n-\alpha-1]\kappa)y}$$

Of course, we are ultimately interested in the limit $n \to 0$ of $\frac{1}{n}\langle [\Sigma x_\alpha] \rangle$, so we need to reorganize things a bit – Performing the sum over $\alpha \Rightarrow$

$$\sum_{\alpha=1}^{n} \int_0^\infty dy\, e^{-(\lambda + [2n-\alpha-1]\kappa)y} = \int_0^\infty dy\, e^{-[\lambda + 2(n-1)\kappa]y} \frac{e^{n\kappa y} - 1}{e^{\kappa y} - 1}$$

allows us to take the necessary limit:

$$[l_p] = \int_0^\infty dy\, \kappa y \frac{e^{-(\lambda-\kappa)y}}{1 - e^{-\kappa y}}$$

which implies that for $\kappa \ll \lambda$, one has $[l_p] \sim \frac{1}{\lambda}$ for vanishing $\lambda \leftarrow$ nothing but the thermal depinning result from three lectures ago. For the problem at hand the disorder-induced delocalization transition occurs as $\kappa \to \lambda$. Letting $x = (\lambda - \kappa)y$, we have

$$[l_p] = \frac{\kappa}{(\lambda-\kappa)^2} \underbrace{\int_0^\infty dx\, x \frac{e^{-x}}{1 - e^{-\frac{\kappa}{\lambda-\kappa}x}}}_{= 1 \text{ at transition}}$$

$\Rightarrow$

$$[l_p] \sim \frac{\kappa}{(\lambda-\kappa)^2}$$

MEAN POSITION OF INTERFACE DIVERGES "QUADRATICALLY"

Comment on "Depinning Due to Quenched Randomness"

The statistical mechanics of interfaces in random media, as illustrated, for example, by disorder-induced critical wetting and roughening phenomena, has been a subject of great interest since the seminal work of Huse and Henley [1], Kardar and Nelson [2,3], and Lipowsky and Fisher [4]. The purpose of this Comment is to bring to resolution an outstanding issue that has remained at the heart of this matter for several years now. It concerns the liberation exponent ψ for interfacial depinning due to quenched randomness. One considers a 2D Ising model on a semi-infinite square lattice in which there is a energetically favorable row of weak bonds along the edge. The imposed boundary conditions are such that at low temperatures and in the absence of strong disorder there is a 1D elastic interface running through these weak bonds, localized by the contact pinning potential along the edge of the sample. As the quenched randomness in the bulk is augmented, however, the interface wanders increasingly further from the edge, searching for minimal energy configurations. Eventually it undergoes a depinning transition. Kardar [2], in his original work on the subject, used Bethe-ansatz techniques within a replica formalism to determine that the mean position of the 1D interface diverged *quadratically* as the disorder strength in the bulk was raised to its critical value. That $\psi=2$ for critical wetting in 2D random-bond Ising models can also be established via bead and necklace model ideas of Lipowsky and Fisher [4], who found that $\psi=\zeta/(1-\zeta)$, where $\zeta_{RB}=\frac{2}{3}$ is the interfacial wandering exponent. Attempting to verify this novel surface critical phenomena, Kardar [2] performed a series of numerical simulations for disorder-induced depinning both from a wall and in the bulk. Somewhat paradoxically, though, his numerical efforts in this regard revealed only an *approximately linear* divergence, which he attributed to an inability to reach asymptotic scaling behavior. Examining this depinning transition using more advantageous scaling variables and with the benefit of somewhat greater computational power, we have managed to access the true critical regime, thereby observing the elusive quadratic divergence.

In Fig. 1, we show the results of our simulation, based on Kardar's solid-on-solid model in the presence of random bonds. In this formulation, the interface runs parallel to the x axis on a square lattice with $y \geq 1$, one end being pinned to (0,1) and a particular configuration described by the set of integer heights $\{y(x)\}$. Whenever $y(x+1)=y(x)\pm 1$, the interface jumps vertically, incurring an elastic energy cost K, with associated Boltzmann weight $\gamma=\exp(-K)$. The horizontal segments along the edge $\mu(x,1)=\mu_e$ are weaker than those in the bulk, which are assumed to be independent random variables drawn uniformly from the interval $[\mu_a-s/2,\mu_a+s/2]$. The total Boltzmann weight of interfaces connecting (0,1) to (x,y) is calculated recursively by transfer-matrix

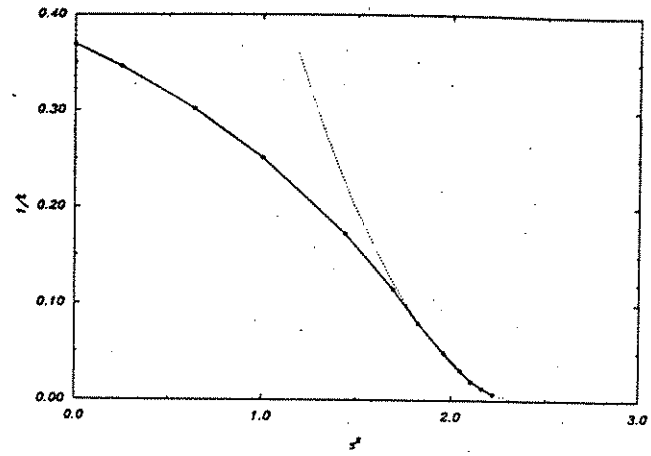

FIG. 1. Interfacial delocalization by quenched randomness from an edge contact potential. The inverse localization length, given by the reciprocal of the mean position of the interface, vanishes *quadratically* as the variance of the bulk disorder strength attains its critical value.

techniques [2]. We have used $\gamma=0.3$ and $\mu_a-\mu_e=0.34$, as in Kardar's original paper, and typically performed the disorder average over 500–1000 realizations of randomness. We estimate $s_c=1.54\pm0.01$. However, path lengths as large as 5.0×10^4, 7.5×10^4, 10^5 were necessary to achieve saturation for $s=1.45$, 1.47, 1.49, respectively. The figure shows the inverse localization length versus s^2, the latter being the most appropriate abscissa since the replica theory predicts $l^{-1}\sim(\text{const}-\kappa)^2$, where $\kappa^{-1}=48\gamma/s^2$. Note that although the quadratic behavior becomes apparent as $s^2\to s_c^2$, it is inevitably so only with the inclusion of the final three data points alluded to above, indicating the extreme difficulty of the problem. We find similar results for disorder-induced depinning in the bulk, but with a slightly larger critical regime. All this is in sharp contrast to the much less stubborn case of complete wetting in random media, for which it is considerably easier to elicit asymptotic scaling [5].

This research was supported by a grant from Petroleum Research Fund of the American Chemical Society.

Martin Zapotocky and Timothy Halpin-Healy
Department of Physics
Columbia University
New York, New York 10027

Received 13 August 1991
PACS numbers: 05.70.Jk, 68.45.−v, 75.60.Ch, 82.65.Dp

[1] D. A. Huse and C. L. Henley, Phys. Rev. Lett. 54, 2708 (1985).
[2] M. Kardar, Phys. Rev. Lett. 55, 2235 (1985).
[3] M. Kardar and D. R. Nelson, Phys. Rev. Lett. 55, 1157 (1985).
[4] R. Lipowsky and M. Fisher, Phys. Rev. Lett. 56, 472 (1986).
[5] M. Huang, M. Fisher, and R. Lipowsky, Phys. Rev. B 39, 2632 (1989).

* see also the work of Wuttke & Lipowsky, Phys. Rev. B44, 13042 (1991).

"DEPINNING BY QUENCHED RANDOMNESS"

THEORY:
M. Kardar
PRL 55, 2235 (1985)

CONFIRMED:
M. Zapotocky & J. Halpin-Healy
PRL 67, 3463 (1991)

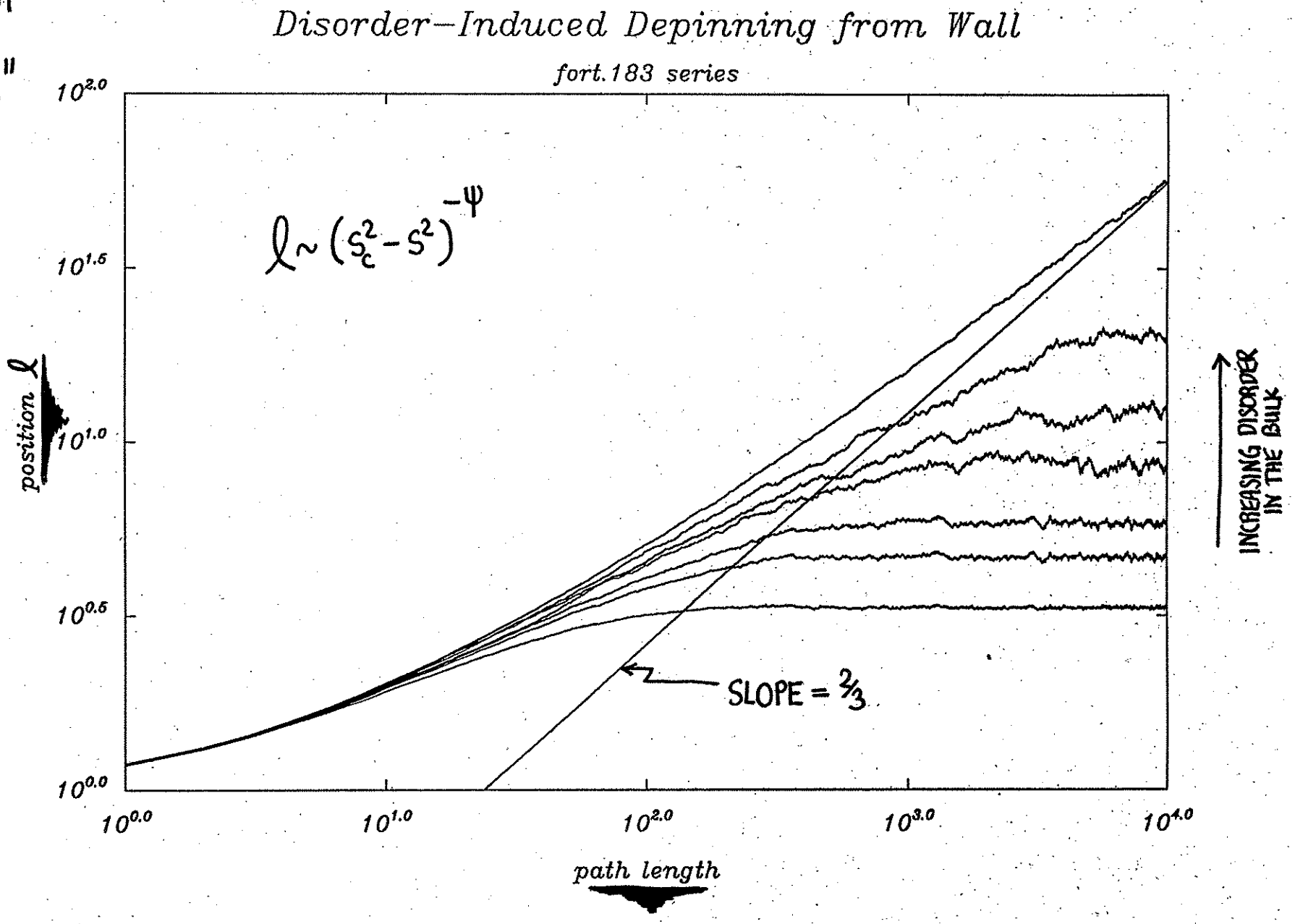

Disorder–Induced Depinning